DEPARTMENT OF MECHANICAL & AEROSPACE ENGINEERING

University of Strathclyde Engineering

Droplet Behaviour in Microfluidic Devices

Pınar England

A thesis presented in fulfilment of the requirements for the degree of Doctor of Philosophy

2018

Declaration of Authenticity and Author's Rights

This thesis is the result of the author's original research. It has been composed by the author and has not been previously submitted for examination which has led to the award of a degree.

Signed: 

Date: 07.June.2018

Publications Arising from this Thesis

I. Y. Zhang and P. Ozdemir. Microfluidic DNA Amplification – A Review. Anal Chim Acta, 638(2) pp. 115-125, 2009. DOI: 10.1016/j.aca.2009.02.038.

II. P. Ozdemir, S. Mohr, C. Wang, M.T. Stickland, N.J.Goddard, P.R. Fielden, and Y. Zhang. Self-Organised Droplet Flow Patterns in Microchannels. 2nd Micro and Nano Flows Conference, West London, UK, 2009.

III. P. England, H.H. Liu, Y.H. Zhang, S. Mohr, N. Goddard, P. Fielden, C.H. Wang. Experimental study of droplet formation at microfluidic T-junctions. In: Proc. 2nd European conference on microfluidics (Microfluidics 2010), Toulouse, France, Paper No. 187, 2010.

IV. P.Ozdemir and Y.Zhang. DNA Analysis in Droplet‐Based Microfluidic Devices. In: Molecular Analysis and Genome Discovery, pp. 56-80, John Wiley & Sons, 2011. DOI: 10.1002/9781119977438.ch4

Abstract

This work is a study to understand the various aspects of a microfluidic device. In the first half we take the role of an end user, experimenting to learn how best to use the device efficiently. In the second half we are the manufacturer, trying to fabricate a user friendly, and fully functioning microfluidic device.

As the end user, we have three different T-junction droplet generator devices, with similar geometries. We start investigating by generating water droplets in an oil medium. They self-organise into various flow patterns: single-profile, double-helix profile and triple-helix profile. We document how, with increasing flow rate ratio and capillary number, we observe more densely packed droplet flow patterns. The device with the deeper expansion channel provides more space for the droplets and they self-organise the triple-helix pattern in 3-dimension.

We then use the same devices to generate droplets for which we can calculate the volume. The fluid flow in a microchannel happens in four different regimes: ballooning, squeezing, dripping and jetting regimes. In single-cell and single-molecule analysis devices, the ability to create droplets on demand and of a certain volume is a desired capability. This can be achieved by understanding and learning how to use the fluid flow characteristics accurately. We experiment with the three different sized microfluidic devices, to measure the droplet volume throughout the squeezing to dripping regimes. This is achieved by manipulating the capillary number and the flow rate ratio. We observe a similar result as with the flow patterns: that the capillary number has an impact on the

droplet volume. As the capillary number increases the droplet diameter decreases. Further, for a set capillary number we can fine tune the droplet diameter by changing the flow rate ratio. As the flow rate ratio increases the volume of water droplets increases, despite the fact the capillary number is set. These coincide with our flow pattern results. Our results fit to the scaling law to predict the droplet size introduced by Tan et al. in 2008 [51]. Unlike some other authors in the literature, we did not observe a critical capillary number where the droplet volume changes suddenly. However, we did observe a transition area where we cannot define the regime of the fluid flow.

As the manufacturer we designed and fabricated our own planar free standing microfluidic devices using a polymer called SU-8. After looking into the weaknesses and the strengths of using SU-8, we describe how we successfully fabricated working devices and developed a new procedure in adhesive low temperature bonding. We finish by considering the challenges of connecting micro sized structures to a macro sized syringe pump, and fabricated a chip-holder inspired by applications in industry.

Acknowledgements

This PhD has been a very long journey for me.

My home changed…

My name changed…

My family changed…

There have been several severe bumps on the way.

But I have been pulled back in,

By love,

By passion,

By the forces of nature.

So thank you all, named & unnamed heroes of mine from the bottom of my heart.

Meliha & Ferit Özdemir

Matthew England

Sue & Cliff England

Also I would like to thank my supervisor Professor Yonghao Zhang for his patience and Dr. Changhai Wang for our collaboration in microfluidic device fabrication.

Pınar (Özdemir) England

For *Adam Demir* (aka **Ironman**) *England*

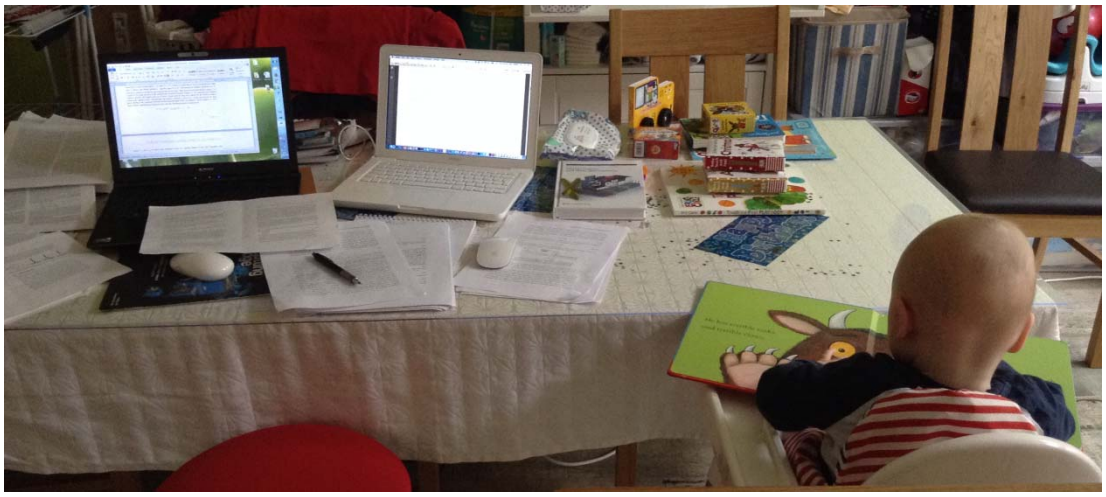

Table of Contents

List of Tables

List of Figures

Nomenclature

Greek symbols

α	Fitting constant
β	Fitting constant
σ	Interfacial surface tension
δ_Γ	Dirac delta
η	Dynamic viscosity
ρ	Density
κ	Local interface curvature
λ	Viscosity ratio
ν	Kinematic viscosity

Latin symbols

$\overline{b}$	Dimensionless length of droplet
Ca	Capillary number
Ca_{cr}	Critical Capillary number
d	Dimensionless droplet diameter
f_s	Surface tension force
g	Gravity
G	Shear stress rate
h	Channel depth in T-junction area
h^*	Height to width ratio
h_e	Channel depth in the expansion area
k	Fitting constant

l	Length of the immiscible slug
L	Characteristic length of a flow
n	Unit normal to the interface
p	Pressure in Navier-Stokes equation
p_{surf}	Surface pressure drop in Young-Laplace equation
Q	Volumetric flow rate ratio
Q_c	Continuous flow rate
Q_d	Dispersed (aqueous) flow rate
r	Final droplet radius
R	Radii of the curvature in Young-Laplace equation
Re	Reynolds number
t	Time
$t_{n,ref}$	Critical droplet formation time
u	Mean fluid velocity
u_c	Continuous flow velocity
V	Dimensionless droplet volume
$V_{c,ref}$	Critical volume at Ca=1
w_c	Continuous flow channel width
w_d	Aqueous (dispersed) flow channel width
w_e	Expansion channel width
∧	Intersection ratio

Acronyms

CSF	Continuum surface force

DEP	Electro-kinetic forces, Electrophoresis
EWOD	Electro-hydrodynamic forces, Dielectric
fps	Frames per second
LOC	Lab on a chip
μ-TAS	Micro total analysis system
MEMS	Micro Electro Mechanical Systems
PC	Polycarbonate
PDMS	Polydimethylsiloxane
PMMA	Polymethylmethacrylate
rpm	Rotation per minute
SEM	Scanning electron microscope
SU-8	A negative tone photoresist
UV	Ultraviolet

Chapter 1

1. Introduction

The history of science goes as far back as the history of humanity. Throughout there have always been gadgets and devices invented with the aim of making our lives better or easier. Not every invention was a success but all were a step towards eventual improvement. Within this timeline, the evolution of machines has not only been towards increased functionality, but also a shift towards ergonomics and compactness. The biggest challenge is not imagining the devices on a micro scale but to manufacture and make them function on this scale. We cannot be sure how the creators of Star Trek imagined their geological, meteorological and biological diagnostic device "The Tricorder" was engineered. While I accept we still have a long way to go in developing such a device (especially one with so many functions), I am sure that micro / nano fluidics and micro-electro-mechanical systems (MEMS) are the right pathway to it.

From the macro world to the micro world, manipulation of fluids has served humanity a great deal. Examples include generating electricity through a hydroelectric dam, managing the watering of crops in challenging environments, and placing a stent into a patient's artery to regulate their blood. We are all made of atoms which create molecules which come together to create the components of n-bodies with various boundary conditions. These n-bodies can be macro sized like celestial objects, the subject in astronomy; or micro sized like liquid molecules, the subject in fluid mechanics. The main aim when exploring the

behaviour of these subjects is to create solutions for both known and unknown problems; from alternative energy to personalized drugs for individuals.

Put simply, microfluidics is a multidisciplinary field which studies the behaviour and manipulation of liquid(s) or liquid-gas mixtures in a micro / nano scaled and constrained space. This makes microfluidic applications very appealing due to requiring only small amounts of sample fluid (e.g. a blood sample), and offering the parallel integration of functions with a quick reaction time. Microfluidics is still a discipline in its infancy. It branched out from the developing techniques of *Micro Electro Mechanical Systems*, or MEMS for short, which originated in the 1960s (see for example the lecture by Feynman in 1959 which identified the possibilities of this technology [1]). We also refer readers to the early review article by Fujiita [2] which foresaw the coming miniaturisation applications. The first and most commercially consumed microfluidic device is the inkjet printer head [5].

Microfluidic technology has many advantages including faster diagnosis time, less energy consumption, less volume consumption and therefore lower costs of agent-reagents. However, scaling the fabrication processes to micro sizes has proved challenging and much improvement is required. Microfluidics offers a variety of applications in various disciplines: chemistry, biology, medicine and engineering. As well as inkjet printer-heads by Hewlett-Packard, microfluidic devices are used in micro-turbomachinery. Liquid based applications are an active research topic due to the potential applications in the life sciences [10, 72]. As the need for more complex electrical and electronic devices increases, the manufacturing technologies are improving. The technology of small

devices, in our case MEMS allows us to fabricate components like pumps [3, 7, 8, 12], sensors and valves [9, 17] on simple, integrated structures [31, 32, 33]. These systems are commonly known as *Lab-on-a-Chip* (LOC) or *Micro-total-analysis-system* (μ-TAS) [6]. Functions like specimen pre-treatment, separation, chemical reactions or detection have now become comparatively quicker and less costly.

There are a large variety of microfluidic devices demonstrated successfully in the literature [11-15, 18] for various applications. These devices are providing increased control and cost effective solutions compared to conventional devices, especially in medicine and biology [16, 47, 57].

1.1 Main research aims

- ***To generate a droplet of a desired volume***.

  Microfluidic devices are difficult to use due to the miniaturization. In microscale the dominant forces may be very different from the ones found in a conventional device. To generate a droplet of a desired volume needs an accurate understanding of underlying mechanisms. First we learn the abilities of our three microfluidic devices by documenting the self-organizing droplet flow patterns observed in our experiments: single-profile, double-helix profile and triple-helix profile. We follow this by learning how these flow patterns are affected by the capillary number, the flow rate ratio and the device geometry. In the later stage, we observed that single-profile is an area between the two important flow regimes: the squeezing and the dripping regimes. Then we designed and conducted a numerical experiment to measure the droplet

diameters. The results of this experiment coincide with the power law proposed by Tan et al. [51]. This power law is a function of the capillary number and the flow rate ratios, as given in Equation (4.18).

- **To fabricate a free standing, fully working polymeric microfluidic device in less than two hours.**
  We designed and fabricated a planar polymeric microfluidic chip. The chip is fabricated in two separate structures. In the top layer the interconnections and the device geometry are fabricated, while on the bottom layer a thick structure. A low temperature, leak free adhesive bonding procedure is developed, and we demonstrate that all this can be done less than two hours, significantly faster than any previous demonstrations.

1.2 Thesis outline

We setup a new laboratory to conduct the microfluidic device based experiments. In Chapter 2, we describe this process, and the decisions that were taken in regard to managing the budget efficiently. We utilized some equipment that we inherited (a high speed camera) and designed our own spatial filter, to delay a costly microscope investment.

In Chapter 3, we focus on the chip fabrication, dimensions and the measurements of the fluids used in conducting the experiments.

Chapter 4 summarises the physics behind the fluid flow, and then present a literature review about generating microdroplets and the scaling law. We outline how the key constant numbers are derived.

Chapter 5 documents and discusses the data we collected using our three chips (labelled Chips 1, 2 and 3). In the first part, we focus on the self-organising droplet patterns: identifying them and explaining the reasons for their behaviour. Later on in the chapter, we look at how the droplet size is affected by the capillary number, flow rate ratio and the device geometry. Also we introduce a scaling law which predicts the size of the droplets generated.

In Chapter 6 we describe how we designed and fabricated a polymeric based microfluidic device and then Chapter 7 introduces a new procedure for a low temperature adhesive bonding, demonstrating working samples. We conclude in Chapter 8 by discussing possibilities for future work.

1.3 Thesis contributions

The major contributions of this thesis are as follows:

1. ***Observed and documented the flow patterns of self-organising droplets (see Chapter 5.1).***

   Thorsen et al. [24] demonstrated the patterns generated by a microfluidic device. We generated droplets in the squeezing to dripping regimes and observed how their patterns are affected by the capillary number, flow rate ratio and the device geometry. We used Chip 1 and 3 to conduct the experiments. Increasing the capillary number reduces the size of the droplets and increasing flow rate ratio increases the size of the droplets. We document how deeper devices create a larger degree of movement for the droplets, and how the triple-helix profile is observed in 3-dimensions.

2. ***Produced droplets of desired volumes in a controlled and consistent manner. Observed and documented this, suggesting an appropriate scaling law (see Chapter 5.2).***

   Using the three microfluidic chips we measured the droplet size in the expansion channel. The measurements are conducted between the squeezing and dripping regimes. We observed that when the capillary number increases the droplet diameter decreases; while for a fixed value of the capillary number, when the flow rate ratio increases the size of the droplet increases. Equation (4.18) suggests that a droplet's dimensionless diameter shows a dependency on the capillary number and the flow rate ratios.

3. ***Designed and fabricated planar polymeric free standing microfluidic devices (see Chapter 7).***

   We demonstrated that the fabrication of a fully functioning planar polymeric free standing microfluidic device can be completed in less than two hours. The SU-8 chips were fabricated in two parts, top and bottom, where the top part has the interconnections and the chip design, and the bottom part has the thick plane surface. These two parts were bonded by a new technique we developed. This technique is quick, efficient and may be performed at low temperatures. We achieved a fully functioning free standing SU-8 microfluidic chip with a channel depth in a range from 12μm to 375μm in between 153 to 173 minutes.

Chapter 2

2. Microfluidics Laboratory Setup

The budget is a key factor for every experimental study. This research included setting up a new microfluidics laboratory to conduct the experiments. Spending an institution's money was a great responsibility and thus required careful thought and planning.

2.1 Experimental setup

The diagram of the experimental setup is presented in Figure 1. To record the droplet behaviour we needed a system for visualization. After getting quotations for inverted microscopes we decide to utilize the equipment left over from a previous research project. The laboratory has the Photron Fastcam Ultima 1024 model high speed camera with a CMOS sensor. This camera can utilize an image of 500 fps (frames per second) at 1024x1024 full resolution and at lower resolutions frame rate can go up to 16000 fps. The manufacturers' custom software program was used to capture and record the videos and the images. Droplet generation is a very speedy process and because we aimed to do our analysis based on the image quality, we had some specific needs for the setup.

The widest area we needed to record was the expansion channels of the microchips which were around 500μm each. We used the high speed camera at 1024x512 resolutions at 1000 frames per second. The manufacturers of the camera developed software to control all elements

of the camera through the computer which enables us to trigger the recording.

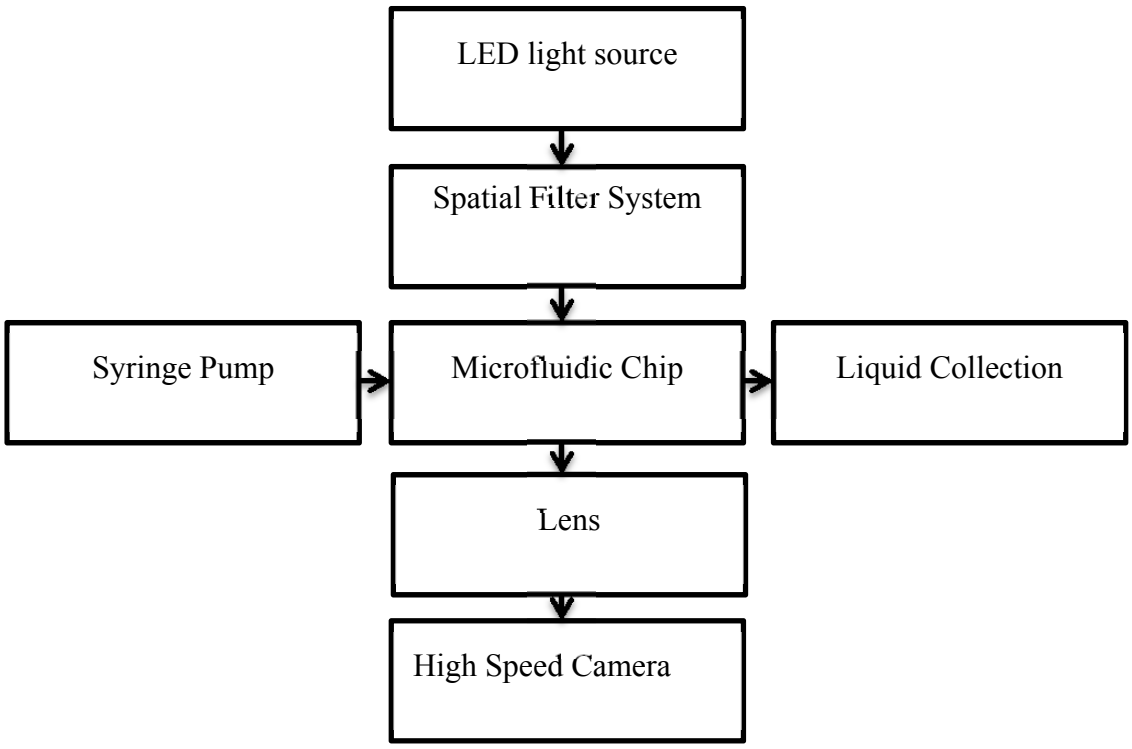

Figure 1: Schematic diagram of the experiment

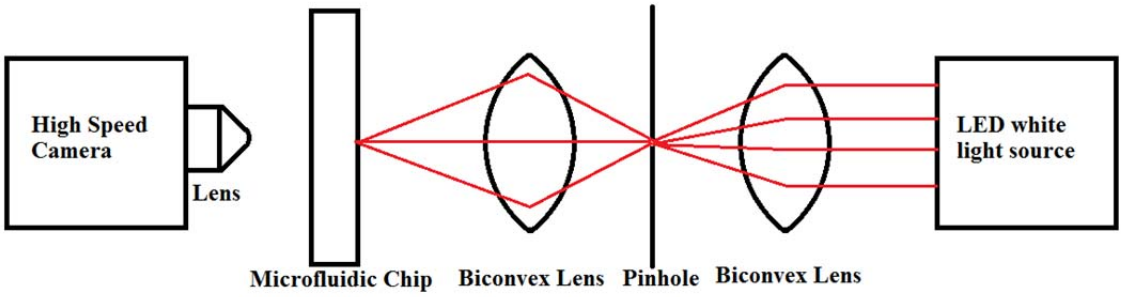

Figure 2: Spatial filter schematic

To get a clear image we needed to eliminate the diverging light beam. We decided to set a spatial filter (Figure 2) using two Ealing equi-convex glass lenses (catalogue number 43-1239) and a pin hole to set it

up. To illuminate the system at first a mercury lamp based system was used, because the camera is high speed, it picked up the frequency of the light. To improve the image we decided to use CoolLED pE-100 white light.

The objective lenses used during the experiments were Carl Zeiss LD Plan Neofluar 20x Corr and 40x Ph2 Corr. To minimize the impact of environment during the experiments we invested in an optical table from Thorlabs. See Figure 3 for a photograph of our optical table setup.

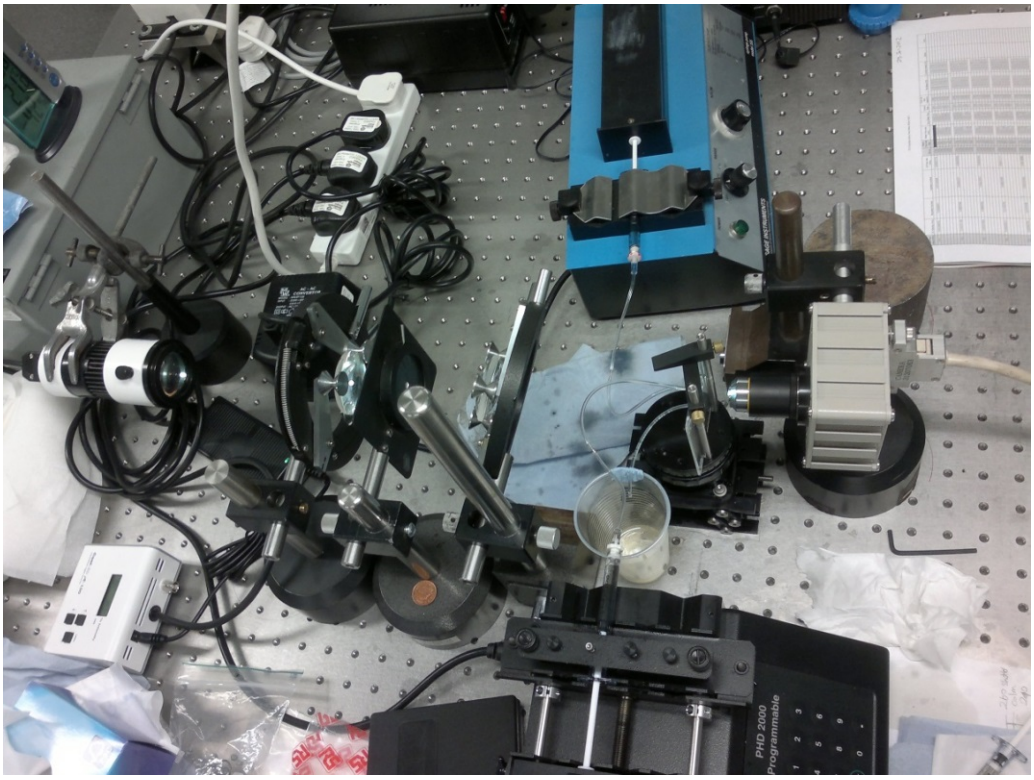

Figure 3: Optical table setup

The microfluidic chips were mounted on Thorlabs MicroBlock 3-Axis positioner with differential micro stage.

We used syringe pumps to pump the fluids. The oil of continuous phase was pumped with the Harvard Apparatus PHD 2000 model syringe pump. This series of pumps have the accuracy of ±1% and

reproducibility ±0.1%. We used 1mL BD Luer-Lok syringes and pumped flow rates from 0.1ml/hr to 1.2ml/hr.

The water of the aqueous phase was pumped using a Sage Instruments 355 model which is an easy tuneable syringe pump. This was a second hand pump without a manual. We needed to know the flow rates and so decided to measure the time it takes to empty a 1mL syringe in X1 at 99.9% flow rate ratio setting. At 20°C room temperature we took 10 readings of time and discarded the highest and smallest readings, then averaged the 8 readings. The result was 23.18 seconds. From there we worked the chart of the flow rates for this syringe pump.

As a procedure, before starting the experiments, oil was pumped through the chip for around 30 minutes minimum to reach the steady state and to prime the chips. Also this routine was carried out every time the syringe needed refilling. We adopted some ground rules to carry out uniform conditions in every set of experiments. The measurements were taken a minimum of 2 minutes apart when the water flow rate changed, and 4 minutes apart if the oil flow rate changed. This created enough time for steady fluid flow.

The maintenance of the microfluidic chips is explained later in Chapter 3.

Chapter 3

3. Experimental Design

In this study we aimed for an alternative way of measuring the size of the droplets. Traditionally researchers presented ways to measure the droplet size visually and modelled it to a scaling law at the T-junction itself (Garstecki et al. [37]; Christopher and Anna [46]; Xu et al. [50]; Glawdel et al. [68, 69, 70]; and Wehking et al. [74]). The problem with this method is the droplet generated in the continuous flow channel is not symmetrical, rather it is approximately bullet shaped in both squeezing and dripping regimes. This causes the volume calculating formulas to not be as effective as is proposed. We looked for an alternative way of measuring the droplets, mainly by having an expansion channel for droplets to relax and be spherical in shape.

3.1 Design and fabrication

The microfluidic devices used in this project were fabricated by machine milling which allowed us to create different depths with each device. The devices were machine milled on Polymethyl Methacrylate (PMMA) sheets at The University of Manchester's laboratories. Interconnections of the devices were drilled on PMMA. The channels end with a reservoir which has an opening towards the back of the PMMA sheet. A suitable sized bootlace ferrule fits in to this opening firmly. The Masterflex Tygon Tubing (1/32´´ inside diameter) attached perfectly to the open side of the bootlace ferrule. For each set of experiment these tubes which have the chip in one end and the syringe pump on the other, were cut 10 cm in length.

Following the milling, the devices were washed and prepared for sealing. For this purpose 100μm thick, self-adhesive acetate Corning Sealing Tape was used. This clear tape is good for optical detection and is compatible with the fluids used during this research. To achieve a good quality sealing the tape is carefully placed and pressed on the device. At this stage it is crucial to eliminate air pockets since they cause a failure in the sealing process. Following this, the devices were left for a few days for a stronger sealing. After each set of experiments were conducted and/or the seal started to lift off, the tape was removed. Then the chips were cleaned and resealed.

The general layout of one of the devices is given in Figure 4, followed by the dimensions of the devices used in this research in Table 1 (see also Figure 5 which shows these dimensions on a diagram).

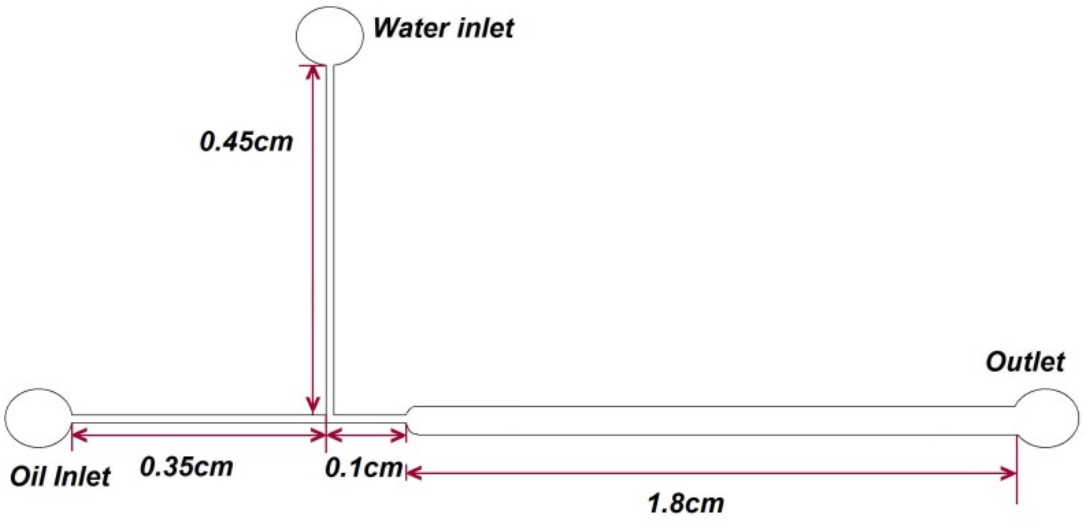

Figure 4: Layout of the microfluidic chip viewed from the top

A degree of randomness in the chip dimensions were caused by the milling machine. For that reason we accurately measured the dimensions

of the devices with an interferometer microscope Zygo , New View 5000 at Heriot-Watt University.

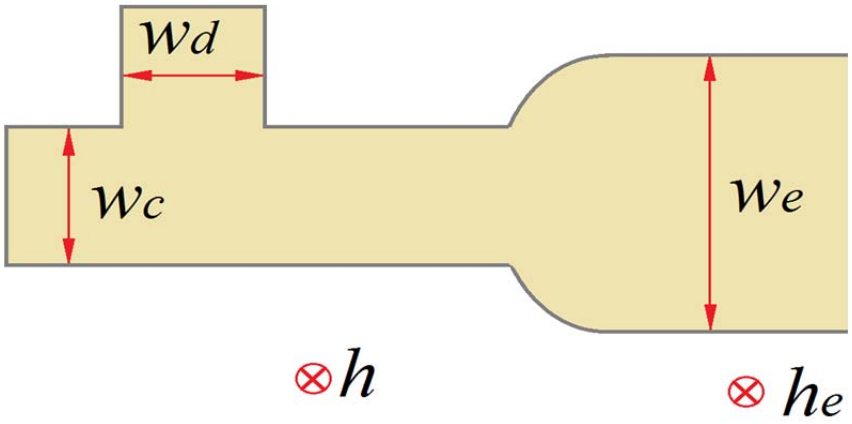

Figure 5: Schematic of the T-junction and the expansion channel where w_c, w_d and w_e are the widths of continuous, aqueous and expansion channels and h and he are the depths.

	Chip 1	Chip 2	Chip 3
Continuous flow channel width (μm) w_c	129	130	129
Aqueous flow channel width (μm) w_d	128	128	124
Channel depth at the T-junction area (μm) h	164	137	140
Expansion channel width (μm) w_e	516	500	511
Channel depth at the expansion area (μm) h_e	330	145	220

Table 1: Dimensions of the microfluidic chips

3.2 Important physical properties of fluids

The first fluid property we will consider is the density, ρ, which is defined as mass divided by unit volume. In our experiments, the flows are incompressible. Throughout the experiments we used water and rapeseed oil as the immiscible fluids. As density of a fluid depends on the pressure and temperature of the system, it is important to run experiments in a controlled environment. The temperature of our experiments was controlled at 20 ±1°C. The properties of the rapeseed oil and distilled water (DI water) used are listed in Table 2 in the following subsection.

Next, the surface tension, σ, as implied by the name, describes work or energy utilized to increase the interfacial area. To understand this property we need to look at it at the molecular level. The liquids tend to take the shape of a sphere to minimize its surface to volume ratio (see for example, de Gennes, Brochard-Wyart et al. [20]). The molecules at the interface are exposed to an unequal field of force, energy input is required to move the molecules in the bulk to the interface.

Generally the surface tension of a certain liquid is measured at the solid-liquid-gas (air) contact line. To observe these behaviors in 1891, Agnes Pockels designed an experiment to measure the tension on the surface of the water [21]. She observed that up to certain strength, water tries to keep the specimen. Her sample was a shirt button, in touch with the surface of the water. As the temperature of the liquid increases the surface tension tends to decrease. This is where the "*magic*" comes into our experiments, droplets form because of this behaviour.

The resistance, a physical property, when a fluid is in motion against the applied shear stress is called viscosity, η. Like density it has a dependency on temperature. Newtonian fluids have a viscosity independent of flowfield, showing a linear correlation between shear stress and shear rate

Both of the fluids we are using in the experiments are Newtonian fluids. Most of the materials used in microfluidic systems (including water, oil and air) are Newtonian fluids. When we first look into a microfluidic device the analysis starts by defining the boundaries and continues by identifying the interactions with the system's surroundings.

3.2.1 Density, viscosity and surface tension measurements

To design an experiment it is important to measure the physical properties of the fluids (Table 2). The fluids used during the experiments are de-ionized water for the dispersed phase and rapeseed oil for the continuous phase. The physical properties of these liquids were measured at conditions the same as the experiments conducted; the set room temperature was 20°C. The densities were measured with a density bottle. The dynamic viscosities were measured using a Thermo Scientific Gilmont Falling Ball Type viscometer. Finally the surface tensions of both liquids, which are free of surface-active contaminants and surfactants, are measured using ColePalmer Surface Tension Apparatus.

			Rapeseed Oil	DI Water
Density	ρ	(kg/m^3)	913.4	998.3
Dynamic viscosity	η	(kg/m s)	0.05196	0.0010
Kinematic viscosity	ν	(m^2/ s)	5.689×10^{-5}	1.0017×10^{-6}
Surface tension	σ	(mN/m)	33.0	73.0

Table 2: Density, Viscosity and Interfacial surface tension measurements of rapeseed oil and distilled water at 20^{O}C.

3.3 Fluid handling

Multiphase flows are challenging as they have two or more fluids pumped in a confined system simultaneously. This presents the problem of choosing the right type of pumping method. The failure possibility of the chip increases depending on: the flexibility of the chip itself; bubbles generated by various reasons and finally the fluids itself clogging. For this purpose we decided to use syringe pumps. The syringe pump offers an easy and quick set up with stable fluid flow.

A stable fluid flow depends on a few factors like the right type of tubing and the right size non-bending syringe. As mentioned in the beginning of the chapter we used Tygon Tubing. The syringe we used was a BD 1ml Luer-Lok Tip Syringe. We could have used a smaller volume syringe but that would have reduced the data collecting time. As a part of the experimental procedure whenever the syringe is refilled, either at the start or during the experiments, before recollecting any data the changed fluid was pumped for at least 18 minutes at the flow rate of 0.6 ml/hr. This reduced instability of the fluid flow. As mentioned in Chapter 2, we used two different syringe pumps. The first one is the Harvard Apparatus PHD 2000 model. This device pumped the continuous phase which is oil. The second one is the Sage Instruments 355 model which was used to pump the aqueous phase. The day before starting the experiments rapeseed oil pumped into the fully sealed chips to prime the chips.

The videos and photo sequences were recorded by the high speed camera and initially analysed using the Image J software package. The calibration of each set of data was important for us: because we have not used a microscope, we needed to know the exact dimensions to calibrate

the Image J program for each microfluidic device. We collected data on 14 consecutive different oil flow rates. In each oil flow rate there were 6 different water flow rates set up, and for each of them the camera took 512 photos. We decided to sample six photos from 512 to carry out the measurements. This was carried out for each three of the devices.

Images were analysed in Image J using a Matlab script. In each image the area of the target droplet, which is the one in the focus of the image chosen, and its area were measured. This was done for each of the three pictures and the average areas of the pixels were calculated. We know the exact width of each expansion channel and the number of pixels there are in each image, so this ratio becomes the scale when we are calculating the diameter of the droplet in each photo. That is the important difference in our measurements compared to [37, 40, 49, 54, 68, 74, 75, 77] and many other studies.

Chapter 4

4. Droplet Generation with T-junction Microfluidic Chips:

Droplet Size and the Flow Regimes

In this chapter the focus will be the scaling of the droplet sizes between the dripping and squeezing regimes. We will address how the geometry, the capillary number and the flow rate ratio affects the droplet size in the T-junction microfluidic device.

First we will look into the concepts of fluid flow and transport within the microchannel. In the early microfluidic devices we see that the devices run in a single phase of fluid (as demonstrated by the ubiquity of single phase devices in the review article [10]). These can be costly if the fluid is an expensive reagent, and also carries the risk of cross contamination of the fluid with the device walls.

4.1 Flow of Fluids

What is fluid? Fluid is any substance which has the capability to flow. It can be in liquid or gas form. The interactions of fluids that flow simultaneously, but where each has a separate volume and velocity field, are known as Multiphase Flows. It is important to study Multiphase Flows because we are surrounded by fluid flows in various forms: water, gases, blood, air, steam, oils, ferrofluids etc. Understanding this motion has been the key for creating many useful applications including steam engines, turbines, dams or plasma propulsion engines, and will be the key for many more.

4.1.1 Newtonian fluids

Newtonian fluids deform continuously under tangential force. This tangential force is commonly known as shear force. The magnitude of deformation is defined by the force applied on the fluid and a physical property of the fluid, the viscosity.

What is Flow? Flow is the action of movement and it is continuous in nature, but not always uniform. There are many types of fluid flows depending on the physical properties of the fluids, such as temperature, viscosity, electromagnetic charge and density, and the boundary interactions like pressure, surface tension and velocity profile. In this work, we are interested in a flow confined in a micro sized volume. In micro scaled devices, fluid flows in parallel layers usually do not mix due to the slow speed.

4.2 The Navier-Stokes equation

The Navier-Stokes equation is the application of Newton's second law to a viscous fluid. Although we have a minimum interaction with this form of it because all the flow equations are already derived and published in a variety of literature, when the right boundary conditions applied it guides us about the interactions between the forces within the system.
In the following u = mean fluid velocity, p = fluid pressure, ρ = density, η = dynamic viscosity, g = gravity and t = time. The Navier-Stokes equation is written as follows:

$$\rho\left(\frac{\partial \vec{u}}{\partial t} + \vec{u}.\nabla\vec{u}\right) = -\nabla p + \eta\nabla^2\vec{u} + \rho g\,. \qquad (4.1)$$

Acceleration (Inertia) = Surface Forces + Body Forces

The forces acting on a fluid split into two groups: short-range forces and long-range forces.

Short-range forces, also known as the Surface Forces originate from the molecule itself when the fluid interacts with other fluids. They are called surface forces because they exist on the surface area. Surface tension and viscosity are the parameters related to forces (4.2) and (4.3).

Long-range forces are also known as the Volume Forces or the Body Forces. These forces are in scale to the volume of the fluid. Gravity and inertia are a typical volume force parameters as in (4.4).

The order of the important forces from micro to nano scale is as follows:

Buoyancy < Inertia ≈ Gravity < Viscous force << Interfacial force

As seen in the order of forces above, in shorter distances the body force becomes very small compared to pressure and viscous forces and it is neglected.

Inertial force = mass × acceleration = $(\rho L^3) \times (u^2/L)$ (4.2)

Viscous force = viscosity × (velocity/distance) × area

$= \eta \times (u/L) \times L^2$ (4.3)

Body force = $\rho g \approx 0$ (4.4)

The concept of continuum is a gradual progression without sudden changes or discontinuities caused by its own continuous mass. Any system which has any energy and mass transfer with the outside is considered as closed, and over time its mass will remain the same. This is known as the principle of mass conservation. This conserved mass

with constant density (incompressible flow) has a unidirectional flow: the velocity vector and the velocity gradient tensor disappear. Hence

$$\vec{u}.\nabla\vec{u} = 0. \tag{4.5}$$

The other simplification to the Navier-Stokes equation comes from the flow being laminar:

$$\frac{\partial\vec{u}}{\partial t} = 0 \tag{4.6}$$

$$0 = -\nabla p + \eta\nabla^2\vec{u} \tag{4.7}$$

Equation (4.7) is known as the linear Stokes equation.

4.2.1 Surface tension and the Navier-Stokes equation

Because of surface tension, there is a pressure jump across the droplet interface which can be described by the Young-Laplace equation, i.e. Equation (4.8), where Δp_{surf} is the pressure difference, and R_1 and R_2 are the radii of the curvature of the two fluids surfaces.

$$\Delta p_{surf} = \sigma(\frac{1}{R_1} + \frac{1}{R_2}) \tag{4.8}$$

To describe droplet dynamical behaviour, the Navier-Stokes equation, Equation (4.1) needs to consider the surface tension force acting on the droplet surface. If a continuum surface force (CSF) model is adopted, which converts the surface tension force into a body force, the above Navier-Stokes equation can be modified to have an additional body force term f_s, at the right side of Equation (4.1). The surface tension force acting on the droplet surface can be modelled as [107]:

$$f_s = \sigma\ \kappa\ n\ \delta_\Gamma \tag{4.9}$$

where σ is the interfacial tension, κ is the local interface curvature, n is the unit normal to the interface, and δ_Γ is the Dirac delta function used to localize the force explicitly at the interface.

4.3 Derivation of constant numbers and their meanings

The Navier-Stokes equation is the motherboard for the continuum fluid mechanics: nearly every formulation is derived through it. When we are fabricating microfluidic devices, we can decide how the following related dimensionless parameters (see Table 3) will have an impact.

Dimensionless numbers	Definition	Formula	Scaling
Reynolds Number (Re)	Inertia/Viscous	$\frac{\rho L u}{\eta}$	1
Capillary Number (Ca)	Viscous / Interfacial	$\frac{\eta u}{\sigma}$	0

Table 3: Scaling Chart of Dimensionless Numbers

4.3.1 Reynolds number

In 1883 Osborne Reynolds published an experimental paper about the fluid motion in a tube [17].

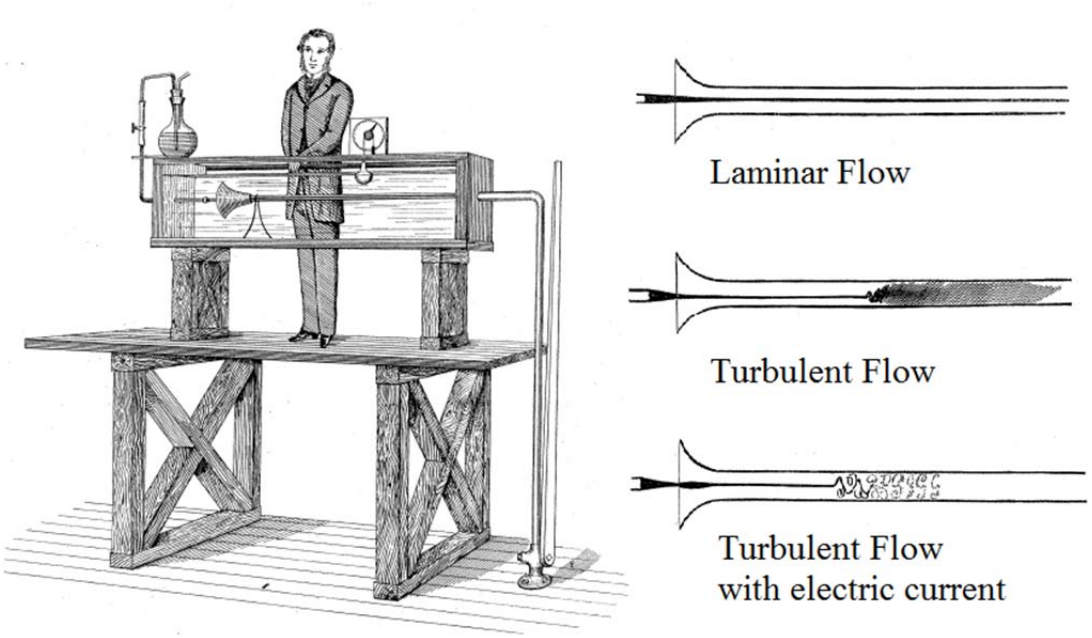

Figure 6: Experimental set up and the recorded observations by Osborne Reynolds.

Reynolds observed the transition from turbulent "sinuous" (as he named it) to laminar flow can be determined by a dimensionless constant which is calculated by viscosity, density, characteristic length and the velocity of the fluid (Figure 6).

Although Reynolds experimentally calculated it, the Reynolds Number is derived through non-dimensionalisation. If we non-dimensionalise the Navier-Stokes equation: coordinates with a characteristic length L, time with a reference time, the velocity with a characteristic mean velocity, and finally the pressure with a characteristic viscous shear stress; then in front of the acceleration forces we find the Reynolds number (4.10).

$$Re = \frac{\rho L u}{\eta}. \qquad (4.10)$$

The Reynolds number represents the ratio of the energy spent on acceleration (kinetic energy) of the fluid to the energy dissipated due to friction. The Reynolds number provides the information for the type of

the fluid flow. As Squires and Quake [22] explain in their review article, most of the microfluidic set ups have a very small Reynolds number. This is because the value viscous forces are far bigger than the inertial forces and the flow is laminar and that makes the Reynolds number the most irrelevant parameter.

4.3.2 Capillary number

The *Capillary Number* is the correlation between viscous and capillary forces, defined as

$$Ca = \frac{\eta u}{\sigma}. \qquad (4.11)$$

In microfluidics, because the fluid flow is slow, it is expected to be in a range from 10^{-3} to 1.

4.3.3 Volumetric flow rate ratio

The *Volumetric flow rate ratio,* Q_n, is the ratio of the dispersed fluid flow rate, Q_d, against the continuous fluid flow rate, Q_c:

$$Q_n = Q_d / Q_c. \qquad (4.12)$$

The volume of droplets generated at a fixed capillary number can be increased or decreased by changing the dispersed fluid flow rate and the flow rate ratio provides the information between these parameters.

4.4 Generating droplets in a microchannel

It is important to know the volume and frequency of the droplets; mainly to be able to plan the functionality (biological, chemical or mechanical) which they are designed to serve. See for example [35, 38, 41, 48, 52, 53].

There are two ways to generate droplets in a microchannel: active and passive. The main differences between these methods are that the active method generates droplets on demand and in smaller volumes ranging from nano-litre to pico-litre. The passive method is chosen when the application requires higher volumes like micro-litre sized droplets and in high frequency [60, 80].

The active method manipulates the fluid by external non-mechanical originated force. Some examples are:

- Electro-kinetic forces, Electrophoresis (DEP),
- Electro-hydrodynamic forces, Dielectric (EWOD),
- Magnetic forces,
- Thermo-capillary forces,
- Surface acoustics forces, and
- Optical forces.

The passive method uses a mechanical pump to simultaneously drive the immiscible fluids inside the channels using the downstream flow against the interfacial surface tension and generate a stream of droplets. The types of device preferred for the passive method are planar in structure with no moving parts and functions in laminar flow. Many passive droplet generator devices have been designed and successfully demonstrated. They can be categorized into three main groups (Figure 7):

- T-junction and Y-junction (Thorsen et al. [24]; De Menech et al. [54]; Li et al. [71]; and Husny and Cooper-White [42]).
- Flow-focusing and Cross-junction (Anna et al. [29] and Ward et al. [34], Lu et al. [76]).

- Co-flowing (Hua et al. [45] and Umbanhowar et al. [25]).

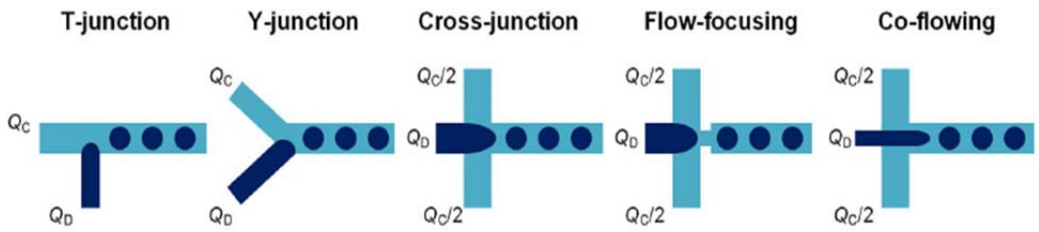

Figure 7: Schematic diagrams of microfluidic droplet generators: T-junction, Y-junction, Cross-junction, Flow-focusing and Co-flowing. Continuous and dispersed phase fluid flows are labelled. (Wang & Luo [23])

All these group of devices have the same characteristic, using immiscible fluids and promoting the droplet growth by patiently waiting for the surface tension to minimise the surface area in the downstream flow. For the experiments we used T-junction devices. The motivation was that although it is a known fact that the device geometry, flow rate ratio and capillary number impacts may be observed, the scaling law suggestions in the literature differ in every experimental study.

We summarise the T-junction microfluidic chip droplet generation stages:

i. The continuous flow fluid is mechanically pumped into the microchannel. This fluid is generally preferred to be a kind of oil due to oil's non-polarity property. The mechanical pump which drives the fluid controls either the pressure or volumetric flow rate. The pressure change in the downstream of this channel has an impact on the generation of the droplet. For that reason in the design of the T-

junction device, the width of the channel does not change for a fixed distance. That certain distance depends on the size of the droplets and the function of the microfluidic chip.

ii. As with the continuous flow, the immiscible aqueous flow fluid is mechanically pumped into the system. This channel is located perpendicular to the carrier phase channel, the contact angle of the two channels are generally at right angles but could be increased or decreased depending on the design. For medical and biological applications, this phase is preferred to be water.

iii. The breakoff of the droplet happens either in the vicinity of the intersection area or within the main channel depending on the flow regime. In the squeezing regime, the droplet fully fills in the main channel. During the break off the pressure profile of the continuous flow fluctuates [67] meaning following a break up in the continuous flow channel the new droplet faces a bigger pressure profile.

In 2014 Bashir et al. [75] reported that droplet break up position does change according to the wetting properties of the walls of the chip. As the hydrophobicity of the walls decrease, the amount of time to fully block the main channel increases.

The impact of the larger channels was discussed in 2015 by Korczyk et al. [77]. The larger channels create larger volume droplets which are more beneficial for certain chemical applications like crystallization of proteins.

4.5 The flow regimes

In this research we mainly focused on T-junction devices. When two or more immiscible fluids driven through inlets towards an intersection, depending on the flow rates, a variety of flow patterns are generated.

As observed by many researchers, a droplet forms by the filling of the fluid to the carrier channel followed by necking and pinching off.

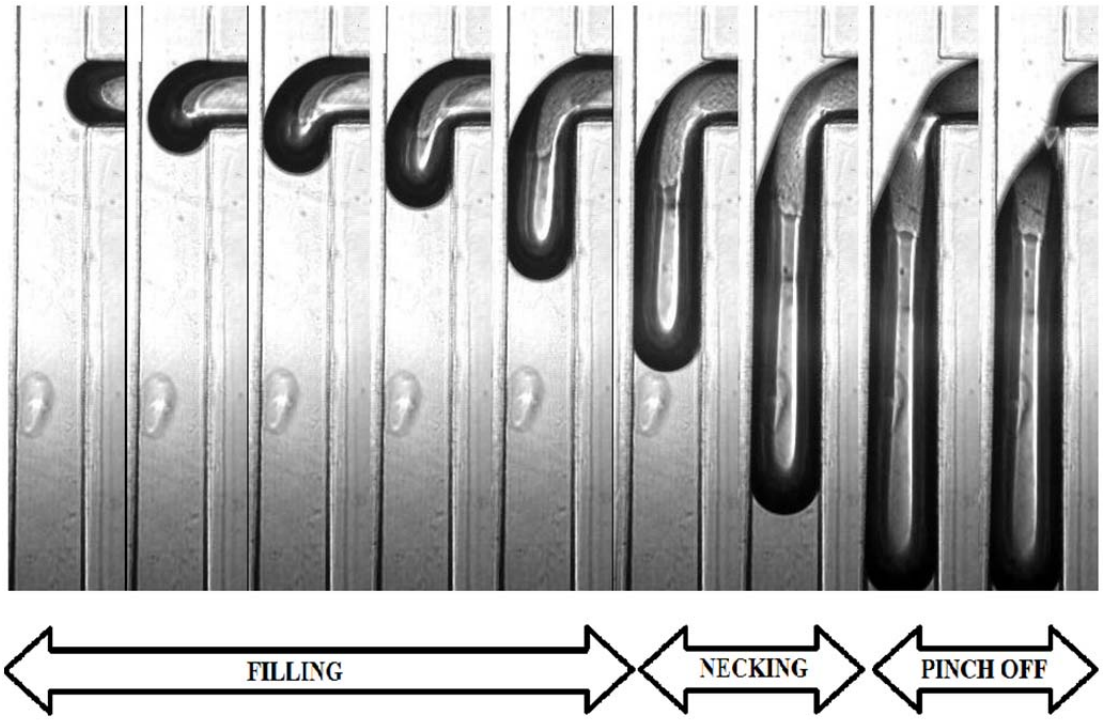

Figure 8: The droplet generation in Chip1 in the squeezing regime with Ca= 0.0036 and Q=1.2. The frame rate is 4000fps, and the magnification rate is 40.

A microfluidic application can be designed to generate a high number of droplets (>1 kHz). For a system working at such high speed, it is important to know the volume of the droplets for different operation parameters of the device. In the next section, first we will look into the change in flow patterns, and then how the droplet size changes in different flow regimes.

A T-junction device consists of two channels; the perpendicular channels naturally intersect in a junction. Simply by changing the flow rate of any fluid flowing in these channels the breakup behaviour in the intersection can be manipulated.

There are four different flow regimes experimentally observed: jetting, dripping, squeezing, and ballooning.

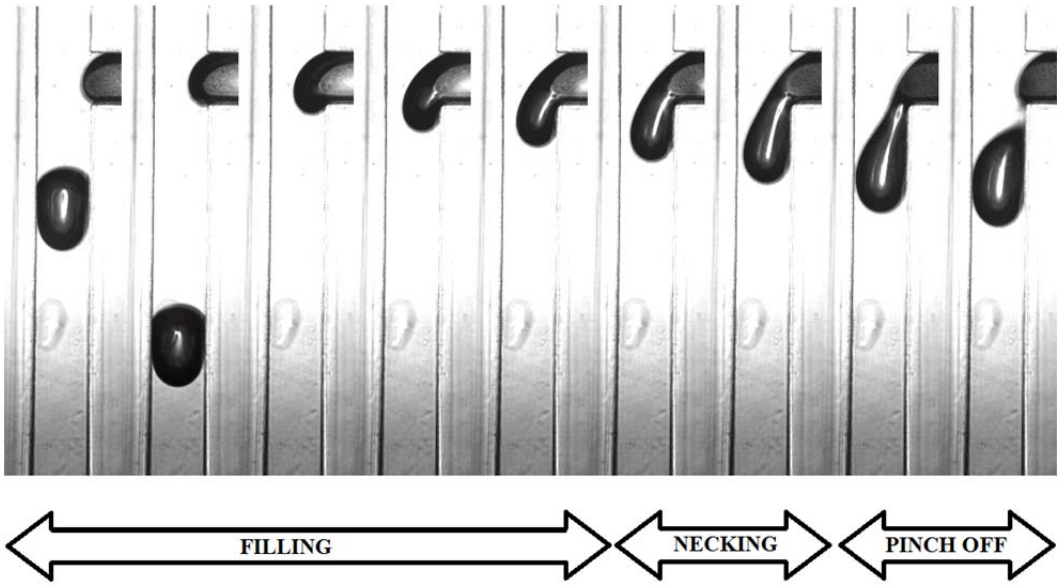

Figure 9: The droplet generation in Chip 1, the dripping regime with Ca=0.019 and Q=1. The frame rate is 4000fps, and the magnification rate is 40.

The fine boundaries of the flow regimes, especially from dripping to squeezing regime are not very clear but the descriptions are definitive.

The squeezing regime, as demonstrated in Figure 8, happens when the emerging fluid flow manages to fully block the junction region of the fluidic device. The force caused by the interfacial surface tension becomes dominant over the viscous drag and extends the flow into the main channel. In 2006 Garstecki et al. [37] demonstrates the droplet

generation describing the droplet break-up mechanisms and the differences between the regimes. The squeezing regime is observed with (around a 10^{-2} value of) the capillary number $Ca < 0.01$.

The dripping regime, as demonstrated in Figure 9, is more dynamic to describe. The interfacial surface tension works on to keep its boundary still but the emerging interface and the viscous drag at the intersection acts against it. While the dispersed phase is trying to fully fill in the downstream channel, the shear force from the continuous phase forces the break up. The value of the capillary number in the dripping regime is considered to be $Ca > 0.01$.

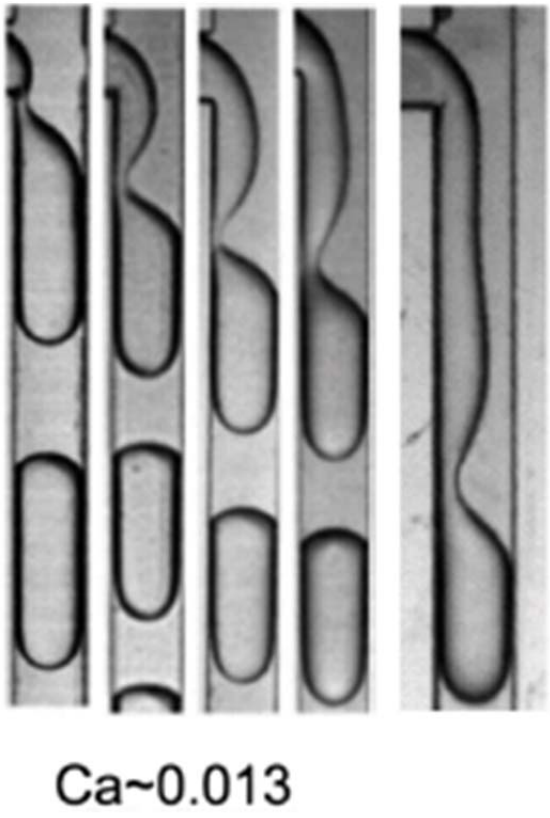

Figure 10: Examples of the jetting regime [77].

The jetting phase occurs when the fluid flow rates are high; it is not a preferred phase for micro droplet based applications (Figure 10).

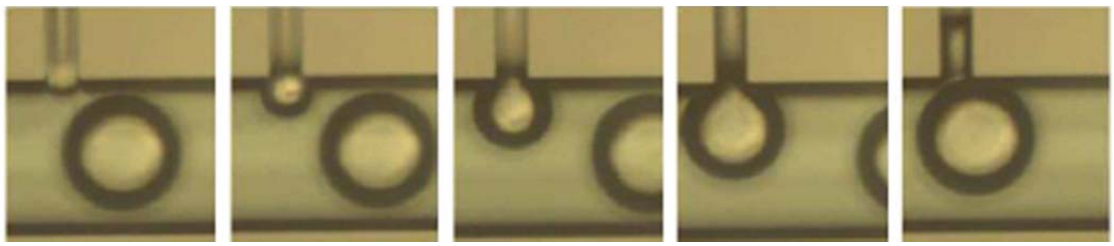

Figure 11: The ballooning regime, channel dimensions w_d=20µm, w_c=100µm and h=46µm. [65]

The ballooning regime recently presented by Tarchichi et al. in 2013 [65], is only observed at very low flow rates and in smaller geometries of microchannel (<50µm) as in Figure 11.

4.6 The scaling law

Droplet based microfluidic devices generally operate in a zone mainly dominated by the dripping and squeezing regimes. For the first time in 2001 Thorsen et al. [24] used a T-junction device to generate water-in-oil droplets. This study documents the flow patterns and suggests a droplet size calculating mechanism. They emphasised the impact of the shear forces which is gained by the design, which is bringing the immiscible fluids in contact at a perpendicular angle. They predicted the droplet radius by balancing the Laplace pressure (interfacial tension) against viscosity of the continuous phase multiplied by the shear stress. The change in the viscosity and the continuous flow rate is the dominant impact on the droplet size: as these parameters increases the droplet size decreases. They calculated the droplet diameter as below, where the break up happens when G, the shear stress rate, dominates against the capillary force at around Ca ≈ 1 in the jetting regime.

$$r \cong \frac{2\sigma}{G\eta} \qquad (4.13)$$

Although their droplet volume calculations are not accurate this study emphasises the developing silicon based microfabrication technology and thus creates a great opportunity for microfluidics to develop.

The problem with this model is that it is not predicting the droplet size when the capillary number is very small. That is because of the regime change: in 2002 Nisisako et al. [26] documented this behaviour in their experiments. They observed the linear decrease of the droplet size as they increase the continuous phase flow rate at a constant aqueous (dispersed) flow rate till a critical point where the behaviour changes, also see Cristini and Tan [30].

The droplet based microfluidic device reported by Tice et al. in 2003 [27], demonstrated how to generate droplets for high-throughput devices whilst controlling the reaction time in droplets that are made of three different coloured fluids at low value of the capillary number ($Ca < 0.1$). In this case the mixing fluids were all water, and the carrier fluid was oil. As they stated in their work, the device is running in low Reynolds number, and has a laminar flow. But this study suggested the flow velocity has a weak impact on the length of the plugs and the flow patterns.

The impact of the confined geometry of the T-junction on droplet generation is recorded by Garstecki et al. in 2005 [36] and 2006 [37]. They also documented that when the capillary number becomes smaller than a critical point ($Ca_{CR}<10^{-2}$) the droplet break up is stimulated by the filling of the aqueous fluid in the main channel, named as the squeezing regime.

The squeezing regime (Ca<0.01) is observed by Garstecki et al. [36]. In this regime the emerging droplet from the aqueous flow creates a big pressure against the continuous flow. The size of the plug depends on the flow rate ratio, Q. Garstecki et al. formulated the droplet length against the flow rate ratio [36]. In here α is a fitting constant of order unity and calculated as 1 by Garstecki et al. [36, 37] and 1.1 by Fu et al. [64].

$$\frac{l}{w_c} = 1 + \propto \left(\frac{Q_d}{Q_c}\right) \tag{4.14}$$

In 2008 De Menech et al. [54] published a numerical and experimental study of a T-junction microfluidic channel acting at low capillary number. They did observe the impact of the capillary number throughout the squeezing regime to the jetting regime. As the capillary number starts to get smaller the size of the droplet increases which is also observed by the transition of the flow regime. Their study looks behind the dynamics of droplet size by examining the change in the capillary number, flow rate ratio and viscosity ratio. In the square profiled channels they observed a critical capillary number $Ca_{cr} \approx 0.015$ where the droplet volume changes significantly. In the dripping regime smaller droplets were generated when the viscosity ratio was big. The shear stress is dominant in this regime. Their work (and those of others) deepened and supported the findings by Garstecki et al. [37, 56, 66].

A 2008 study by Christopher et al. [49] focused their results in the transition region, highlighting that the viscous forces are important. The droplet size always depended on the capillary number and the flow rate ratio. The significant change in the volume of the droplet happens around the critical value of the capillary number which was around

$Ca_{cr} \approx 0.009$. They formulated the dimensionless length of the droplet ($\bar{b}$) in Equation (4.15), where $\Lambda = \frac{w_d}{w_c}$.

$$\frac{l}{w_c} = \bar{b} + \frac{\Lambda}{\bar{b}} Q \tag{4.15}$$

In their model droplet generation happens when the squeezing pressure and the viscous forces becomes bigger than the capillary force, which is working against the droplet break up.

$$(1 - \bar{b})^3 = \bar{b}\,\mathrm{Ca} \tag{4.16}$$

At low capillary number their results coincided with Garstecki et al. [36, 37] and Fu et al. [55, 79].

Guillot and Colin [39] observed in 2005 the change in behaviour of the droplet break up. For any given continuous phase fluid rate, when the dispersed phase fluid flow rate increases the break up location moves from T-junction to the channel.

In articles of 2005 and 2006 by van der Graaf et al. [40, 43], droplet generation is defined as a two-step mechanism. At first a droplet grows until the capillary force reaches a balance level against the drag force caused by the continuous phase. Then a droplet continues to grow in this stage because of the pumping mechanism. Finally it pinches off. They predict the volume of the droplet by Equation (4.17) below.

$$V = V_{c,ref} Ca^m + t_{n,ref} Q_d Ca^n \tag{4.17}$$

Their simulation for a square profiled T-junction chip (100µm X 100 µm) finds the critical volume at Ca=1 $V_{c,ref} = 2.5 \times 10^{-5}$ µL, and the critical droplet formation time $t_{n,ref} = 135$ µs when m=n = -0.75.

Tan et al. [51] proposed the power-law, Equation (4.18), initially for the cross-junction device. It is also suitable for T-junction devices where k, α and β are fitting parameters.

$$\frac{l}{w_c} = k\left(\frac{Qc}{Qd}\right)^{\alpha} Ca^{\beta} \tag{4.18}$$

In this work the fluid flow rate ratio defined as Q_n must be bigger than 1. Their model is valid when the capillary number is smaller than 0.1. In the case of k = 1.59, α = 1/5 and β = -1/5, when all the forces (interfacial tension and the shear force of the continuous flow) acting on the capillary number are in equilibrium, the capillary number is only influenced by the continuous flow channel.

In the literature (De Menech et al. [54], Gupta et al. [58] and Gupta and Kumar [59]), the following 6 dimensionless parameters are used, to highlight the characteristics of a T-junction microfluidic chip. They are the Reynolds number (Re), the capillary number (Ca), the flow rate ratio (Q), the viscosity ratio (λ*), the intersection ratio (Λ), and height-to-weight Ratio (h*). The Reynolds number is very small, so it is not used. But the volume calculations can be written as a function of the remaining: V*=f(Ca, Q, λ*, Λ, h*).

Chapter 5

5. Experimental Data

Earlier we discussed the present and potential applications for microfluidic devices. When the samples / specimens are expensive or small in volume, it is better to trap them in a medium to stop them interacting with each other and/or with their surroundings. Trapping them in micro / nano sized droplets is one way to do this.

This section focuses on the droplet generation in two major regimes (dripping and squeezing) and observes the behavioural changes during the transition between the regimes. The comparisons are based on change in the capillary number, geometry, and flow rate ratio. Also we looked into the current scaling laws for the volumes of the droplets generated and how our data fits to the challenge.

5.1 Flow patterns: self-organizing microdroplets

In this part of the experiments, we experiment to understand the self-organised water droplet flow patterns in oil continuous flow. Before looking into the scaling and investigating the changing phase of droplet generation from dripping to squeezing regimes in confined space we focused on understanding the complex flow patterns in dripping regime in microfluidic devices. We observed the patterns caused by the change of fluid flow at the expansion of the channel. These patterns are classified as follows: the single profile, the double helix profile and the triple helix profiles.

The flow rates applied to the continuous phase channel were ranged from $2.7x10^{-5}$ ml/sec to $5.55x10^{-4}$ ml/sec by the Harvard Apparatus PHD 2000 syringe pump. The flow rates applied to the aqueous phase channel were ranged from $1.59x10^{-4}$ ml/sec to $4.3x10^{-3}$ ml/sec by the Sage Instruments 355 syringe pump.

We analysed the data under three sections: the capillary number, the flow rate ratio and comparison of the geometries of the chips 1 and 3 which were used for collecting data.

5.1.1 Impact of the flow rate ratio

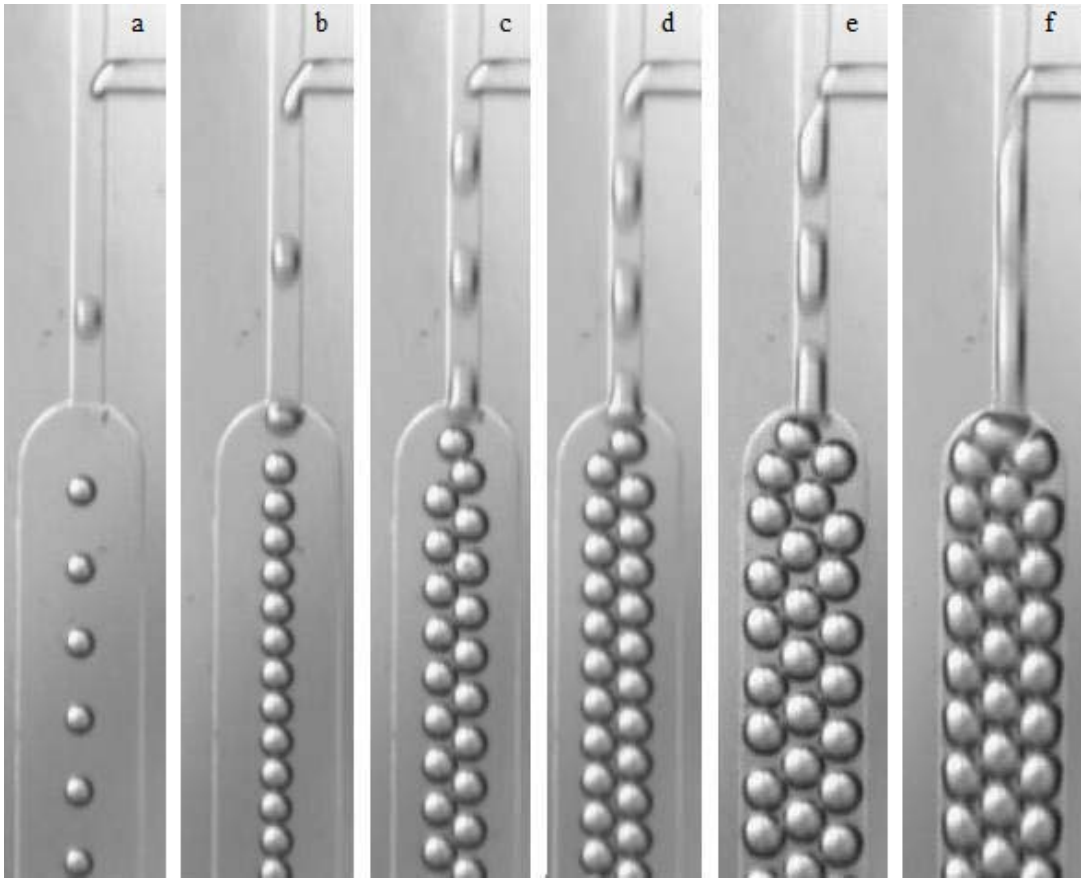

Figure 12: Various flow patterns in Chip 3. Droplet patterns from left to right: a-Single profile, b-Touching single profile, c & d-Double helix profile, e & f-Triple helix profile. The flow rate ratios, Q, are: a- 0.62, b-

1.72, c- 3.13, d- 4.38, e-5.94 and f-15.49.The oil flow rate is $2.78x10^{-4}$ mL/s, Re=0.03487 and Ca=0.0199. The flow regime is dripping.

We explain the impact of the flow rate ratio using Figure 12. When the oil flow exceeds the water flow and stops it entering into the main channel, no water droplet flow is observed. When the water stream starts to increase we start to observe dispersed single profile droplet flow. The droplets flow through the centre as expected from a pressure driven laminar flow (a). As the water pressure increases the number of droplets increases, the distance between the droplets decreases and finally the droplets start to touch each other and form a touching single profile flow (b). As the periodicity of droplet generation increases the droplets start to push each other (c), and a double helix profile forms (d). Finally a Triple helix profile forms, the droplet chain is touching the channel walls, visually the droplets are still spherically shaped and bigger looking then in the double helix profile (e). When the water flow rate is considerably high but not blocking the oil flow we do observe (f).

Similar behaviour of the flow rate ratio is observed in Chip 1, documented in Figure 13. As the flow rate ratio increases the number of water droplets increases which causes the droplets to pack densely. We also observed that the droplet size gets bigger [37, 62, 63, 73]. Note that the difference between Figure 12 and Figure 13 is the geometry of the device, as discussed in Section 5.1.3

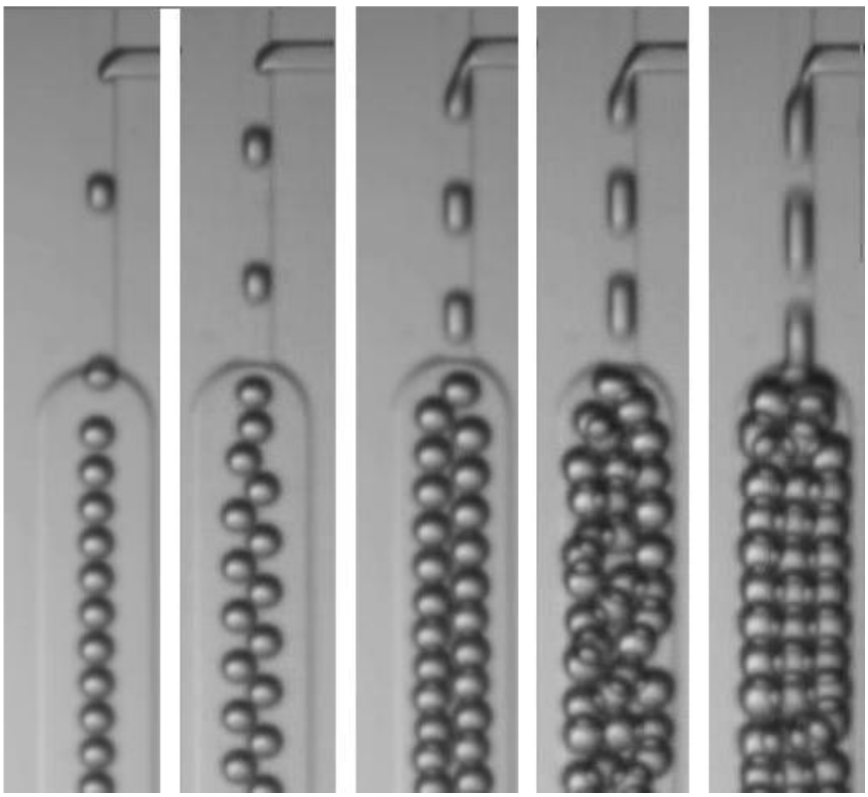

Figure 13: Various flow patterns in Chip 1. The droplet flow patterns, with various flow rate ratios 1.25, 2.5, 3.75, 6.88, and 12.5 from left to right. The oil flow rate is 1.39×10^{-4} ml/s, Re=0.0174, Ca=0.0099.The flow regime is dripping.

5.1.2 Impact of the capillary number

Figure 14 and Figure 15 below show the impact of the capillary number. In Figure 14: the first image on the left is with Ca=0.0039; in the middle image the capillary number is 5 times bigger; and in the image on the right has the capillary number is 10 times the first one. We do observe the flow pattern changing from single file profile to double helix profile. Although the flow rate ratio is kept at 3.13 during the recordings, as the capillary number increases the droplet size becomes smaller (see also Garstecki, et al. [37]).

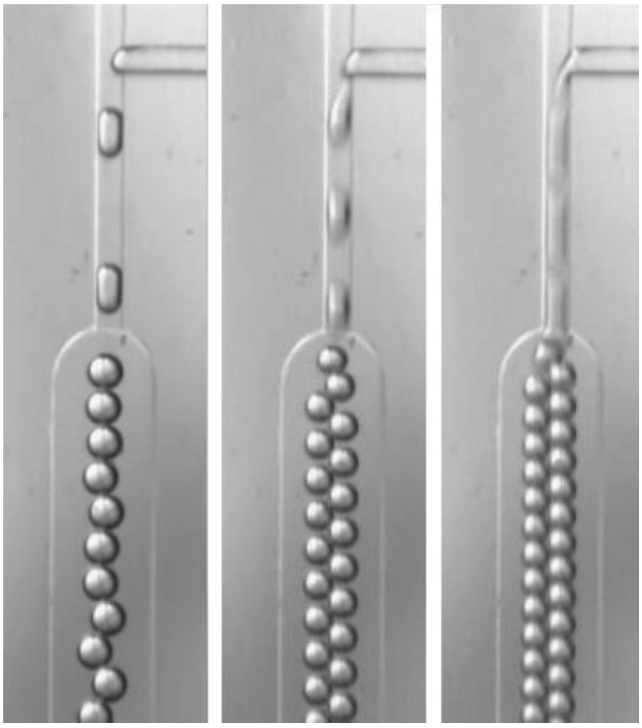

Figure 14: The impact of the capillary number on droplet flow patterns in Chip 3, where Ca=0.0039, 0.0199, and 0.039 (from left to right). The water/oil flow rate ratio is fixed at 3.13.

Figure 15 has the four images of Chip 1. In image (a) the oil flow rate is $2.7x10^{-4}$ ml/sec and water flow rate is $1.3x10^{-3}$ml/sec and the flow rate ratio is 4.3. Although the flow rate ratio of image (b) is the same at 4.3 as in image (a) the oil flow rate is $5.5x10^{-4}$ ml/sec and water flow rate is $2.6x10^{-3}$ ml/sec. So the capillary number of a Ca= 0.017 doubles in value in image (b) to Ca=0.034. As a result of this increase the droplet sizes get smaller and the number of droplets generated increases. Further, the droplets arrange more densely. Similar observations are visible within the images (c) and (d). Image (c) has the capillary number of 0.017 and the image (d) has the capillary number of 0.034. They both operate in

7.74 flow rate ratio but the droplets in image (d) are smaller and more densely packed because of the increase in the capillary number.

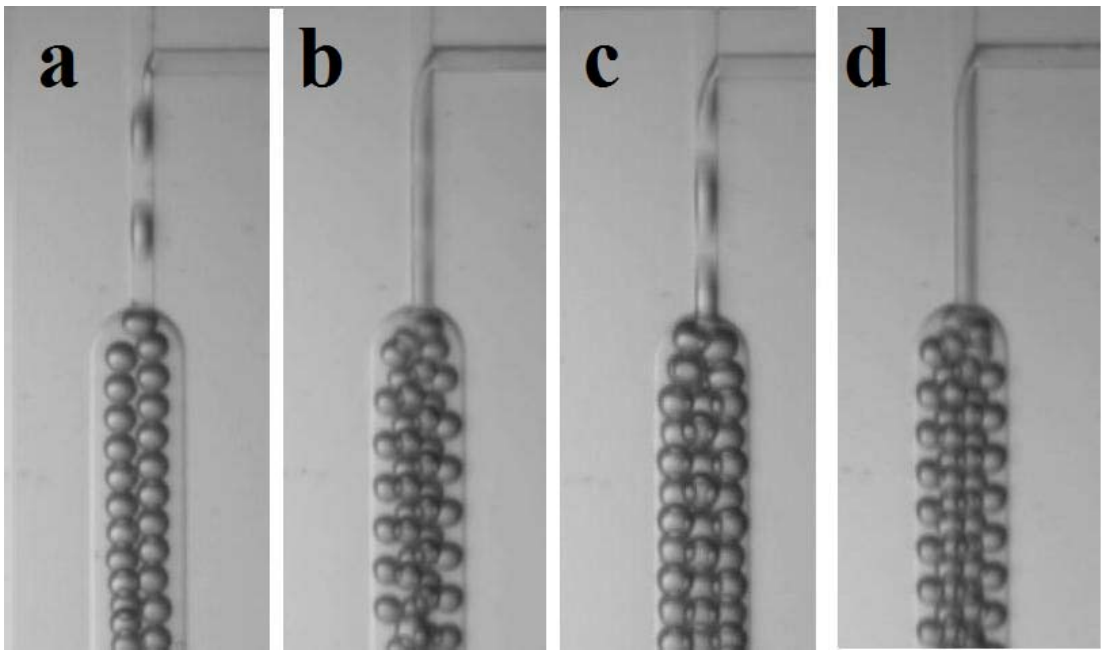

Figure 15: The impact of the capillary number on droplet flow patterns in Chip 1. Images (a) and (c) Ca=0.017 and Re=0.029, and images (b) and (d) Ca=0.034 and Re=0.059. The flow rate ratio is fixed at 4.3 (a) and (b), and 7.74 in (c) and (d).

5.1.3 Impact of the chip geometry

To understand the impact of the geometry of the devices on the flow patterns we discuss Figure 16.

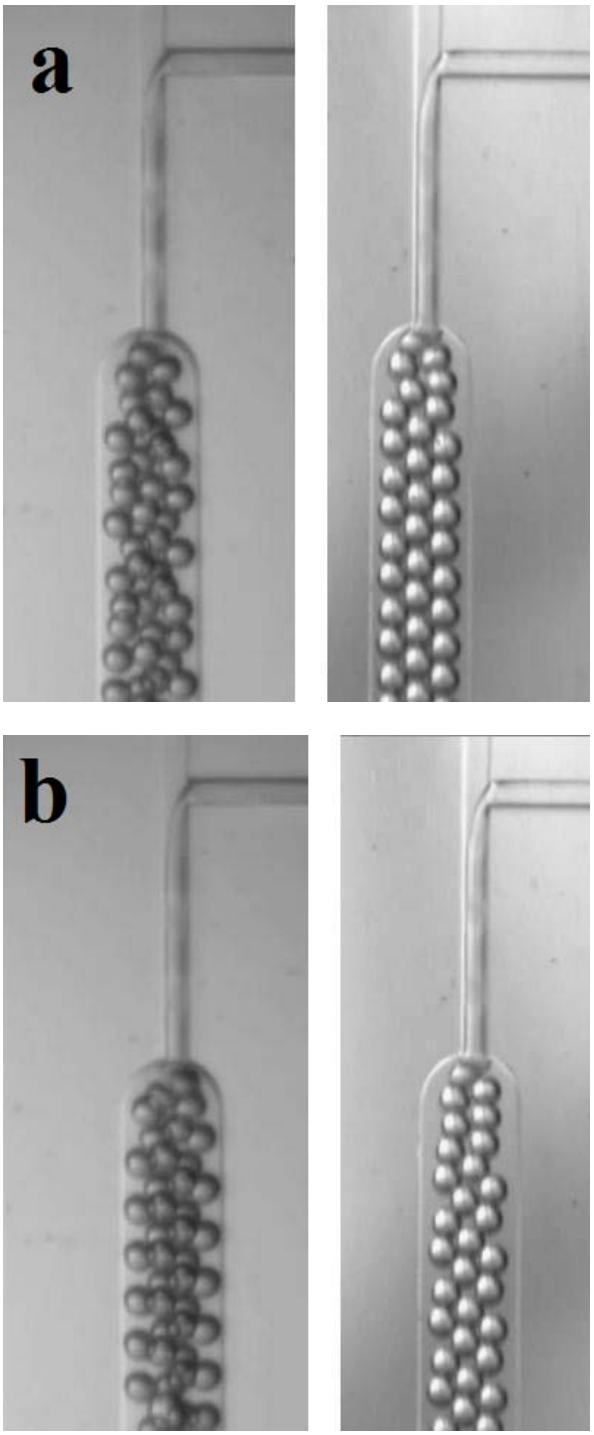

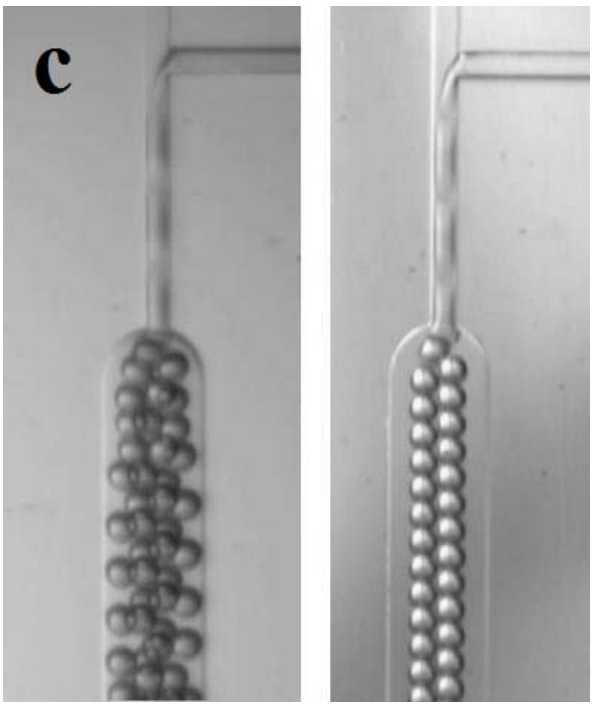

Figure 16: The impact of the geometry. In images (a), (b) and (c) the pictures on left hand are from Chip 1, Ca=0.034, Re=0.059. The images on right hand are from Chip 3, Ca =0.039, Re= 0.069. The flow rate ratio is (a) 3.91, (b) 4.69 and (c) 5.47.

In Figure 16 there are 3 sets of images: in each set the image on the left hand is from Chip 1 and the one on the right hand is from Chip 3. The capillary number and the Reynolds number of Chip 1 are 0.034 and 0.059, and for Chip 3 are 0.039 and 0.069. In the expansion area the device dimensions are listed in Table 2 (Section 4.1). Chip 1 has 516µm width and 330µm depth. Chip 3 has 511µm width and 220µm depth. The flow rate ratios of images are (a) 3.91, (b) 4.69 and (c) 5.47.

Since the images in Figure 13 have the same operating conditions like the capillary number and the flow rate ratios, the droplets generated in T-junction are approximately same sized. But Chip 1 is deeper and the droplets inside are more densely packed. This is due to the rapid drop of the flow rate. We observe the same situation in Figures 12 and 13. Also

as seen in Figure 13 the droplets self-organise the triple helix pattern in 3-dimensions, unlike the droplets in Figure 12.

5.2 Results: Scaling law

This is an experimental study to understand the change in the droplet size and how it is influenced by the capillary number, the flow rate ratio, and the geometry of the T-junction device.

This experimental study was designed with three microfluidic T-junction devices. For the droplet volume calculations we used the data collected in the expansion channel. The challenge here is to experimentally measure the droplet volume in the T-junction intersection area, which is essential to validate the scaling laws developed to predict droplet size (Garstecki et al. [37]; Christopher and Anna [49]; De Menech et al. [54]). We decided to reduce the complication of guessing the droplets volume by measuring its area in the expansion channel where the fluid flow slows down and the droplet becomes the relaxed spherical shape. In the previous section we discussed the fluid flow in expansion channels and the flow profiles.

The parameters we collect data on are listed below and the full Excel charts of the calculations for the observations are presented in Appendices A, B and C (one for each of the 3 chips).

Minimum and maximum values of the Reynolds and the capillary numbers are as listed in Table 4. The viscosity ratio, the intersection ratio and the height-to-width ratios of the each microfluidic device are as listed in Table 5.

	Range of the Re		Range of the Ca	
Oil Flow Rate	0.1 ml/hr	1.2 ml/hr	0.1 ml/hr	1.2 ml/hr
Chip 1	0.002977	0.035729	0.0017055	0.020467
Chip 2	0.003564	0.042771	0.002026	0.024312
Chip 3	0.003487	0.041854	0.001997	0.023975

Table 4: The Reynolds and the capillary numbers for the minimum and maximum Oil flow rate for each device.

Data was collected for the following Oil flow rates Q_c (ml/hr): 0.1, 0.2, 0.3, 0.4, 0.5, 0.55, 0.6, 0.65, 0.7, 0.8, 0.9, 1.0, 1.1 and 1.2. For each oil flow rate listed above the following flow rate ratios Q were recorded and measured: 0.05, 0.1, 0.15, 0.2, 0.25 and 0.3.

		Chip 1	Chip 2	Chip 3
Viscosity Ratio	$\lambda = \frac{\eta_d}{\eta_c}$	0.019		
Intersection Ratio	$\Lambda = \frac{w_d}{w_c}$	0.992	0.9846	0.9612
Height-to-width Ratio	$h^* = \frac{h}{w_c}$	1.279	1.053	1.085

Table 5: The viscosity ratio, the intersection ratio and the height-to-width ratio of Chips 1, 2 and 3.

The dimensionless droplet diameter, d, is calculated by dividing the measured droplet size from experimental data to hydraulic diameter of the continuous flow channel. For the calculation of the scaling law

equations in Section 5.2.2 the dimensionless droplet diameter is used. All the figures are created with the measured droplet diameters, micrometre in unit, which are listed in Appendix D with the standard error results. For our measurements biggest the standard error result was ±2.5 μm. This value is considerably small against its counterpart, measured droplet diameter 159.3μm.

5.2.1 Influence of the capillary number

One of the important parameters that has influence on droplet size is the capillary number. Garstecki et al. [37] and De Menech et al. [54], both observe that the droplet size becomes smaller as the capillary number increases. Figures 18, 20 and 21 show some of the experimental data we collected for the three chips. In each, column A is recorded in the squeezing regime, columns B and C are in the transition regime and finally column D is in the dripping regime. The droplet generation is documented step by step: the lag stage, the filling stage, the necking stage and finally the detachment of the droplet. In the bottom line of the figure the droplet is documented at the expansion channel, which is a deeper and wider structure (Table 2).

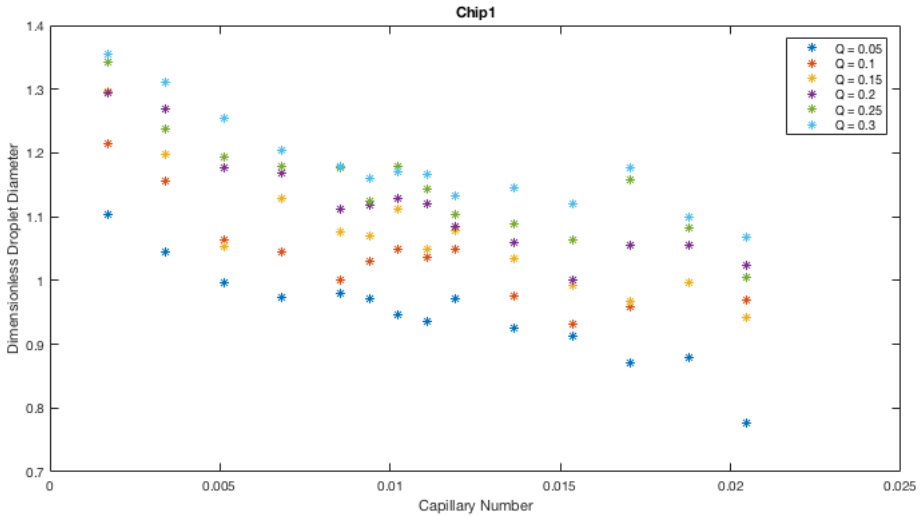

Figure 17: The impact of the capillary number on the droplet diameter at flow rate ratios 0.05, 0.1, 0.15, 0.2, 0.25 and 0.3 for Chip 1.

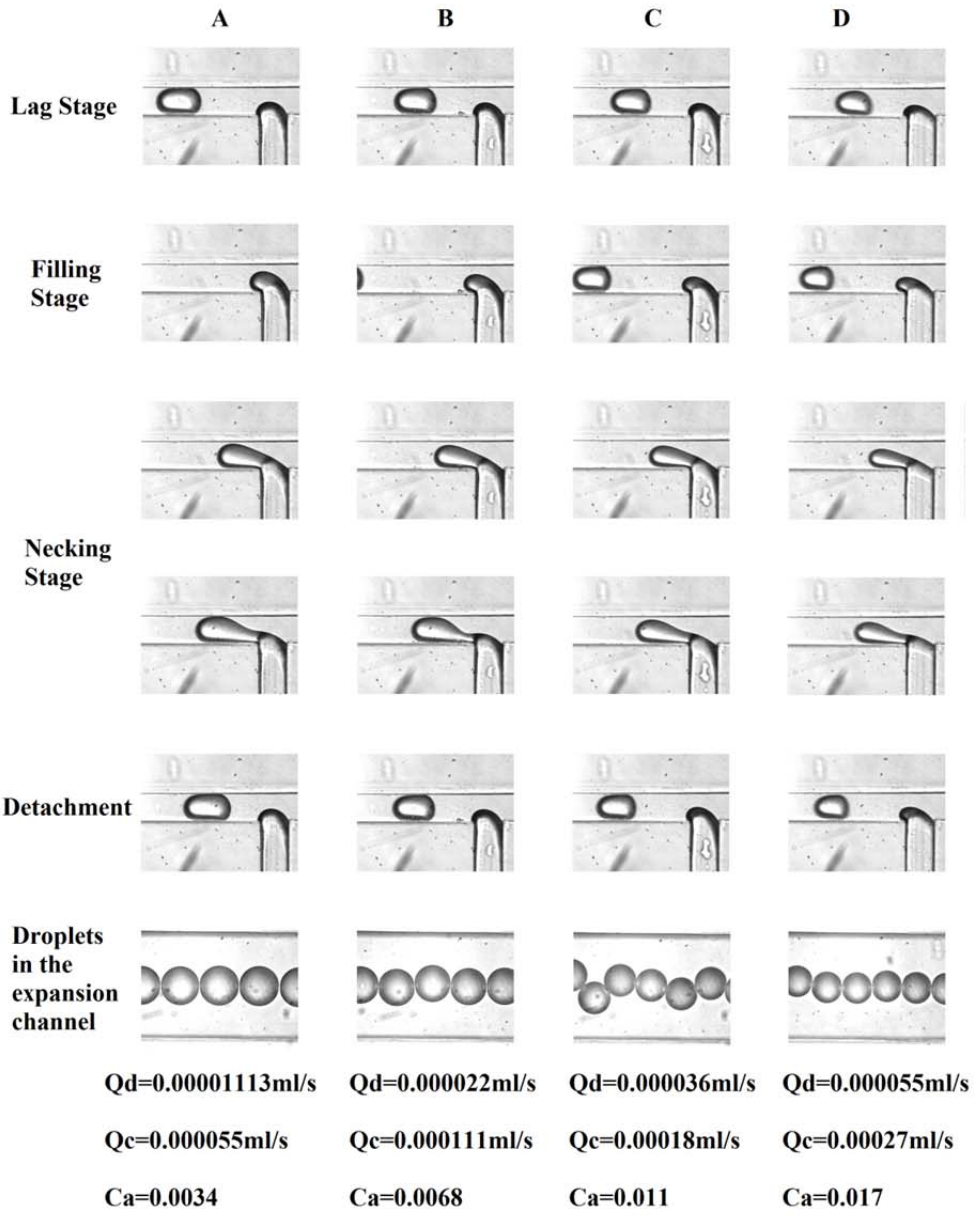

Figure 18: Chip 1 in squeezing, transition and dripping regimes.

We have conducted a series of experiments to measure the droplet volume in certain conditions in T-junction devices. In the flow pattern experiments we observed the impact of the capillary number on droplet size visually: the devices were mainly operating in the dripping regime

since Ca > 0.01. For certain microfluidic devices like microfluidic reactors (Tice et al. [28], Song et al. [[44], Tan et al.[51]), it is important to have accurate control of the sample sizes (Zhu and Wang [53], Anna [80]).

The droplets generated in the squeezing regime are larger than the continuous flow channel which is observed in Figures 18 A, 20 A and 21 A. When the capillary number is 0.0020 and the flow rate ratio Q is 0.2 Chips 2 and 3 display similar conditions in column A, but the droplet diameters as 209.7 µm and 204.1µm show the impact of the chip geometry.

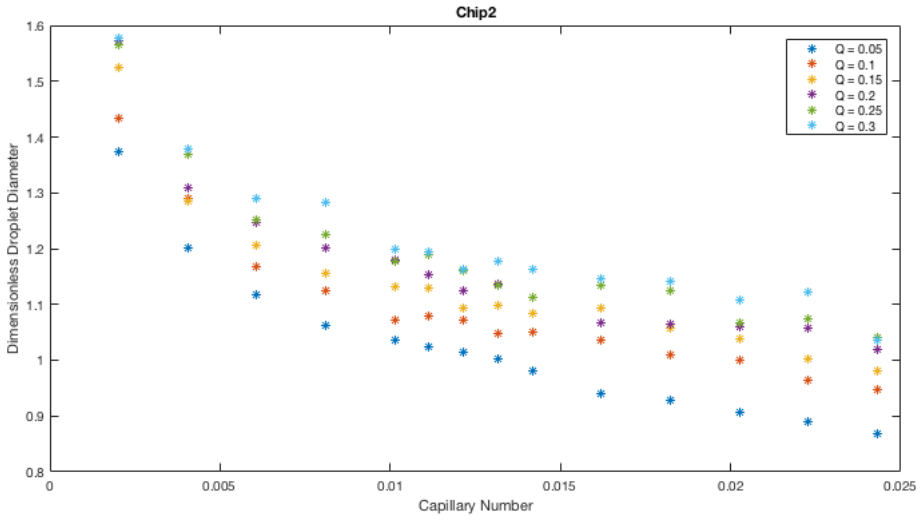

Figure 19: The impact of the capillary number on the droplet diameter at flow rate ratios 0.05, 0.1, 0.15, 0.2, 0.25 and 0.3 for Chip 2.

We achieved the smallest value of the capillary number 0.0017 with the biggest height-to-width ratio 1.279, which is Chip 1 (Figure 18). Although the value of h* is not that different between Chips 2 and 3, we did observe that the droplets generated with Chip 3 (Figure 21) were bigger in diameter than with Chip 2 (Figure 20).

In some numerical and experimental studies, a critical value of the capillary number Ca_{cr} is observed where the droplet breakup regime transitions from the squeezing to the dripping regime. De Menech et al. [54] observed the critical capillary number at $Ca_{cr} \approx 0.015$ while in 2009 Liu and Zhang's numerical experiment [56] observed $Ca_{cr} \approx 0.018$. On the other hand in an experimental study in 2008 Christopher et al. did not observe such a critical value at all [49]. Similar to De Menech et al. [54] and 2009 Liu and Zhang [56], we did observe a trend line change. For each chip the critical Capillary number was slightly different but around $Ca_{cr} \approx 0.01$. From Equation (4.17) we know the Capillary number is bigger when the droplet diameter is smaller. In Figures 17, 19 and 22 we did observe a break in trend line around Ca_{cr} and as the droplet diameter gets smaller the impact of the Capillary number decreases.

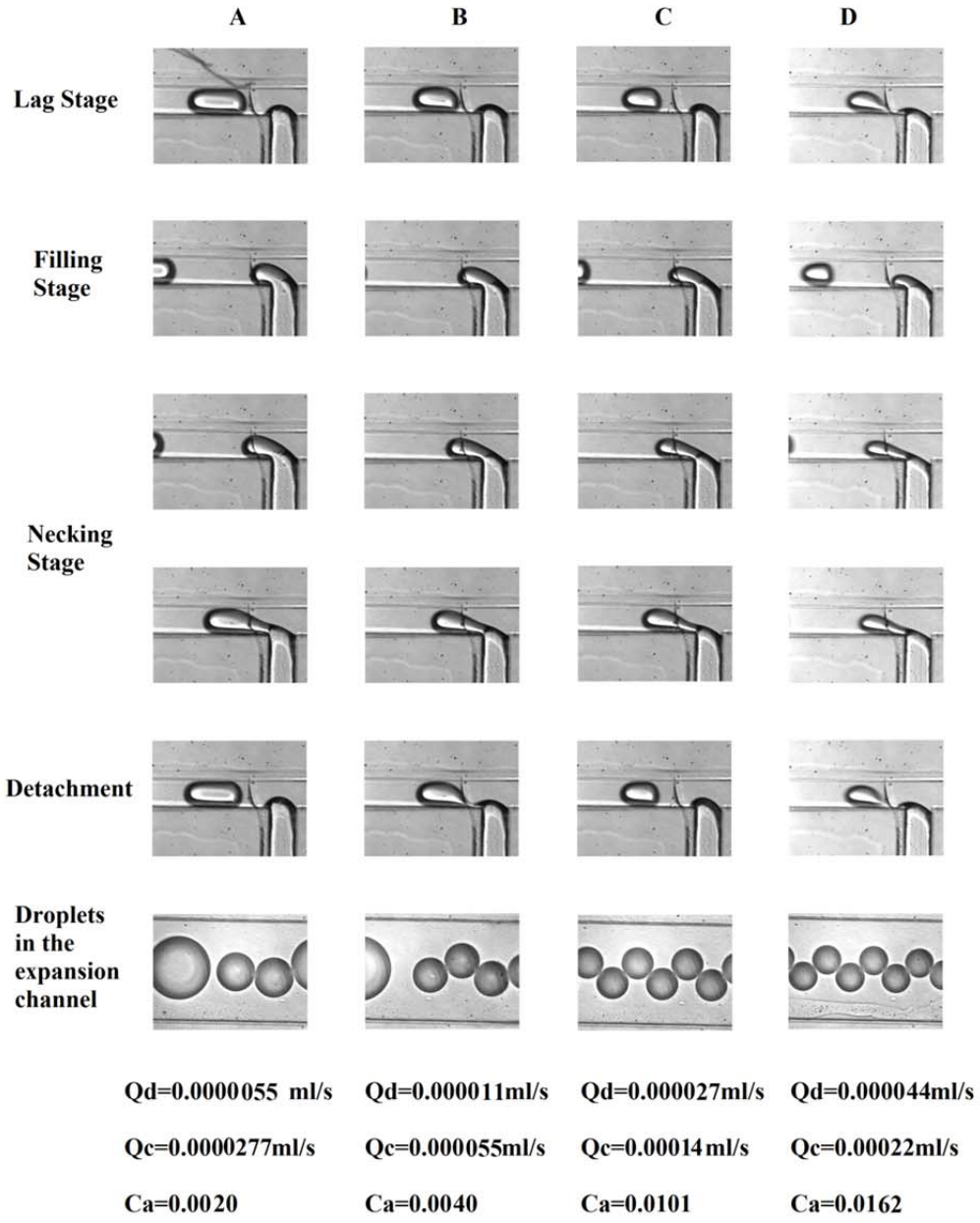

Figure 20: Chip 2 in squeezing, transition and dripping regimes.

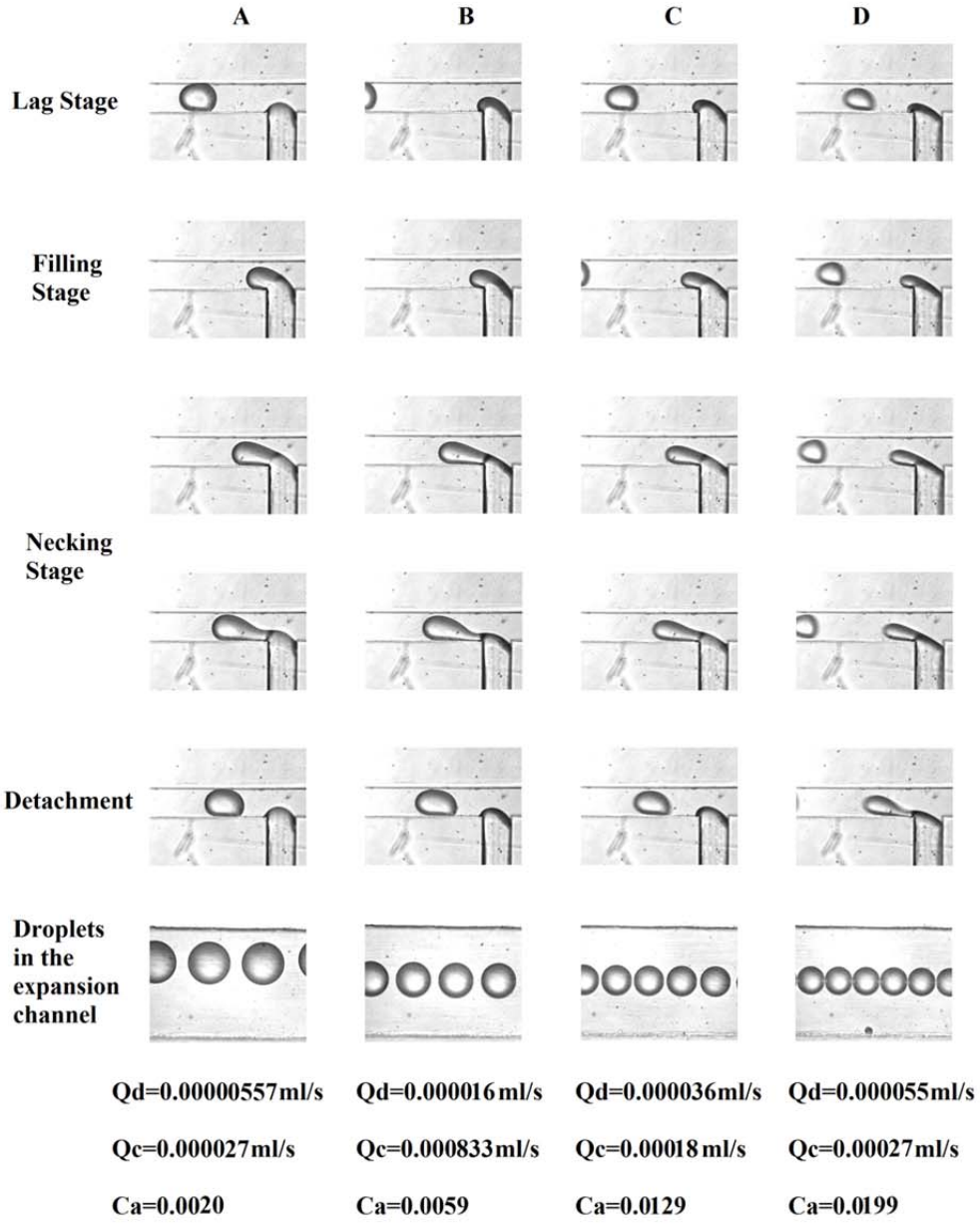

Figure 21: Chip 3 in squeezing, transition and dripping regimes.

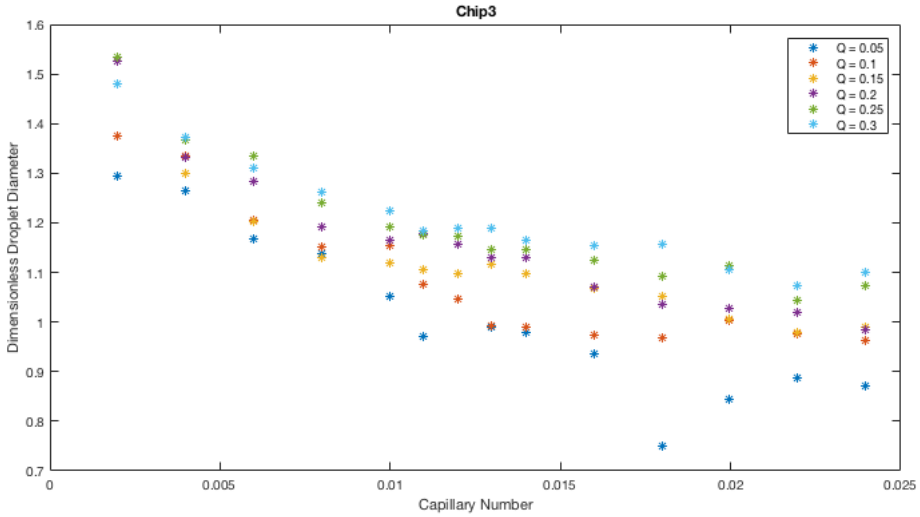

Figure 22: The impact of the capillary number on the droplet diameter at flow rate ratios 0.05, 0.1, 0.15, 0.2, 0.25 and 0.3 for Chip 3.

5.2.2 Influence of the flow rate ratio

The flow rate ratio creates a great opportunity to change the droplet volume in any set value of the capillary number the full results are listed in Appendix D. The capillary number is calculated using the oil velocity and oil velocity is the amount of oil flowing through the cross section area of the chips dispersed channel.

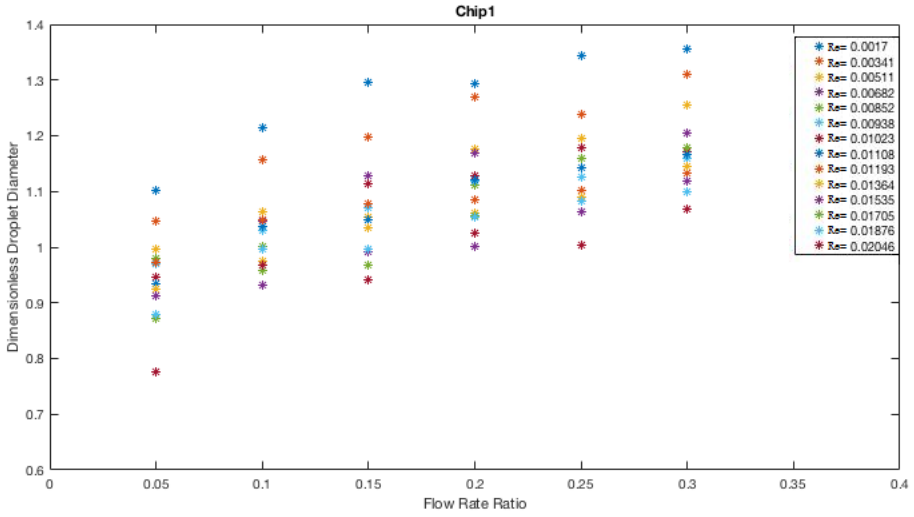

Figure 23: The impact of the flow rate ratio on the droplet diameter at the capillary number in a range from 0.0017 to 0.0204 for Chip 1.

To change the flow rate ratio, we need to change the amount of the aqueous flow rate. When the flow rate ratio is small, the droplet is generated at the corner of the T-junction chip.

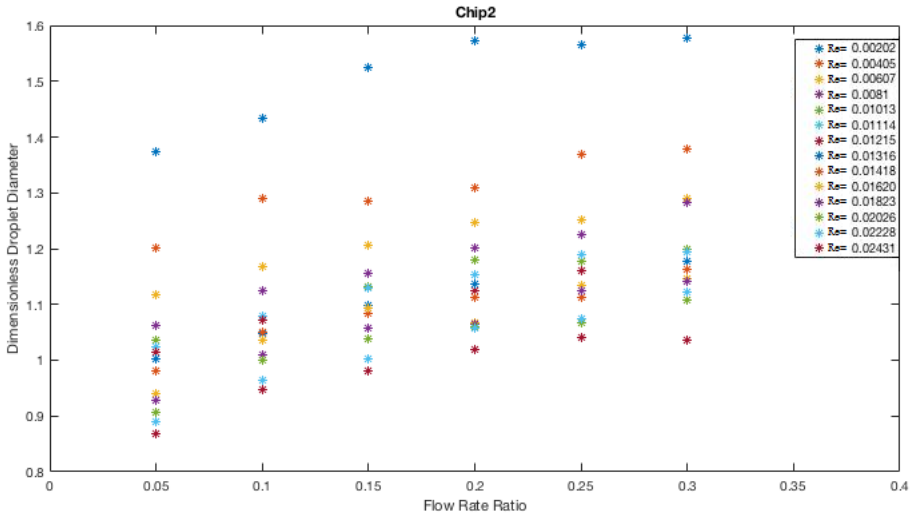

Figure 24: The impact of the flow rate ratio on the droplet diameter at the capillary number in a range from 0.0020 to 0.0243 for Chip 2.

When the flow rate ratio starts to increase, meaning the amount of water in the system is increasing, the droplet itself starts to move towards the downstream and break up happens at the downstream channel [49, 54,

and 56]. In Figures 23, 24 and 25 the droplet size is biggest at the smallest capillary number.

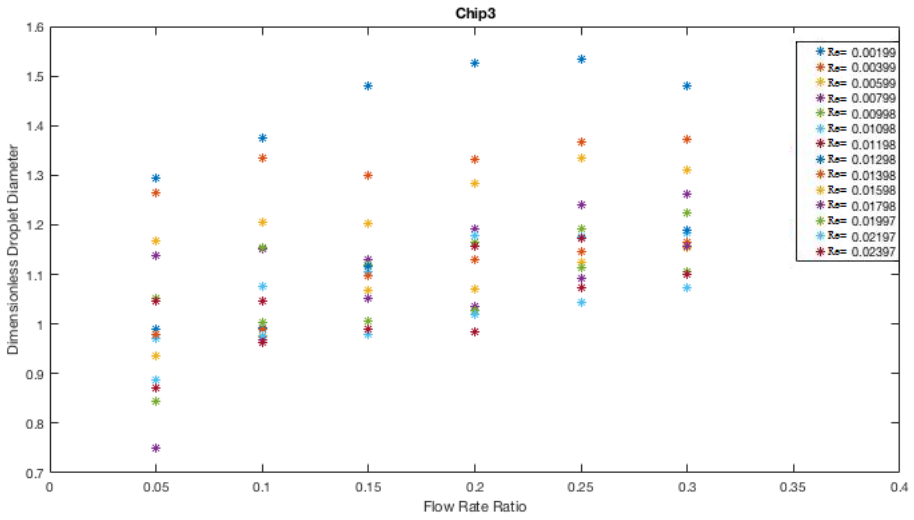

Figure 25: The impact of the flow rate ratio on the droplet diameter at the capillary number in a range from 0.0019 to 0.0239 for Chip 3.

Unlike the Capillary number, flow rate ratio has a strong and continuous impact on the droplet diameter.

5.2.3 **The scaling law**

We used Equation (4.18) proposed by Tan et al. [51] to calculate the dimensionless value of the droplet diameter as the function of the capillary number and the flow rate ratio. Figures 17, 19, 22, 23, 24 and 25 are the power fitting results of the experiments. We rewrite Equation (4.17) as Equation (5.1) to see the correlations between the parameters. The superscript β is a negative value, meaning interfacial surface tension has direct influence on the droplet diameter as well as the dispersed phase flow rate ratio. The continuous flow velocity u_c is calculated as (Q_c/w_ch), and from Equation (5.1) we observe that the droplet diameter decreases as the continuous phase flow rate ratio and the capillary number increases.

$$d = kQ^{\alpha}Ca^{\beta} \quad (5.1)$$

We now describe the power law fitting for the three chips.

Chip 1 $d=0.5611\ Q^{0.08812}\ Ca^{-0.1749}$ (5.2)

Matlab calculations of coefficients of Chip 1 with 95% confidence bounds are; k = 0.5611 (0.4329, 0.6892), α = 0.08812 (-0.003748, 0.18) and β =-0.1749 (-0.2575, -0.09229).

Chip 2 $d=0.4501\ Q^{0.1019}Ca^{-0.246}$ (5.3)

Matlab calculations of coefficients of Chip 2 with 95% confidence bounds are; k = 0.4501 (0.3793, 0.5208), α = 0.1019 (0.03462, 0.1692) and β =-0.246 (-0.3065, -0.1855).

Chip 3 $d=0.5089\ Q^{0.02994}\ Ca^{-0.187}$ (5.4)

Matlab calculations of coefficients of Chip 3 with 95% confidence bounds are; k = 0.5089 (0.4057, 0.6122), α = 0.02994 (-0.05649, 0.1164) and β =-0.187 (-0.2647, -0.1093).

Equations (5.2), (5.3) and (5.4) represent the correlation between the droplet diameter and the flow rate ratio and the capillary number.

In this study the conditions for a regime change are given as follows:

- The droplets in the squeezing regime considered to have a droplet diameter bigger than the depth of the continuous channel ($d > h$).
- The droplets in the transition regime has the droplet diameter smaller than the depth of the continuous channel but bigger than the width of the continuous channel ($w_c < d < h$).

- The droplets in the dripping regime considered to have a droplet diameter bigger than the width of the continuous channel ($w_c > d$).

Figure 26: Flow patterns as the function of the capillary number versus the flow rate ratio for Chip 1.

The above conditions were used to plot the Figures 26, 27 and 28 for the three chips.

In our experiments we collected data with similarly sized chips and although our ranges for the Reynolds and Capillary numbers were not big either, we did manage to observe different results. Chip 2 was the smallest one and produced the most stable results.

Chip 1 has the biggest height-to-width ratio, and smallest capillary number range from 0.0017 to 0.0204. As a result of that we manage to observe the transition from the squeezing to the dripping regime. The trend of this distribution shows similarities with Liu and Zhang [66] (Figure 26).

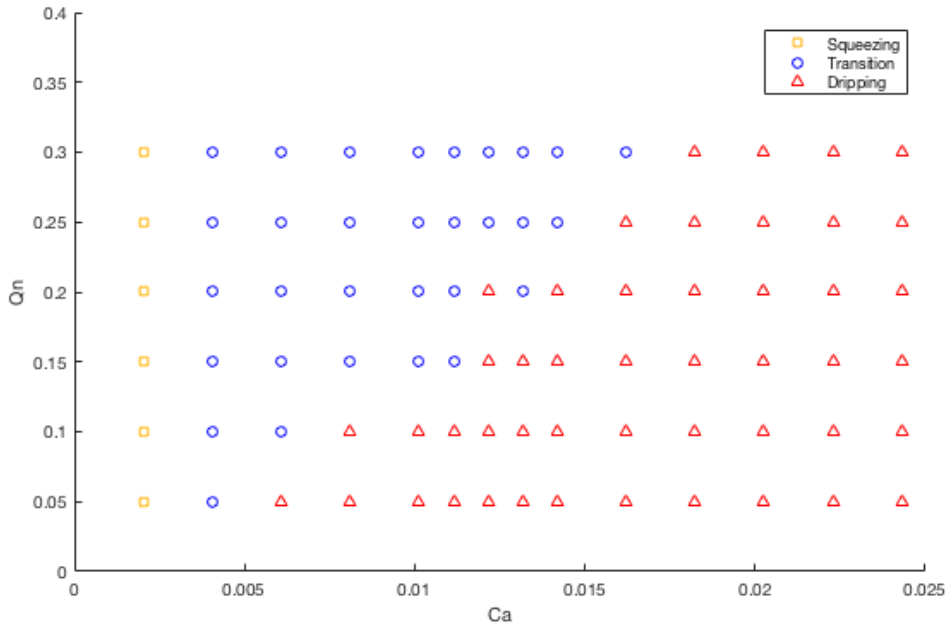

Figure 27: Flow patterns as the function of the capillary number versus the flow rate ratio for Chip 2.

In Figure 27, we do observe the squeezing regime, transition and the dripping regime. The transition regime was more dominant in low capillary numbers where we would expect the squeezing regime to dominate.

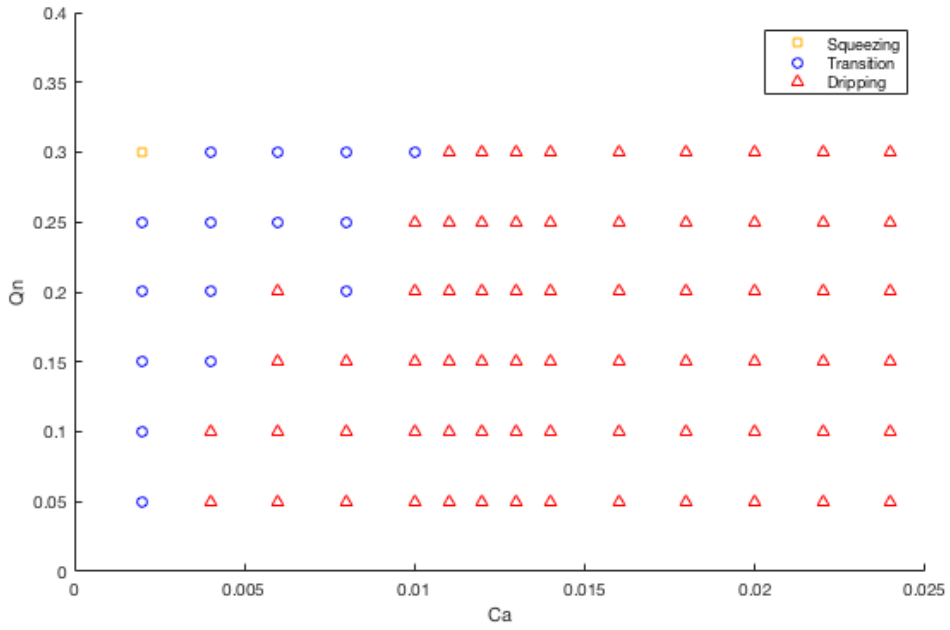

Figure 28: Flow patterns as the function of the capillary number versus the flow rate ratio for Chip 3.

In Figures 26, 27 and 28 we observe for the higher flow rate ratios the transition from dripping to squeezing regime starts in bigger Capillary numbers.

For example, for Chip 1 in Figure 26, for Q=0.3 the transition regime is in between 0.009<Ca<0.02. But for Q=0.05 the regime change happens more quickly: 0.001<Ca<0.006.

Similar observations are made for Chip 2 in Figure 27, for Q=0.3, 0.004<Ca<0.018 is the transition regime, but for Q=0.0 it is 0.002<Ca<0.006.

For Chip 3 in Figure 28, in Q=0.05, we do not observe the squeezing regime at all, but the transition finishes in 0.004. For Q=0.3, the transition happens in a range between 0.002<Ca<0.01.

5.3 Conclusions

The flow patterns are investigated by the impact of the flow rate ratio, the capillary number and the channel geometry. It is observed that the microdroplets become densely packed as the flow rate ratio, Q_n, starts to increase due to the number of droplets increasing. Similarly as the capillary number increases we documented that the flow pattern becomes tightly packed and the droplet size becomes smaller. The deeper structured chip offered bigger space to the droplets, even when the droplets have similar size; the flow pattern changed from double helix pattern to triple helix pattern in 3-dimensions.

Throughout our experiments we clearly observed the squeezing and the dripping regimes at low and high capillary numbers. But also we observed a transition area where the regime of the flow is neither squeezing nor dripping. The droplet diameter decreased as the capillary number increased. In the range of parameters for which we collected data: we have observed a critical change of the droplet diameter where the trend slows down in shrinking due to the regime change around the capillary number $0.01 < Ca < 0.015$.The increase in flow rate ratio has the impact of increasing the droplet size. Chips 1 and 2 had a better range to observe the transition from the squeezing to the dripping regimes. The power laws in Equations (5.2), (5.3) and (5.4) were calculated by the trends illustrated in Figures 17, 19, 22, 23, 24 and 25.

Chapter 6

6. Polymeric based microfluidics device fabrication

In the previous chapter we investigated the droplet size and the scaling law of a microfluidic chip. One of the major results was the geometry of the chip having a direct impact on the droplet size. In this chapter we will look into the fabrication process of a polymeric microfluidic chip, an alternative way of adhesive bonding will be demonstrated, and then finally we will show an application: using microfluidic devices to build Logic Gates. The driving force of this project is to fabricate a microfluidic device which is low cost, reliable and durable, quick and easily processed, and finally, not environmentally dangerous.

6.1 Background

Microfluidics branched out as a product of Micro Electro Mechanical Systems (MEMS) technologies. It has been around since the late 1980s. The most common application is inkjet printing heads as micro nozzles [5]. Despite the fact these applications are very commonly used, microfluidics real potential is in its infancy and requires more research for mass production of commercial devices. The key requirements for commercial production are a simple fabrication procedure and a low cost. In this chapter we will look into how to fabricate a durable microfluidic device.

Microfluidics devices are in the scale of 1 to 500μm in cross sections, which the conventional manufacturing techniques cannot easily deliver. In the evolution of process technology, MEMS follows from semiconductor device fabrication [86].

For microfluidics the most common materials are in the following three groups [84]:

- Inorganic Materials (silicone, glass or ceramics);
- Polymers (Elastomers and Thermoplastics);
- Paper.

The wide diversity of the materials means that there are a number of different techniques for processing. Fabrication of devices simply can be grouped into two: direct and replicative fabrication. Direct fabrication includes the techniques like photolithography, mechanical or laser bulk machining, and chemical etching. On the other hand replicative fabrication uses a master to reproduce the device like injection moulding or hot embossing. Replicative fabrication is more common in polymeric structures.

The earliest microfluidic devices were on glass and silicon. For glass, a combination of various etching techniques, power blasting and laser ablation produces a variety of cross-sectional profiles. In the case of silicon, etching is preferred due to its easier machining properties [84]. These materials are commonly used in MEMS because they are a good fit for mass production, the anodic bonded structures are durable, they perform well optically, and they are chemically stable (solvent compatibility and surface stability). However, they are not preferred in Microfluidics because they are expensive, time consuming to fabricate, and also need surface treatment to use water.

6.2. Polymeric devices in microfluidics

Photolithography is the technique that has been used to fabricate polymeric devices. Scientists need to prototype, demonstrate their research, and discover the potential applications of microfluidics

quickly. Since the 2000s the choice of materials for microfluidics has shifted to polymers and plastics. The fabrication of multifunctional structures with electric / electronic components is easier with polymeric structures because most of the polymers are transparent which enables the integration of optical detection and manipulation systems. Another important advantage of using polymers is that their chemical formula can be modified to the researcher's needs.

For microfluidics the most affordable and commonly used materials are polymers, and polymers [82, 84, 85]. Limitations like chemical (tend to absorb water in long-term use), thermal stability or optical properties are some of the important criteria when choosing the right material.

The choice of material and the design depends on the use of the microfluidic based product. The most commonly used polymers are PDMS, PMMA, PC and SU-8 due to their biocompatibility, but there are many varieties of substances to experiment with. A detailed comparison review is published by Nge et al. in 2013 [84]. A simplified version of a table from their work is included below as Figure 29.

material	optical clarity	UV transparency	surface chemistry	surface charge
glass	good	>280 nm	silanol	negative
silicon	opaque	none	silicon/silanol	requires oxidation
LTCC	opaque	none	aluminum oxide	negative
Ormocer	moderate	>300 nm	[a]	negative
PDMS (native)	good	>220 nm	silanol	negative
PDMS (oxidized)	good	>220 nm	silanol	negative
TPE	moderate	>400 nm	polyester	requires oxidation
PFPE	moderate	>350 nm	fluorocarbon	[a]
PS	good	>300 nm	phenyl	requires oxidation
PC	good	>360 nm	phenyl/ carbonate	requires oxidation
PMMA	good	>340 nm	acrylate	negative
PEGDA	good	>300 nm	acrylate/PEG	negative
PEGDA/ PMMA	good	>300 nm	acrylate/PEG	negative
PDMS-*co*-PEO (5%)	moderate	>440 nm	silanol/PEO	negative
PDMS-*co*-PEO (10%)	moderate	>440 nm	silanol/PEO	negative
FEP/PFA	moderate	[a]	fluorocarbon	[a]
COC	good	>360 nm	cydic olefin	requires oxidation
thiol ene	moderate	[a]	thiol/allyl	[a]
PU (castor oil)	moderate	[a]	carbamate/ ricinoleic acid	negative
PU (tecothane TT-1095A)	moderate	>300 nm	carbamate/ phenyl	negative
zein	moderate	[a]	zein	[a]
SU-8	moderate	>360 nm	epoxy/phenyl	negative
paper	opaque	none	cellulose	[a]

[a] Information that was not reported in the literature.

Figure 29: Summary of the materials that could be used in microfluidic devices (Nge, 2013) [84].

Figure 29 lists the materials that could be used in microfluidic devices. It documents for each material the optical clarity, UV light transparency, composition as the surface chemistry and finally surface charge.

PDMS (Polydimethylsiloxane) devices offer researchers a quick and less costly solution. It is silicon based organic polymer and it is good for fabricating valves and pumps [4, 9, 80]. The master of the design, fabricated on silicon or SU-8, is coated by a thick layer of the liquid form of PDMS for the fabrication process. This is followed by the curing of the PDMS under a pressure chamber. The problems with this material are its short lifetime, and its bending during high pressure operations due to its low elastic modulus.

6.3 SU-8

For our microfluidic device fabrication, SU-8 is chosen. SU-8 is a high contrast, epoxy based negative polymer photoresist. It was developed and patented by IBM in 1989 to improve the resolution of advanced semiconductor devices during fabrication process. SU-8 photoresist can be fabricated from 0.5 micrometre to up to 2 millimetres with the typical aspect ratio greater than 20 (higher ratios have been achieved via single coat spinning [86]). This big range makes it suitable to use in several microfluidic applications like cantilever [86], microneedle [100], and free standing microfluidic chips [91].

MicroChem Inc. and Gerstel SA are the main suppliers of the resin and liquid forms. In recent years MicroChem released newer formulations to improve the adhesion and the range of thickness. SU-8 is a thermosetting polymer: it cures irreversibly. It is commonly used in moulding the PDMS. When it is fully cured, it becomes very resistant to high temperature and most of the solvents.

The benefits of using a single material to build up a microfluidic device are:

- better symmetry of the mechanical stresses, and;
- better thermal and electrical isolation.

The polymeric structures manufacturing was carried out at Heriot-Watt University, Institute of Sensors, Signals and Systems class 1000-10000 clean room MISEC laboratories.

6.3.1 Composition:

SU-8 is cross-linked in two steps, first by exposure to UV light followed by the thermal process. For this project we mixed our own formulation using the manufacturers' guidelines. The thickness of the end product desired lead us to the SU-8 65/35 formulation for fabricating the microfluidic devices but for the bonding process it is MicroChem's SU-8 3000 that has been used. This product has improved adhesion. The thickness can be changed by changing the ratio of Gamma Butyrolactone (GBL) which affects the viscosity of the mixture.

100 ml of SU-8 65/35 formulation contains:

- 65 mg of SU-8 epoxy resin,
- 29 ml of Gamma Butyrolactone (GBL) as the primary organic solvent, and
- 6 ml of CYRACURE photo initiator (UVI-6974).

The ground epoxy resin is mixed with GBL in a dark coloured, tightly closed container which later on placed in the ultrasonic bath at least a

day. This is done to increase the speed of homogenous mixing of the formula. Two hours after this initial mixing the mixture is photosensitized by adding triarylium-sulfonium salt. During this project due to the lab opening times the mixture is left at least a week in the ultrasonic bath. There is no harm in leaving the formula in the ultrasonic bath as long as its cap is tightly closed in a dark coloured jar.

Figure 30 shows the ladder like molecular structure of SU-8 before crosslinking. When the SU-8 is exposed, an electron is released from the photo initiator (HSbF6) which gets attracted by the oxygen bridges of the structure; this turns the structure into a strong, Lewis acid. Following the exposure the structure is post baked to achieve high crosslinking density.

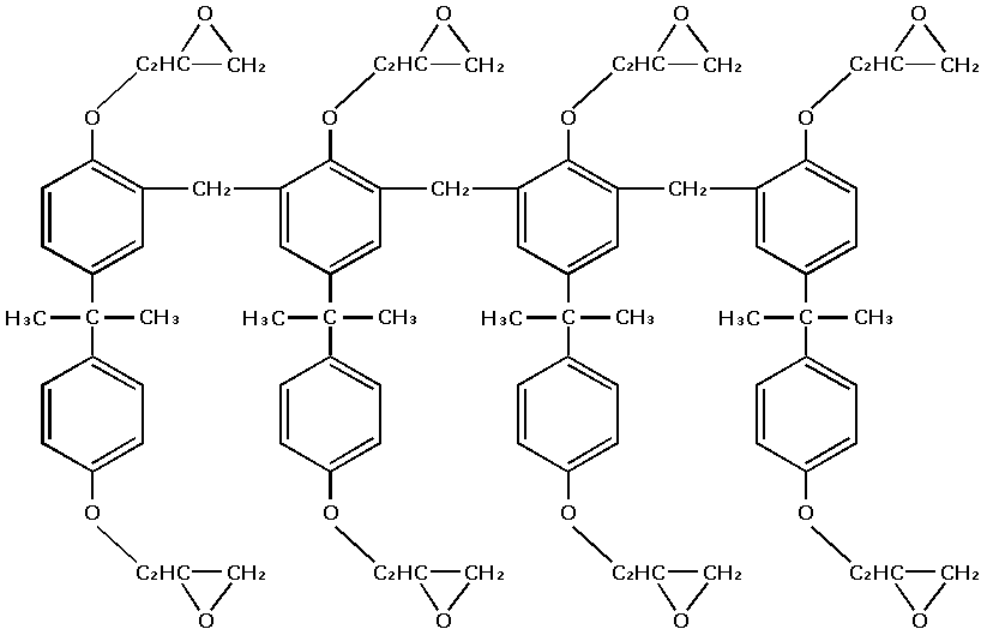

Figure 30: SU-8 before crosslinking

All varieties of SU-8 mixtures are advised to be processed in several lithography techniques like e-Beam, X-ray and UV radiation (350 –

400nm) [81, 83]. We summarise below the standard process steps as detailed on the manufacturer's data sheet. In this project the same process structure was followed. To create free standing microfluidic devices Kapton film has been used.

6.3.1.1 Fabrication process – Crosslinking:

- **Substrate cleaning:** It is standard to wash the wafers and all other components used in fabrication. To eliminate the tiny particles to contaminate the fabrications, as a common practice, all hard surfaces get a cleaning and dehydration treatments. For cleaning the substrates placed in a beaker filled with distilled water (DI) and Decon 90 detergent. This beaker stays in the ultrasonic bath for a minimum of two hours. Following that the beaker and its contents are washed with DI water and refilled with DI water and placed in the ultrasonic bath again at least a minimum of one hour. Decon 90 can be disposed directly down the sink since it is not a dangerous fluid to the environment. The washed and cleaned substrates dried with pressured nitrogen gas and dehydrated on a hot plate at 65°C at least for 15 minutes. The Kapton film needs longer dehydration at the oven 1 hour at 65°C.

- **Spin Coating:** The spin coating speed is the first parameter to be set. It is important because it defines the thickness of the polymer film and it has a direct effect on the soft baking time. Throughout this research the depth from 12µm to 375µm achieved in two and three layer fabrication.

  The spin coating steps are:

a. A pipette placed in SU-8, because of its thick viscosity this takes about a minute.
b. The coating parameters input to the spin coating machine.
c. The Kapton film attached wafer placed on the chuck. Kapton film tends to bend when it is placed directly on the chuck.
d. To keep the wafer straight to achieve a smooth coating of SU-8, the vacuum pump turned on.
e. SU-8 spread on the Kapton film starting from the centre.
f. Chose the program, which set at step b, and press start.

It is crucial to avoid bubbles on the wafer surface before starting the spin coating since they can cause deformities over the surface, using a clear pipette to suck them up helps. But also an elevated rate of spinning helps to achieve a smoother SU-8 surface topology. During this research two different formulations of SU-8 are used but for both of them the spread cycle parameters were the same. Spread cycle parameters were 500rpm with 200 rpm/second acceleration for 20 seconds.

The Spin cycle parameters define the thickness of the thin film, and were in range of 1000rpm to 3000rpm with 200 rpm/second acceleration for 30- 60 seconds.

- **Soft Bake:** This is the step before UV exposure. The smoothly SU-8 coated substrate needs to evaporate the solvent before lithography. This curing process is known as soft bake or pre-exposure bake (PEB). The SU-8 film becomes denser in a more controlled way. The manufacturer advises to ramping or stepping up the hot plate temperature for baking. During this research two

hot plates were used. Although the fully cured SU-8 is compatible for medical applications, uncured SU-8 has to be handled carefully so these hot plates were located under the extractor fan bench.

The first hot plate was set to 65°C and the second one was to 95°C. The curing on the first hot plate is always shorter than the second hot plate. Especially with the deeper and multi layered structures it is better to use two separate hot plates to avoid the uneven, wrinkly surface of the SU-8. Before the exposure the wafers were left to rest no more than 10 minutes. It is observed that the wafers adjusted back to room temperature had no sticking problem when they get to contact with the mask during the exposure.

- **UV Light Exposure:** The manufacturers' data sheet specifically advises the use of 350-400nm wavelength for setting the SU-8 structures. All the fabrications have been carried out on Tamarack Scientific MODEL 152R with interchangeable i-line filter (365nm) for thick film lithography. Tamarack delivers collimated light by a high pressure mercury UV lamp. i-line filter is recommended for best resolution.

  The UV lithography steps are:

  a. The SU-8 coated wafer is positioned on the Tamarack table on top of the vacuum suction channels.

  b. The printed side of mask is positioned on the wafer and pressed softly to remove the air in between.

  c. The vacuum is turned on to avoid any dislocations between the wafer and the mask during exposure.

d. Exposure dosage (mJ/cm^2) is set at the Tamarack machine, and the button "Expose" pressed.

e. The vacuum is turned off and the wafer taken to the hot plate for post exposure bake.

Determining the exposure dosage is very crucial. When there is not enough UV light the channels does not form properly. Table 6 shows the correlation between the exposure energy against the thickness of the film from the MicroChem SU-8 3000 Datasheet.

THICKNESS microns	EXPOSURE ENERGY mJ/cm^2
0.5 - 2	60 - 80
3 - 5	90 - 105
6 - 15	110 - 140
16 - 25	140 - 150
26 - 40	150 - 160

Table 6: MicroChem SU-8 3000 Datasheet, advised exposure dosage.

Finally, the wafer is taken back to the extractor fan bench for post expose bake.

- **Post Expose Bake:** This step is similar to soft bake. It is done to cross-link the exposed parts of the structure. As with the pre-exposure bake it is conducted with two hot plates set to 65°C and to 95°C but the baking times are shorter. The wafer should rest and allowed to adjust back to room temperature slowly under the extractor fan bench before development. For multi-layered structures this is the step to return spin coating and building up.

The key factor for multi-layered structures is a carefully designed mask which we will discuss in next section.

- **Development:** This is the step when the channels, structures in the SU-8 film, get their depth. The unexposed photo resist dissolves away in solvent based developer. The choice of solvent during this research was EC solvent (2-methoxy-1-methylethyl-acetate (PGMA), Quarry Park Ltd). After the development the EC solvent must not poured down the sinkhole due to its low toxicity for organisms [87, 88].

6.3.2 Kapton film

Kapton ® HN film, developed by Dupont ™, is a flexible polyimide film which remains durable from -269°C to +400°C temperature. It is preferred for printing flexible electronics and aircrafts, space-crafts and any high vacuumed environment. In this work it is used due to its low adhesion to cross-linked SU-8 and as explained below the structures fabricated on it have better resolution.

Low adhesion between SU-8 and Kapton creates the opportunity to fabricated multi layered devices as demonstrated by Agirregabiria et al. in 2005 [92]. The 125μm thick version of Kapton film is used as a carrier for both the main and top parts of the SU-8 devices. During a previous research it was observed that SU-8 structures form better on a Kapton film than on a glass wafer [106]. This is mainly because of Snell's law ($n_1 \sin \theta_1 = n_2 \sin \theta_2$). The refractive index of each material are: $n_{Glass} = 1.47$, $n_{SU\text{-}8} = 1.67$ (at UV light), $n_{Kapton} = 1.70$. When the UV light is exposed at 90° at a contact lithography travel through the SU-8 with $\theta_{SU\text{-}8} = 39.92°$ refraction angle, but with glass wafer this is $\theta_{Glass} =$

46.45° and with 125 μm thick semi-transparent Kapton film it is θ_{Kapton} = 39.11°. Fabrication on Kapton film creates better cross sectional geometry than fabricating on glass.

6.3.3 Bonding process:

Delicately fabricated micro and nano sized structures need to be carefully integrated to macro sized systems to gain functionality: this is a part of *Packaging Engineering*. The packaging of MEMS and NEMS is known as wafer bonding techniques, with adhesive bonding one of the techniques. A low temperature adhesive bonding of free standing SU-8 devices is demonstrated by Tuomikoski et al. in 2005 [93]. That work was carried at 68°C, and to increase the impact of bonding, pressure has been applied with tweezers during the procedure. They were aware that the under cured SU-8 might fill into the channels they were trying to bond so they incorporated moat channels into their mask design. These moat channels are clearly visible in Figures 37 and 38 in both sides of the main channel.

Wafer bonding enables complex three-dimensional structures fabrication and packaging (Bilenber et al.[90]; Gutierrez-Riveral et al.[101]; Mitri et al. [102]; and Niklaus et al. [104]) Adhesive bonding is also referred as gluing since an intermediate layer is used to bond the two layers of structures and most commonly used materials are SU-8 and BCB (Benzocyclobuten). Important process parameters can be grouped into two. The first group is related to the adherent materials properties, which are: uniform coating thickness, bonding temperature, bonding pressure. The second group is more focused on the materials to be bonded, the interaction of the adherent with them by heat and pressure.

Basically the process includes heat, time and pressure elements and good adhesive bonding can be achieved by good curing.

Good curing means achieving good bonding strength between the adherent and the substance. The most common procedure is to evenly spread the adherent on to one or both of the substrates and bring into contact and clamp them to apply an even pressure. Also depending on the adherent there might be heating, and UV light curing might be involved. The main advantage of adhesive bonding is that it can cut the costs of high temperature, pressure and longer waiting times. But all these can turn into disadvantages: when a good bonding is not achieved, or a short life-time of the bonded structure is obtained or limited heat resistance of the end product. Figure 31 is the schematics of a free standing, all SU-8 microfluidic device.

For the case of microfluidics the adhesive bonding is very sensitive and important because you need to deliver the liquids into the microchip through the interconnections without any leakage. Also in the case of parallel, multilayer structured devices there should be no contamination within the microfluidic device between the channels. Good quality uniform bonding has to be achieved in a bigger area than any MEMS / NEMS devices with an opening to attach interconnections without any breakage or clogging. As is mentioned in Section 6.2, PC, PDMS, PMMA and SU-8 are commonly used polymeric materials in microfluidics. PC, PDMS and SU-8 are generally sealed by adhesive bonding and PMMA prefers thermal bonding.

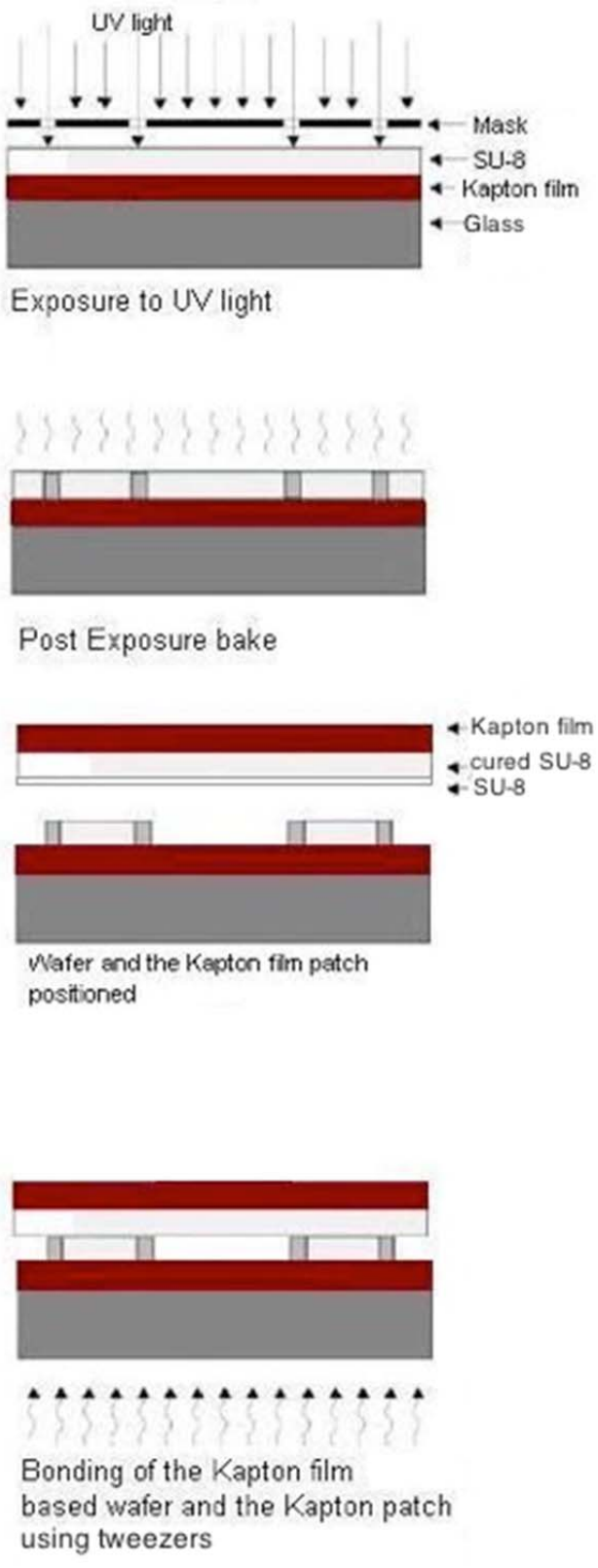

Figure 31: Fabrication schematics of free standing, all SU-8 microfluidic devices.

Chapter 7

7. Rapid manufacturing of microfluidic devices with SU-8

Throughout this project we aimed to achieve results in the most economical way and with the simplest possible solutions. The motivation here is to fabricate a fully functioning microfluidic chip with a uniform technique in optimum time scale. Here we followed the route of generating several hundred well documented results to optimize the technique, to widen our vision and understand the real capacity of the materials we are using.

7.1 Design principles

The continuous flow of droplet generation at high frequency devices is an active research topic with a lot of interest due to the possible number of applications like PCR-on-a-chip device or fluidic based electronic circuit components. All these possibilities come to life through correct visualization of the chip followed by the execution – fabrication. The first learning step is the design, throughout this project there have been five different masks drawn. For each mask the experimental data collected helped to improve the subsequent mask. In this study we first fabricated T and Cross-junction microfluidic chips followed by Logic gate devices.

For the T and Cross-junction several dimensions were designed. Many dimensions from 50μm width to 150μm width parameters are used in designs. At the beginning of this project, we searched into the commercially available microfluidic products, their choice of material, fittings and their choice of packaging. Some of the companies whose

products we like are: Micronit Microfluidics, Dolomite and Translume. They all offer as well as custom made polymeric products, their main products were quartz / glass based.

It is a well-known fact that any glass and silicon microfluidic chip needs a surface treatment to reduce the absorption of fluids (Kopp et al. [105]). That is because the glass is a hydrophilic material. We bought some samples from Translume and Micronit. Translume's fluidic chip uses the luer-lock fittings directly glued on the inlets which avoid the problem of packaging but luer-lock connections have a big volume of fluid capacity for a microfluidic chip, in practice it is not preferred. Micronit Fluidics and Dolomite both offer better and sophisticated products. We choose Micronit Fluidics for two reasons: (1) flexible variety set of connectors like Upchurch Chromatography fittings and (2) Fluidic Connect 4515 Chipholder (Figure 32) which allows you to use it with a number of chips with the same base structure.

Figure 32: Micronit Microfluidics, Fluidic Connect 4515 Chipholder.

The design of this chip-holder is the cause of the first limitation on the design feature. For experimental purposes we need to be able to clearly

see the T-junction and cross-junction areas where the droplet forms. Micronit microfluidics chip droplet generator was located 7.5 mm × 7.5 mm away in the X (horizontal) and Y (vertical) direction from the left hand side midpoint of the chip. It was not visible due to the chip-holder design; thus in our chips we shifted it in the X direction to 13.5mm so our optical systems could observe it.

The second limitation on the design feature was the power of the UV light machine Tamarack. Traditionally this device is used to fabricate MEMS components which are smaller in size compared to microfluidic devices. The deep and narrow channels are harder to fabricate. Despite the fact 50μm and 60μm wide channels were designed, but deep structures were not successfully fabricated due to the limitations mentioned previously.

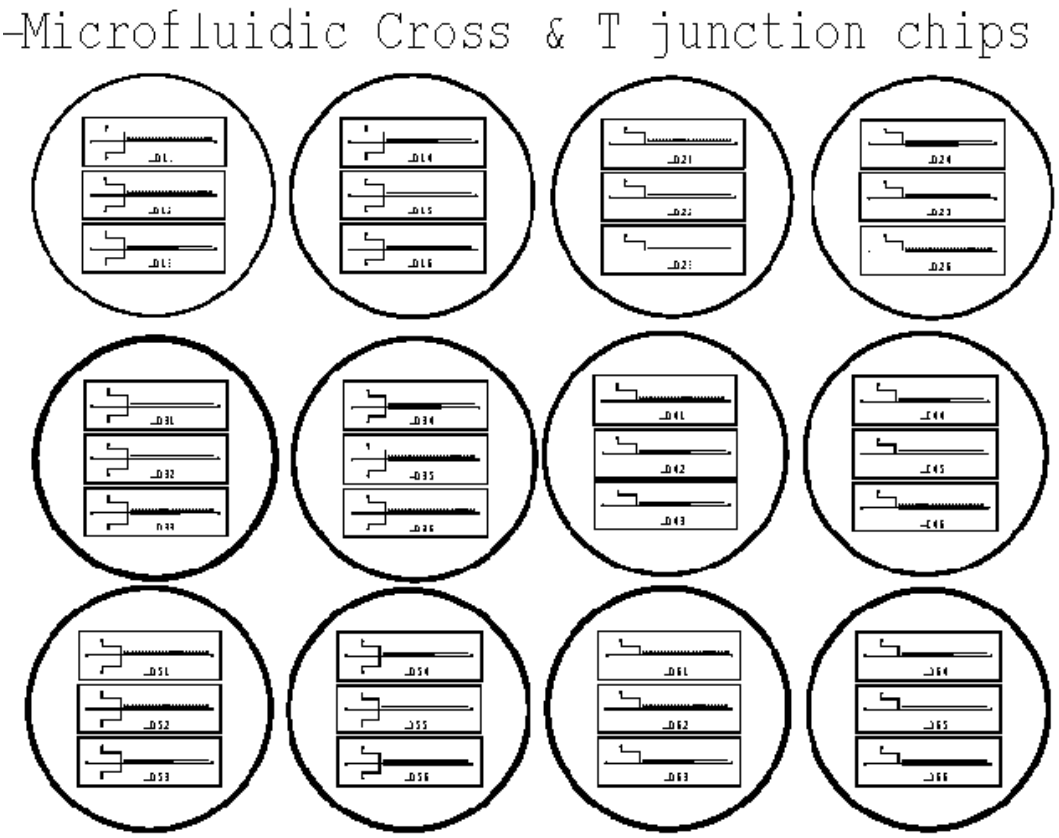

Figure 33: An example for a mask design.

The first mask aimed to understand the fabrication capabilities, so it consisted of three T-junction and three Cross-junction designs (Figure 33). The second mask was a prototype for a PCR application using logic gates for separation and T and Cross junction devices with a moat channel for improved bonding structure. By the time of designing the third mask we decided to do multilayer fabrication with interconnections on the chip. Finally masks four and five consisted of logic gate device variations. Throughout this project all designs contained a drawing of its name and a ruler within their structure (Figures 34 and 35). In the first mask design: those labelled 1X – 3X and 5X were Cross-Junction, while those labelled 2X – 4X and 6X were T-junction designs. Their dimensions are listed in Table 7. These masks were designed with the

aim of answering the questions like: is SU-8 65 the right material for fluidic structures? What dimensions are in our capability to manufacture?

Design name	Dimensions (µm)	
	w_d	w_c
Des 1X	50	50
Des 2X	50	50
Des 3X	100	100
Des 4X	100	100
Des 5X	150	150
Des 6X	150	150
Des 7X	100	80
Des 8X	100	60
Des 9X	150	100
Des 10X	150	80

Table 7: Dimensions of the designs on the mask.

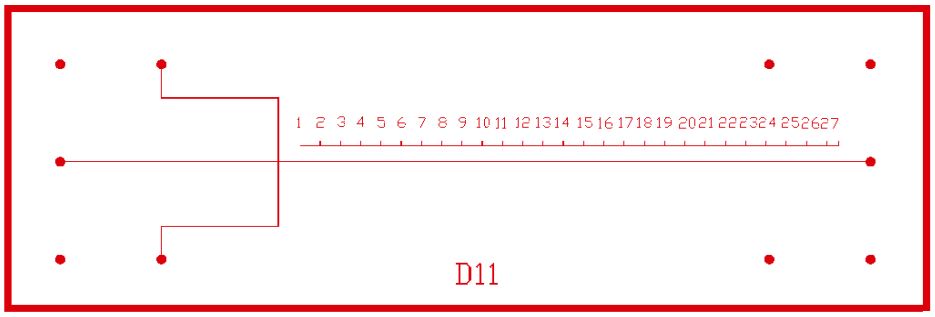

Figure 34: Details from first mask. Cross- junction device.

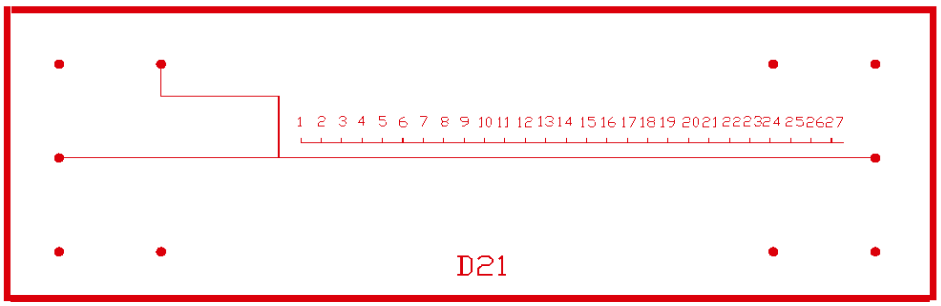

Figure 35: Details from first mask. T-junction device.

We also try to replicate the manufacture of the logic gates devices demonstrated by Prakash and Gershenfeld in 2007 [19]. Figure 36 and Figure 43 are examples of logic gate devices in action. The video from which Figure 36 is taken can be viewed at http://goo.gl/91nAeV.

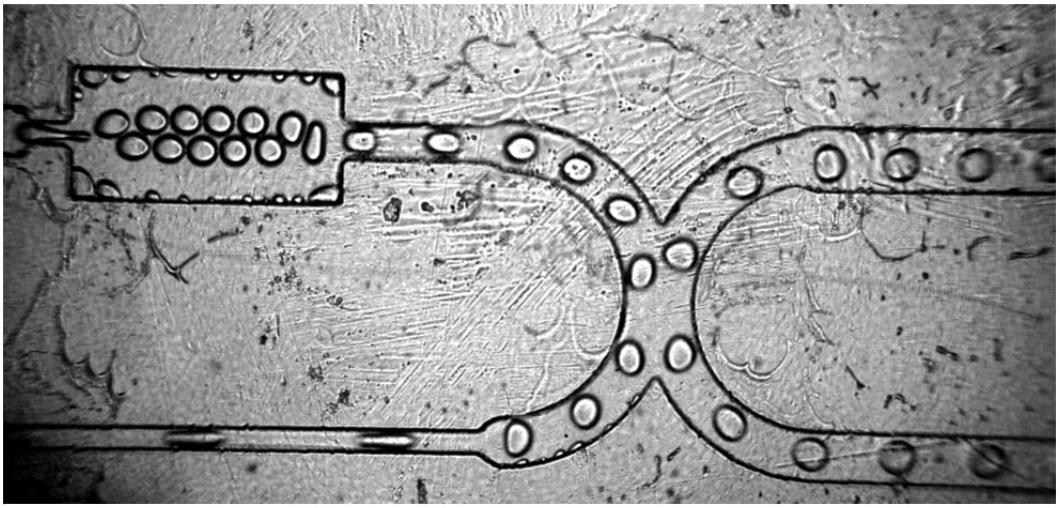

Figure 36: An AND/OR Gate designed and manufactured by the author.

7.2 Experimental results

In this research SU-8 3000 is used on SU-8 65 to achieve good bonding. Because it is the same material and continuous fabrication process, it did not need to have plasma surface treatment, which all other polymeric materials must have for good quality bonding.

As previously mentioned five Polyester Film Photo masks were designed using L-Edit, a Tanner EDA mask editor programme, and commercially printed by the company JD Photo with a 64000 dpi resolution.

One of the main concerns of this research was looking into fabricating polymeric microfluidic devices in various dimensions. From a variety of fabrication methods we chose UV photo-lithography and SU-8 as the medium. Using this material and method we managed to fabricate structures from tens of microns high to hundreds of microns high.

As we mentioned in the previous section, the inlets of the devices were printed as the first layer by the help of a mask. The main structure manufactured on top of this layer was using another mask and in some examples we have manufactured a third layer of increasing the depth of the certain areas in the design. When we use this third layer mask, it is used after the inlets mask. The reason for this is that the development is the final stage in fabricating open top fluidic structures and removes the parts that the UV light has not cured. Also the SU-8 is a transparent material and would pass the UV light to below level. So when designing the multi-level structure masks one should always have to build on the previous layers mask and this approach would be beneficial to place the guidance structures.

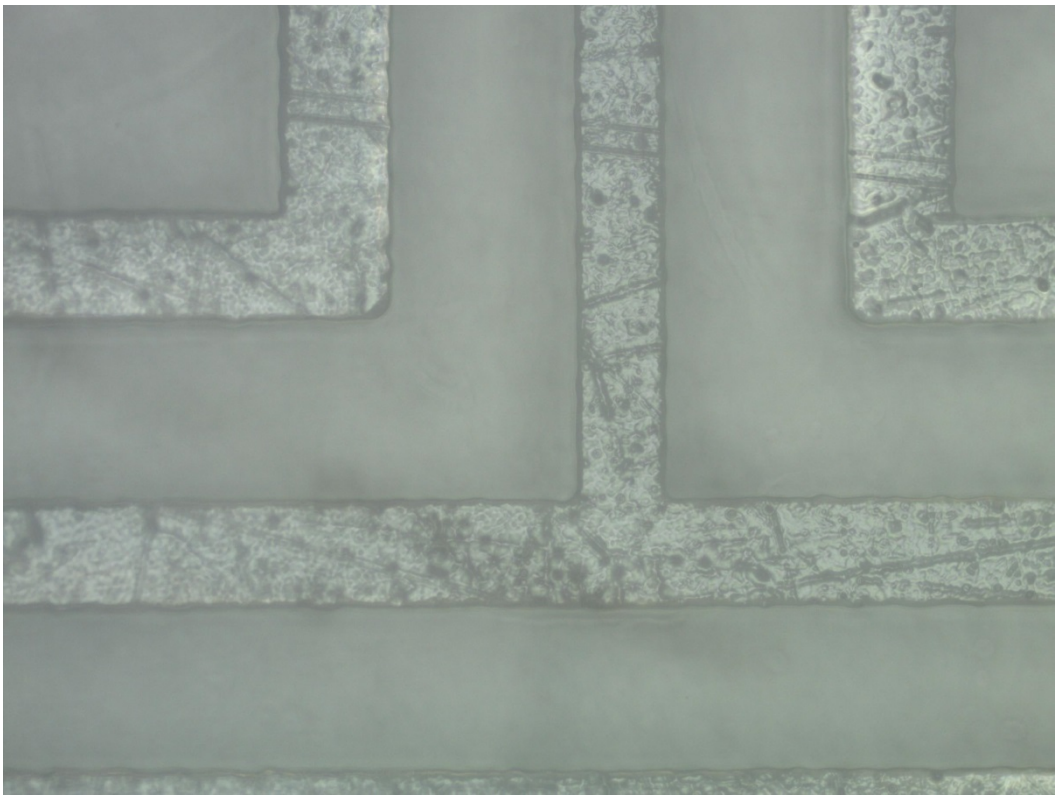

Figure 37: Detail from a T-junction fluidic device.

In the early stages the channels were manufactured on three-inch glass wafers and three-inch sized Kapton films. Later on we used glass slides, Lexan and PVC cuts to fabricate on. During the research, we undertook several options like fabricating the structures directly on inlet drilled Lexan and PVC pieces. For this purpose we used an upright drill. Despite the fact the inlets were de-burred and polished neatly, during the fabrication these pieces turned out to be an unsuccessful choice for micro device fabrication. The failure was caused by two reasons, the inlets either filled in with SU-8 or SU-8 created an orifice around it by the end of the spinning cycle. Silicon, or Pyrex glass structures can be used to build on but they need to be drilled previously and this process is costly. Also it is observed that

the structures on glass substrates are more brittle since the glass suspends their movement.

The fabrication steps in Section 6.3 are always followed as the guidelines for each device but the changing parameters created the variety of depths from 12µm to 375µm depth in single layered structures.

Figure 38: SEM image of a T-junction fluidic device. Its design name is D22, width of the channels are 50µm.

We choose to fabricate free standing devices, and to do that first we needed to attach the Kapton film to another surface which the spin coater can hold without bending. It is better to use an out of date version SU-8 for this because during the development stage this adhesive stays under the Kapton film, meaning that it is not cured, and so would be developed and removed without any difficulty.

7.2.1 Fabrication parameters

After looking into the manufacturers' fabrication methodology, one always has to work out the actual operational parameters. This is mainly due to the device you are trying to build. If you are fabricating cantilever [86], big reservoir [93] or obstacles in a wide channel [96], it is better to reduce the time for development and exposure of the structures. On the other hand if you are fabricating narrow but deep channels which have high aspect ratio then you need to increase and optimize the parameters. By adopting our fabrication parameters we managed to achieve a fully sealed and fully functioning, free standing SU-8 microfluidic chips. The other important achievement was to be able to manufacture a fully working microfluidic chip in less than two hours.

We looked into other studies to understand and design our own fabrication parameters. The first group we read had published many journal papers, including Ruano-Lopez et al. [97]; Blanco et al. [89]; Agirregabiria et al. [92]; Agirregabiria et al. [95]; and Fernandez et al. [100]. They have demonstrated successfully fabricated devices, using SU-8 50. The fabrication parameters they adopt in most cases are using low exposure dosage which has positive impact on bonding which we will discuss in the next section. The two spin coating parameters they used are 3000rpm and 5000rpm followed by soft bake 6 min at 65°C and 20 min at 90°C for the first one and 7 minutes at 90°C for the second, exposed to UV light with the dosage of 150mJ/cm^2 and 130mJ/cm^{2}consecetively. Finally post baked by 1 min at 65°C and 7 min at 90°C and 3 min at 90°C resulted with 30µm and

20µm depth in their structures. In their various works, they used Kapton film as the carrier phase. The idea of using a low adhesion material has been demonstrated by Steigert et al.[99] as well: instead of Kapton film they used 100µm thick Polyester (PET) film. Their structures are fabricated separately: bottom one is built on a metallized (Ti/Au) silicon or pyrex wafer, and the top one is on handling wafer attached with PET film. They use SU-8 3025 and 3050 of the 3000 series which has better adhesion properties. As with the first group they go for low exposure dosage of UV light, 120-180mJ/cm^2 and they fabricate structures around 25µm depth.

In 2007 Chen et al. [98] showed in their experiments that changing the concentration of the surfactant in SU-8 25 and 50, and achieve structures around 40µm depth. Another group who inspired our research published the following papers: Tuomikoski and Fransilla [91]; Tuomikoski and Fransilla [93]; Sikanen et al. [94]. Their fabrication parameters are not as detailed in the publications but it is mentioned that SU-8 50 and SU-8 100 were used to fabricate structures in a range of 10 µm depth to 500 µm depth. Another important difference in their work is the high exposure dosage they use 800-1500 mJ/cm^2.

Our chips were built as two separate structures and in the final stage they are bonded permanently. The top layer is called the structure and the bottom layer is called the cover. The structure layer is built on Kapton film and the first part of it is the interconnections, meaning the inlets and the outlets of the microfluidic chip. This is a simple

layer fabricate, it needs to be thick and smooth. Ideally a more viscous version of SU-8 can be used to build this layer. If or when that is preferred, the development time should be tested. Some thick structures needs higher exposure dosage and longer development and that can damage the layers built on top of the initial layer.

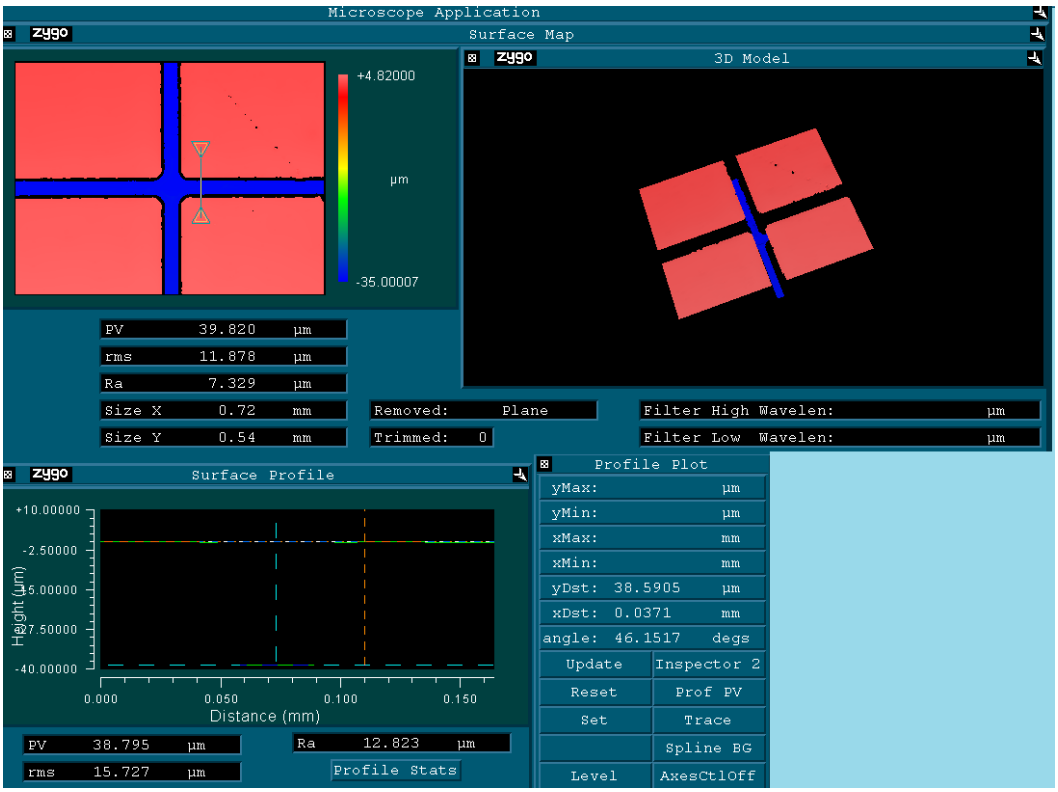

Figure 39: Example Measurement with Zygo.

We created and followed a very strict routine for this layer fabrication: 1000 rotations per second of SU-8 65 formulation on a Kapton film followed by soft baking stage - 5 minutes at 65°C and 20 minutes at 95°C. For cooling down to room temperature all substrates were rested 10 minutes which is followed by UV light exposure dosage of 400mJ/cm^2 using i-line filter. Then post exposure bake 1 minute at 65°C and 6 minutes at 95°C. After the substrate cooled down to room temperature it is developed approximately 4 minutes

30 seconds. A datasheet of the fabrication parameters is presented in Appendix E.

The quality of fabrication was initially checked in the laboratory with Zygo, an interferometer microscope (an example structure is in Figure 39). An image with a dark-field image microscope is in Figure 37. Some structures observed with SEM imaging in Figure 38.

Fabrication Steps	Process time (min)
Main Structure	
Wafer cleaning (Kapton film at 200^{O}C)	5
Dehydration bake at 200^{O}C	60
Cooling	5
Spincoating (Kapton film to glass wafer)	2
Soft bake	9
Cooling	5
Spincoating 1st layer (inlets)	2
Soft bake	25
Cooling	10
Exposure	2
Spincoating 2nd layer (main channels)	2
Soft bake	7
Cooling	10
Development	5 to 25
Bonding	2
Exposure	2
Total	153 to 173

Table 8: The approximate timeline of fabrication the main structure

Table 8 and Table 9 list the steps of chip fabrication with the processing time.

7.2.2. Bonding procedure

The next step for a functioning microfluidic device is to seal the open structures fabricated previously. There are a few types of bonding techniques used for SU-8 structures. We used a low temperature and have managed a good quality bonding using SU-8 3000 as the adhesive glue. Similar to the main structure fabrication, first a thick layer of carrier level is fabricated on Kapton film. The top level spin coated with SU-8 65, 1000 rotation per second followed by soft baking stage, 5 minutes at 65°C and 30 minutes at 95°C. It is very important that the top level fully cures, that is the reason why we baked it longer at 95°C.

Fabrication Steps	Process time (min)
Bonding Layer	
Spincoating (Kapton film to glass wafer)	2
Soft bake	9
Spincoating (fully cured SU-8 wall)	2
Soft bake	35
Exposure	2
Spincoating (bonding layer)	2
Soft bake	5
Total	57

Table 9: The approximate timeline of fabrication the bonding layer

The bonding layer was spin coated at 2000 rotation per second, followed by soft baking procedure, 1 minute at 65°C and around 2:50 to 3:10 minutes at 95°C on a hot plate. The soft baking time on 95°C hot plate is a dynamic decision, because we do not want the bonding

layer to be too dry or too wet and the other samples using the hot plate may not be uniform the surface temperature of the hot plate.

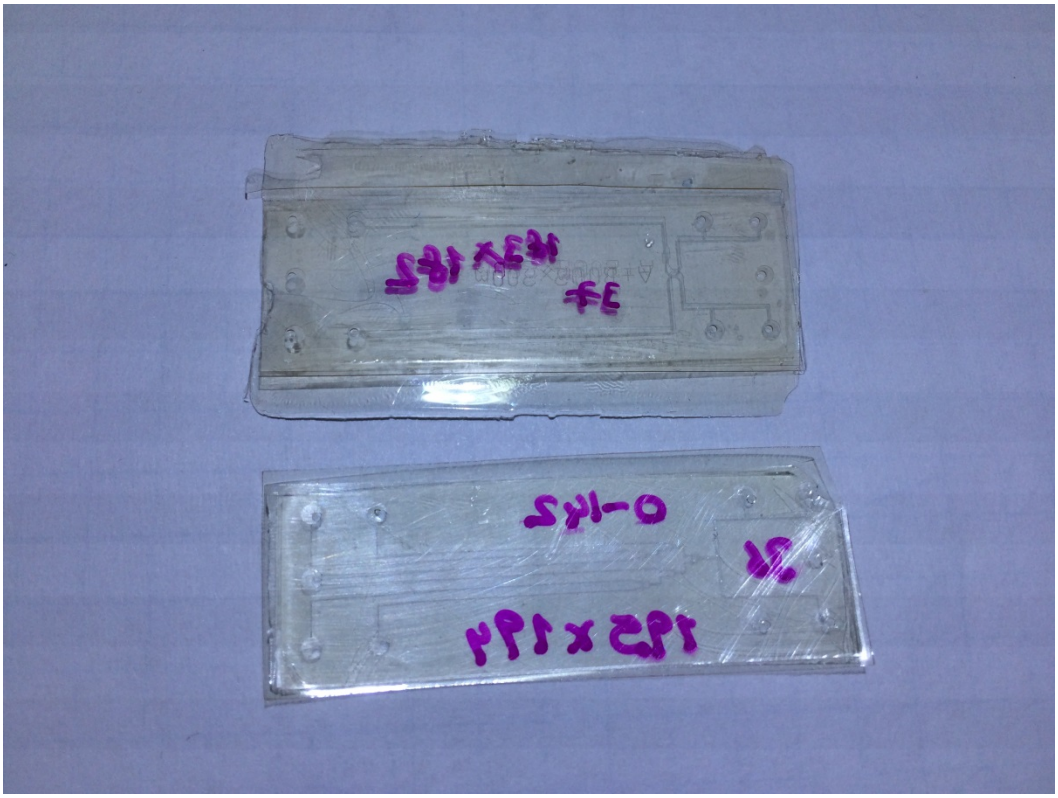

Figure 40: Some fully bonded free standing SU-8 microfluidic devices.

The Kapton film with the main channels was warmed up using a metal weight, the temperature of the weight is around 50°C ± 5°C. This is done to reduce bonding failure, both Kapton film and developed SU-8 becomes smoother under low temperature. We warmed up some main channels on 65°C, which was observed to be too warm and thus the bonding failed due to the SU-8 filling in the channels. When both top and bottom wafers are ready, we brought the structures in contact and slightly pressed with a finger. It does not need much pressure - the pressure is to avoid any bubbles and reduce the possibility of unbounded areas due to the surface irregularities. At this point the bonding immediately occurs but we need to peel off

the Kapton film on the bottom layer and expose the bonded structure to UV light exposure a low dosage of 400mJ/cm2 using i-line filter. In Figure 40 we demonstrate fully bonded, free standing SU-8 devices. To reduce a mix up they are labelled with a felt pen. The top one is design 37, with the dimensions of 183µm X 182µm in the T-junction area. The bottom one is design 36, with the dimensions of 195µm X 194 µm in the T-junction area.

7.2.3. Packaging

Manufacturing free standing polymeric chips has its own issue: the packaging. Our free standing chips are rather thin, and brittle which makes it hard to glue tubing to its inlet and outlets. We decided to build a chip-holder where we can clamp the SU-8 devices without breaking.

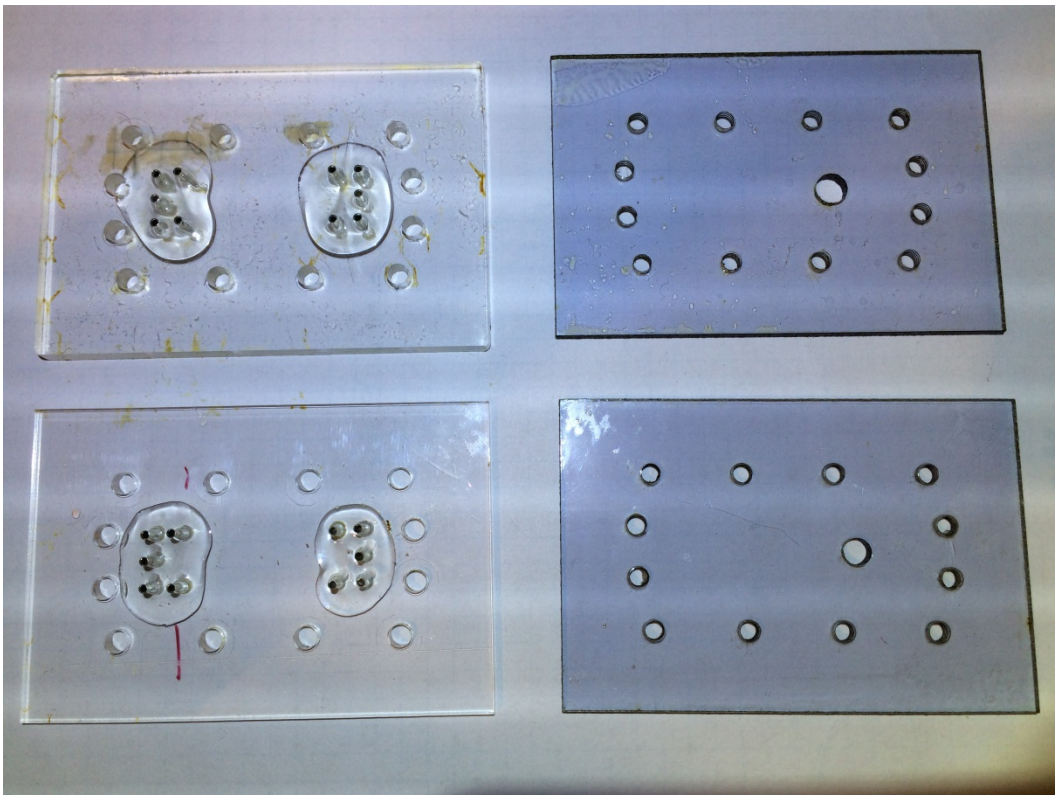

Figure 41: Top and bottom layers of the chip-holder.

Figure 41 is a picture of the chip-holders before assembly. At the left hand side of the picture we see the PC (Polycabonate) as the top layer. We used 3mm and 5mm thick PC. At the right hand side we see the bottom layer cut off from 3mm and 5mm PVC material. To plug the tubing we drilled interconnection holes and attached bootlace ferrules and to make this structure strong and leak free we used NOA68 UV light curable glue. This is done to reduce areas not visible. But any observations of a microfluidic device require a short distance between the sample and the optical lens. That is something to be improved in the design of our chip-holder.

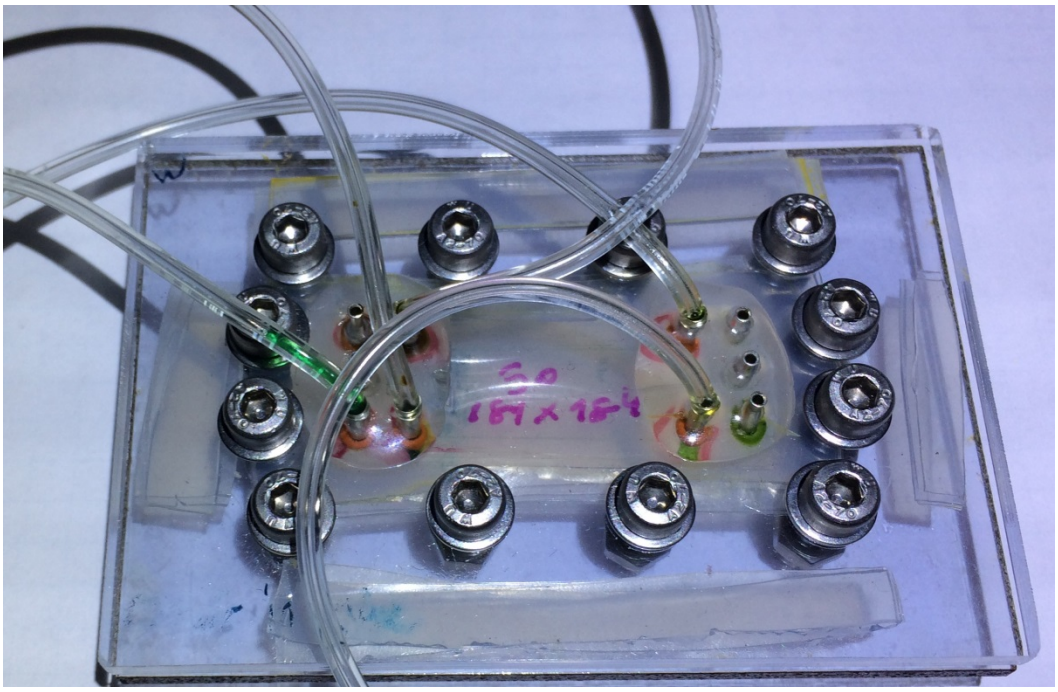

Figure 42: Assembled chip-holder.

In Figure 42, we observe a free standing SU-8 chip fitted in a chip-holder and ready to use. At this point the chip is sandwiched between layers of silicone tape. This silicone tape protects the chip from breaking but also creates O-ring like structure around the interconnections.

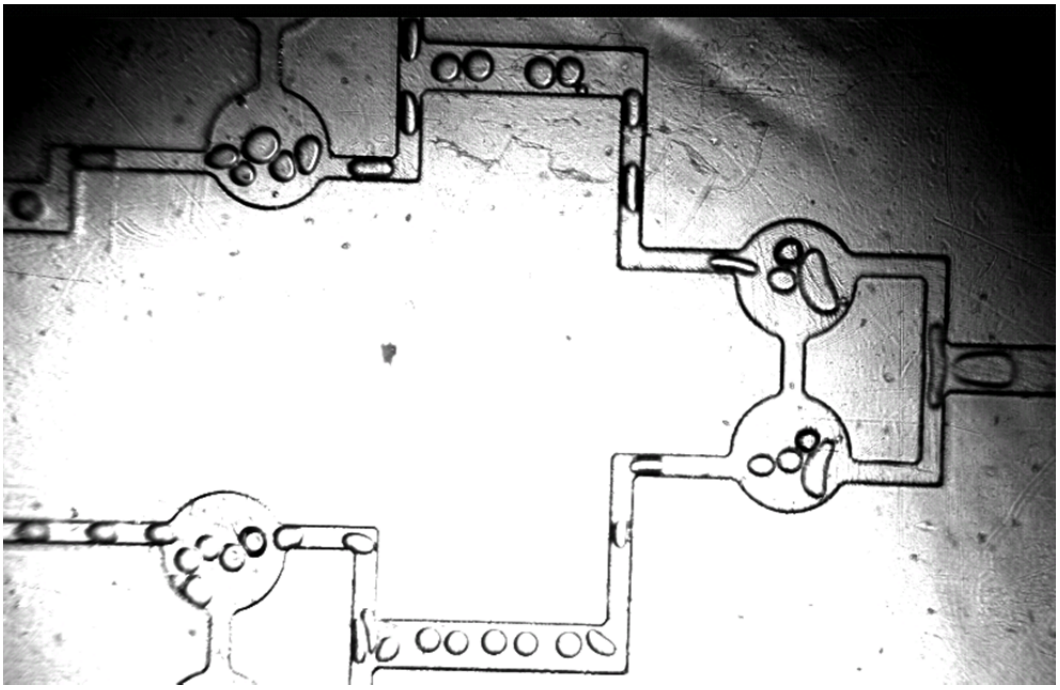

Figure 43: An attempt to fabricate a flip-chip.

Figure 43, is one of our chips: fabricated, bonded and ready for experiments. Unfortunately there was a leak at the inlets, and also the design was not right. Looking through the video from which Figure 43 was extracted, it is obvious that the dispersed phase channel needs to be wider to generate bigger sized water droplets.

7.3 Conclusion

SU-8 is a delicate and unreliable material for mass production but we have demonstrated that it can be the material for niche, complicated structured and individually built products. Gut [103], looks in to the attenuation of scattered light on SU-8 structures and finds the attenuation of light in SU-8 structures are rather small so it is feasible for fabricating optical sensors. In the chapter we went through the steps of design, fabrication, bonding and packaging. In bonding we

demonstrated a new improved bonding technique. With carefully planned use of equipment Table 8 and Table 9 processes were carried out in parallel time, so all process of prototyping a fully functioning free standing SU-8 microfluidic chip were achieved in between 153 to 173 minutes in 12μm to 375μm channel depth. We also fabricated the structures demonstrated by Prakash [19] but although they worked, they showed design failures.

Chapter 8

8. Future research

As the review articles mentioned above [11, 14, 48, 52, 72, 80] show that microfluidics has great potential for simple but efficient medical, biological, and chemical applications.

In the first part of this thesis, as the end user, we conducted experiments using microfluidic chips manufactured by us. The ratios that we had planned for the chips were different to those which we ended up with; but we decided to continue with the available devices. Our chips have very similar continuous and aqueous channel width but different depths at the T-junction and at the expansion areas; we documented similar trends in droplet size against the capillary number and the flow rate ratio. We think the most interesting area of future work would be experimenting with deeper structures.

When we were studying the scaling law, we choose the maximum values of oil flow rate 1.2ml/hr. Because we measured the size of the droplet at the expansion channel we preferred the droplets to be in either single or double single profile flow pattern so they can be in spherical shape. By using wider and deeper structured chips the experiment can be conducted in higher oil flow rate.

In the second part of the thesis we manufactured polymeric microfluidic chips. There are a variety of materials that may be used to fabricate chips [84], and the main challenge is packaging. For SU-8 structures it is important to keep in mind their brittle nature and we

suggest a fruitful path for continued development would be a chip holder which might apply uniform pressure throughout. This can be achievable with thin glass or Pyrex slides, possibly with the interconnections drilled on them.

Bibliography

[1] R. Feynman. *There's plenty of room at the bottom [data storage]*. Journal of Microelectromechanical Systems, 1(1): 60–66. IEEE, 1992. Reprint of a lecture from 29 Dec 1959. https://dx.doi.org/10.1109%2F84.232589

[2] H. Fujita. *Future of actuators and microsystems*. Sensors and Actuators A: Physical, 56(1-2): 105-11. Elsevier, 1996. http://dx.doi.org/10.1016/0924-4247(96)01282-4

[3] A. Manz, C.S. Effenhauser, N. Burggraf, D.J. Harrison, K. Seiler and K. Fluri. *Electroosmotic pumping and electrophoretic separations for miniaturized chemical-analysis systems*. Journal of Micromechanics and Microengineering, 4(4): 257-265. IOP, 1994. http://dx.doi.org/10.1088/0960-1317/4/4/010

[4] S.C. Terry, J. H. Jerman and J. B. Angell. *A gas chromatographic air analyzer fabricated on a silicon wafer*. IEEE Transactions on Electron Devices, 26(12), 1880-1886. IEEE, 1979. http://dx.doi.org/10.1109/T-ED.1979.19791

[5] H.P. Le. *Progress and Trends in Ink-jet Printing Technology*. Journal of Imaging Science and Technology, 42(1): 49-62. Society for Imaging and Technology, 1998.

[6] A. Manz , N. Graber, H.M. Widmer. *Miniaturized total chemical analysis systems: A novel concept for chemical sensing*. Sensors and Actuators B: Chemical, 1(1-6): 244-248. Elsevier, 1990. http://dx.doi.org/10.1016/0925-4005(90)80209-I

[7] H.T.G. van Lintel, F.C.M. Vandepol and S. Bouwstra. *A piezoelectric micropump based on micromachining of silicon*. Sensors and Actuators, 15(2): 153-167. Elsevier, 1988. http://dx.doi.org/10.1016/0250-6874(88)87005-7

[8] V. Gass, B.H. Vanderschoot, S. Jeanneret and N.F. Derooij. *Integrated flow-regulated silicon micropump* . Sensors and Actuators A: Physical, 43(1-3), 335-338. Elsevier, 1994. http://dx.doi.org/10.1016/0924-4247(93)00703-7

[9] S. Shoji, M. Esashi and T. Matsuo. *Prototype miniature blood gas analyser fabricated on a silicon wafer*. Sensors and

Actuators, 14(2): 101-107. Elsevier, 1988. http://dx.doi.org/10.1016/0250-6874(88)80057-X

[10] D.B. Weibel and G.M. Whitesides. *Applications of microfluidics in chemical biology*. Current Opinion in Chemical Biology, 10: 584-591. Elsevier, 2006. http://dx.doi.org/10.1016/j.cbpa.2006.10.016

[11] S. Shoji and M. Esashi. *Microflow devices and systems*. Journal of Micromechanics and Microengineering, 4(4): 157–171. IOP, 1994. http://dx.doi.org/10.1088/0960-1317/4/4/001

[12] D.J. Laser and J.G. Santiago. *A review of micropumps*. Journal of Micromechanics and Microengineering, 14(6): R35–R64. IOP, 2004. http://dx.doi.org/10.1088/0960-1317/14/6/R01

[13] P. Woias. *Micropumps—past, progress and future prospects*. Sensors and Actuators B: Chemical, 105(1): 28–38. Elsevier, 2005. http://dx.doi.org/10.1016/j.snb.2004.02.033

[14] P. Gravesen, J. Braneberg and O.S. Jensen. *Microfluidics - a review*. Journal of Micromechanics and Microengineering, 3(4): 168-182. IOP, 1993. http://dx.doi.org/10.1088/0960-1317/3/4/002

[15] H. Song, J.D. Tice, R.F. Ismagilov. *A microfluidic system for controlling reaction networks in time*. Angewandte Chemie Intl. Ed., 42: 768-772. Wiley, 2003. http://dx.doi.org/10.1002/anie.200390203

[16] D.J. Beebe, G.A. Mensing and G.M. Walker. *Physics and applications of microfluidics in biology*. Annual Review of Biomedical Engineering, 4: 261-286. Annual Reviews, 2002. http://dx.doi.org/10.1146/annurev.bioeng.4.112601.125916

[17] O. Reynolds. *An experimental investigation of the circumstances which determine whether the motion of water shall be direct or sinuous, and of the law of resistance in parallel channels.* Philosophical Transactions of the Royal Society of London, 174:935-982, 1883.

[18] I.E. Araci and S.R. Quake. *Microfluidic very large scale integration (MVLSI) with integrated micromechanical valves*. Lab Chip, 12, 2803- 2806. Royal Society of Chemistry, 2012. http://dx.doi.org/10.1039/C2LC40258K

[19] M. Prakash and N. Gershenfeld. *Microfluidic bubble logic*. Science, 315: 832-835. American Association for the Advancement of Science, 2007. https://dx.doi.org/10.1126/science.1136907

[20] P.G. de Gennes, F. Brochard-Wyart and D. Quere. Capillarity and wetting phenomena: drops, bubbles, pearls, waves. Springer-Verlag New York, 2003. http://dx.doi.org/10.1007/978-0-387-21656-0

[21] A. Pockels. *Surface Tension.* Nature 43: 437-439. Nature Publishing Group, 1891. http://dx.doi.org/10.1038/043437c0

[22] T.M. Squires and S.R. Quake. *Microfluidics: Fluid physics at the nanoliter scale*. Reviews of Modern Physics 77(3): 977-1026. American Physical Society, 2005. https://doi.org/10.1103/RevModPhys.77.977

[23] K. Wang and G. Luo G. *Microflow extraction: A review of recent development*. In Press: Chemical Engineering Science, 2016. http://dx.doi.org/10.1016/j.ces.2016.10.025

[24] T.R. Thorsen, W. Roberts, F.H. Arnold and S.R. Quake. *Dynamic pattern formation in a vesicle-generating microfluidic device*. Physical Review Letters 86(18): 4163-4166. APS Physics, 2001. https://dx.doi.org/10.1103/PhysRevLett.86.4163

[25] P.B. Umbanhowar, V. Prasad and D.A. Weitz. *Monodisperse emulsion generation via drop break off in a coflowing stream*. Langmuir 16(2): 347-351. ACS Publications, 2000. https://dx.doi.org/10.1021/la990101e

[26] T. Nisisako, T. Torii and T. Higuchi. *Droplet formation in a microchannel network*. Lab Chip 2:24–26. Royal Society of Chemistry, 2002. https://dx.doi.org/10.1039/B108740C

[27] J.D. Tice, H. Song, A.D. Lyon and R.F. Ismagilov. *Formation of droplets and mixing in multiphase microfluidics at low values of the Reynolds and the Capillary numbers*. Langmuir 19:9127–9133. ACS Publications, 2003. https://dx.doi.org/10.1021/la030090w

[28] J.D. Tice, A.D. Lyon, and R.F. Ismagilov. *Effects of viscosity on droplet formation and mixing in microfluidic*

channels. Analytica Chimica Acta 507: 73–77. Elsevier, 2004.
http://dx.doi.org/10.1016/j.aca.2003.11.024

[29] S.L. Anna, N. Bontoux and H.A. Stone. *Formation of dispersions using "flow focusing" in microchannels*. Applied Physics Letters 82(3): 364-366. APL, 2003.
http://dx.doi.org/10.1063/1.1537519

[30] V. Cristini and Y. C. Tan. *Theory and numerical simulation of droplet dynamics in complex flows - A review*. Lab on a Chip 4(4): 257-264. Royal Society of Chemistry, 2004.
http://dx.doi.org/10.1039/B403226H

[31] T. Nisisako, T. Torii and T. Higuchi. *Novel microreactors for functional polymer beads.* Chemical Engineering Journal 101(1-3): 23–29. Elsevier, 2004.
http://dx.doi.org/10.1016/j.cej.2003.11.019

[32] S. Sugiura, M. Nakajima and M. Seki. *Prediction of droplet diameter for microchannel emulsification: prediction model for complicated microchannel geometries*. Industrial and Engineering Chemical Research, 43(26): 8233–8238. ASC Publications, 2004.
http://dx.doi.org/10.1021/ie0494770

[33] B. Zheng, J.D. Tice, and R.F. Ismagilov. *Formation of arrayed droplets of soft lithography and two-phase fluid flow, and application in protein crystallization*. Advanced Materials, 16(15): 1365-1368. Wiley, 2004.
https://dx.doi.org/10.1002%2Fadma.200400590

[34] T. Ward, M. Faivre, M. Abkarian and H.A. Stone. *Microfluidic flow focusing: Drop size and scaling in pressure versus flow rate driven pumping*. Electrophoresis, 26(19): 3716–3724. Wiley, 2005.
https://dx.doi.org/10.1002/elps.200500173

[35] J.H. Xu, G.S. Luo, G.G. Chen and J.D. Wang. *Experimental and theoretical approaches on droplet formation from a micrometer screen hole*. Journal of Membrane Science 266(1-2): 121-131. Elsevier, 2005.
http://dx.doi.org/10.1016/j.memsci.2005.05.017

[36] P. Garstecki, A.M. Ganan-Calvoe and G.M. Whitesides. *Formation of bubbles and droplets in microfluidic systems*. Bulletin of the Polish Academy of Sciences, Technical

Sciences, 53(4): 361-372. 2005

[37] P. Garstecki, M.J. Fuerstman, H.A. Stone and G.M. Whitesides. *Formation of droplets and bubbles in a microfluidic T-junction–scaling and mechanism of break-up*. Lab Chip 6:437–446. Royal Society of Chemistry, 2006. https://doi.org/10.1039/B510841A

[38] T. Cubaud, M. Tatineni, X. Zhong and C.M. Ho. *Bubble dispenser in microfluidic devices*. Physical Review E, 72:037302. APS Physics, 2005. https://doi.org/10.1103/PhysRevE.72.037302

[39] P. Guillot and A. Colin. *Stability of parallel flows in a micro channel after a T junction*. Physical Review E, 72:066301. APS Physics, 2005. https://doi.org/10.1103/PhysRevE.72.066301

[40] T. van der Graaf, M.L.J. Steegmans, R.G.M. van der Sman, C.G.P.H. Schroen, R.M. Boom. *Droplet formation in a T-shaped microchannel junction: a model system for membrane emulsification*. Colloids Surf. A 266:106–116. 2005 http://dx.doi.org/10.1016/j.colsurfa.2005.06.019

[41] A. Gunther and K.F. Jensen. *Multiphase microfluidics: from flow characteristics to chemical and materials synthesis*. Lab on a Chip 6(12): 1487-1503. Royal Society of Chemistry, 2006. http://dx.doi.org/10.1039/B609851G

[42] J. Husny and J.J. Cooper-White. *The effect of elasticity on drop creation in T- shaped microchannels*. Journal of Non-Newtonian Fluid Mechanics, 137(1-3), 121-136. Elsevier, 2006. http://dx.doi.org/10.1016/j.jnnfm.2006.03.007

[43] S. van der Graaf, T. Nisisako, C.G.P.H. Schroen , R.G.M. van der Sman and R.M. Boom. *Lattice Boltzmann simulations of droplet formation in a T-shaped microchannel*. Langmuir 22: 4144–4152. ASC Publications, 2006. http://dx.doi.org/10.1021/la052682f

[44] H. Song, D.L. Chen and R.F. Ismagilov. *Reactions in Droplets in Microfluidic Channels*. Angewandte Chemie Intl. Ed. 45(44),7336–7356. Wiley, 2006. http://dx.doi.org/10.1002/anie.200601554

[45] J. Hua, B. Zhang and J. Lou. *Numerical simulation of microdroplet formation in coflowing immiscible liquids*. AIChE Journal, 53:2534–2548. Wiley, 2007. http://dx.doi.org/10.1002/aic.11287

[46] G.F. Christopher and S.L. Anna. *Microfluidic methods for generating continuous droplet streams*. Journal of Physics D: Applied Physics, 40(19): R319-R336. IOP, 2007. http://dx.doi.org/10.1088/0022-3727/40/19/R01

[47] L.H. Hung and A.P. Lee. *Microfluidic devices for the synthesis of nanoparticles and biomaterials*. Journal of Medical and Biological Engineering, 27: 1–6. Springer, 2007

[48] S.Y. Teh, R. Lin, L.H. Hung and A.P. Lee. *Droplet microfluidics*. Lab Chip 8: 198-220. Royal Society of Chemistry, 2008. http://dx.doi.org/10.1039/B715524G

[49] G.F. Christopher, N.N. Noharuddin, J.A. Taylor and S.L. Anna. *Experimental observations of the squeezing-to-dripping transition in T-shaped microfluidic junctions*. Physical Reviews E, 78: 036317. APS Physics, 2008. https://doi.org/10.1103/PhysRevE.78.036317

[50] J. Xu, S. Li, J. Tan, and G. Luo. *Correlations of droplet formation in T junction microfluidic devices: from squeezing to dripping*. Microfluidics to Nanofluidics 5(6): 711–717. Springer, 2008. https://doi.org/10.1007/s10404-008-0306-4

[51] J. Tan, J. Xu, S. Li and G. Luo. *Drop dispenser in a cross-junction microfluidic device: scaling and mechanism of break-up*. Chemical Engineering Journal, 136(2-3): 306–311. Elsevier, 2008. http://dx.doi.org/10.1016/j.cej.2007.04.011

[52] A. Huebner, S. Sharma, M. Srisa-Art, F. Hollfelder, J.B. Edel, and A.J. De Mello. *Microdroplets: a sea of applications?* Lab Chip 8:1244–1254. Royal Society of Chemistry, 2008. http://dx.doi.org/10.1039/B806405A

[53] P. Zhu, L. Wang. *Passive and active droplet generation with microfluidics: A review.* Lab on a Chip. In Press (published online). Royal Society of Chemistry, 2016. https://doi.org/10.1039/C6LC01018K

[54] M. De Menech, P. Garstecki, F. Jousse and H.A. Stone. *Transition from squeezing to dripping in a microfluidic T-*

shaped junction. Journal of Fluid Mechanics 595: 141–161. Cambridge University Press, 2008. https://doi.org/10.1017/S002211200700910X

[55] T. Fu, Y. Ma, D. Funfschilling and H.Z. Li. *Bubble formation and breakup mechanism in a microfluidic flow-focusing device*. Chemical Engineering Science, 64(10): 2392–2400. Elsevier, 2009. http://dx.doi.org/10.1016/j.ces.2009.02.022

[56] H.H. Liu and Y.H. Zhang. *Droplet formation in a T-shaped microfluidic junction*. Journal of Applied Physics, 106:034906. AIP, 2009. http://dx.doi.org/10.1063/1.3187831

[57] M. Steegmans, C. Schron and R. Boom. *Generalised insights in droplet formation at T-junctions through statistical analysis*. Chemical Engineering Science, 64(13):3042–3050. Elsevier, 2009. http://dx.doi.org/10.1016/j.ces.2009.03.010

[58] A. Gupta, S.M.S. Murshed and R.Kumar. *Droplet formation and stability of flows in a microfluidic T-junction*. Appl. Phys. Lett, 94(16): 164107. AIP, 2009. http://dx.doi.org/10.1063/1.3116089

[59] A. Gupta and R. Kumar. *Flow regime transition at high capillary numbers in a microfluidic T-junction: viscosity contrast and geometry effect*. Physics of Fluids, 22(12): 122001. AIP, 2010. http://dx.doi.org/10.1063/1.3523483

[60] J. Hong, M. Choi, J.B. Edel and A.J. DeMello. *Passive self-synchronized two-droplet generation*. Lab Chip 10: 2702–2709 . Royal Society of Chemistry, 2010. http://dx.doi.org/10.1039/C005136E

[61] T. Fu, D. Funfschilling and Y. Ma. *Scaling the formation of slug bubbles in microfluidic flow focusing devices*. Microfluidics and Nanofluidics, 8(4): 467-475. Springer, 2010. http://dx.doi.org/10.1007/s10404-009-0471-0

[62] P. Ozdemir, S. Mohr, C. Wang, M.T. Stickland, N.J. Goddard, P.R. Fielden, Y. Zhang. *Self-Organised Droplet Flow Patterns in Microchannels*. 2nd Micro and Nano Flows Conference West London, UK, 1-2 September 2009.

[63] P. England, H.H. Liu, Y.H. Zhang, S. Mohr, N. Goddard, P. Fielden, C.H. Wang. *Experimental study of droplet*

formation at microfluidic T-junctions. In: Proceedings of the second European conference on microfluidics — Microfluidics 2010, Toulouse, 8–10 Dec 2010, paper No. 187. 2010

[64] T.T. Fu, Y.G. Ma, D. Funfschilling, C.Y. Zhu and H.Z. Li. *Squeezing-to-dripping transition for bubble formation in a microfluidic T-junction*. Chemical Engineering Science 65(12): 3739-3748. 2010. http://dx.doi.org/10.1016/j.ces.2010.03.012

[65] N. Tarchichi, F. Chollet and J.F. Manceau. *New regime of droplet generation in a T-shape microfluidic junction*. Microfluidics and Nanofluidics, 14(1): 45-51. Springer, 2013. http://dx.doi.org/10.1007/s10404-012-1021-8

[66] H.H. Liu and Y.H. Zhang. *The mechanism of droplet formation in the squeezing regime in microfluidic cross-junction*. Physics of Fluids, 23:082101. AIP, 2011. http://dx.doi.org/10.1063/1.3615643

[67] J. Sivasamy, T. Wong, N. Nguyen and L.T. Kao. *An investigation of the mechanism of droplet formation in a microfluidic T-junction*. Microfludics and Nanofluidics, 11: 1-10. Springer, 2011. http://dx.doi.org/10.1007/s10404-011-0767-8

[68] T. Glawdel, C. Elbuken and C.L. Ren. *Droplet formation in microfluidic T-junction generators operating in the transitional regime. I. Experimental observations*. Physical Review E, 85: 016322. APS Physics, 2012. https://doi.org/10.1103/PhysRevE.85.016322

[69] T. Glawdel, C. Elbuken and C.L. Ren. *Droplet formation in microfluidic T-junction generators operating in the transitional regime. II. Modelling*. Physical Review E, 85: 016323. APS Physics, 2012. https://doi.org/10.1103/PhysRevE.85.016323

[70] T. Glawdel and C.L. Ren. *Droplet formation in microfluidic T-junction generators operating in the transitional regime. III. Dynamic surfactant effects*. Physical Review E, 85: 026308. APS Physics, 2012. https://doi.org/10.1103/PhysRevE.86.026308

[71] X. Li, F. Li, J. Yang, H, Kinoshita, M. Oishi and M. Oshima. *Study on the mechanism of droplet formation in T-junction microchannel*. Chemical Engineering Science, 69(1):

340-351. Elsevier, 2012.
http://dx.doi.org/10.1016/j.ces.2011.10.048

[72] T. Schneider, J. Kreutz and D.T. Chiu. *The potential impact of droplet microfluidics in biology*. Analytcial Chemistry, 85(7): 3476-3482. ACS Publications, 2013.
http://dx.doi.org/10.1021/ac400257c

[73] J.K. Nunes, S.S.H. Tsai, J. Wan and H. Stone. *Dripping and jetting in microfluidic multiphase flows applied to particle and fiber synthesis*. Journal of Physics D: Applied Physcis. 46(11), 1–20. IOP, 2013.
http://dx.doi.org/10.1088/0022-3727/46/11/114002

[74] J.D. Wehking, M. Gabany, L. Chew and R. Kumar. *Effects of viscosity, interfacial tension, and flow geometry on droplet formation in a microfluidic T-junction*. Microfluidics and Nanofluidics,16(3): 441–453. Springer, 2014.
http://dx.doi.org/10.1007/s10404-013-1239-0

[75] S. Bashir, J.M. Rees and W.B. Zimmerman. *Investigation of pressure profile evolution during confined microdroplet formation using a two-phase level set method*. International Journal of Multiphase Flow, 60(2014): 40-49. Elsevier, 2014.
http://dx.doi.org/10.1016/j.ijmultiphaseflow.2013.11.012

[76] Y. Lu, T. Fu, C. Zhu, Y. Ma and H.Z. Li. *Scaling of the bubble formation in a flow-focusing device: Role of the liquid viscosity*. Chemical Engineering Science, 105(2014): 213-219. Elsevier, 2014.
http://dx.doi.org/10.1016/j.ces.2013.11.017

[77] P.M. Korczyk, M.E. Dolega, S. Jakiela, P. Jankowski, S. Makulska and P. Garstecki. *Scaling up the throughput of synthesis and extraction in droplet microfluidic reactors.* Journal of Flow Chemistry, 5(2): 110-118. Akadémiai Kiadó, 2015.
http://dx.doi.org/10.1556/JFC-D-14-00038

[78] T. Fu and Y. Ma. *Bubble formulation and breakup dynamics in microfluidic devices: A review.* Chemical Engineering Science, 135(2015): 343-372. Elsevier, 2015.
http://dx.doi.org/10.1016/j.ces.2015.02.016

[79] T. Fu, Y. Ma, D. Funfschilling and H.Z. Li. *Dynamics of bubble breakup in a microfluidic T-junction divergence*.

Chemical Engineering Science, 66(2011): 4184-4195. Elsevier, 2011. http://dx.doi.org/10.1016/j.ces.2011.06.003

[80] S.L. Anna, *Droplets and Bubbles in Microfluidic Devices*. Annual Reviews in Fluid Mechanics, 48: 285-309. Annual Reviews, 2016. http://dx.doi.org/10.1146/annurev-fluid-122414-034425

[81] R.J Jackman, T.M. Floyd, R. Ghodssi, M.A. Schmidt and K.F. Jensen. *Microfluidic systems with on-line UV detection fabricated in photodefinable epoxy*. Journal of Micromechanics and Microengineering, 11: 263. IOP, 2001. http://dx.doi.org/10.1088/0960-1317/11/3/316

[82] S. Li, C.B. Freidhoff, R.M. Young and R. Ghodssi. *Fabrication of micronozzles using low-temperature wafer-level bonding with SU-8*. Journal of Micromechanics and Microengineering, 13: 732. IOP, 2003. http://dx.doi.org/10.1088/0960-1317/13/5/328

[83] K.B. Mogensen, J. El-Ali, A. Wolff, and J.P. Kutter. *Integration of polymer waveguides for optical detection in microfabricated chemical analysis systems*. Applied Optics, 42: 4072-4079. OSA Publishing, 2003. https://doi.org/10.1364/AO.42.004072

[84] P.N. Nge, C.I. Rogers, and A.T. Woolley. *Advances in Microfluidic Materials, Functions, Integration, and Applications*. Chemical Reviews, 113(4): 2550-2583. ACS Publications, 2013. https://doi.org/10.1021/cr300337x

[85] W. Hu and B. Yang and C. Peng and S.W. Pang. *Three-dimensional SU-8 structures by reversal UV imprint*. Journal of Vacuum Science & Technology B, 24: 2225-2229. AIP, 2006. http://dx.doi.org/10.1116/1.2335431

[86] Y.K. Yoon, J.H. Park and M.G. Allen. *Multidirectional UV Lithography for Complex 3-D MEMS Structures*. Journal of Microelectromechanical Systems, 15(5): 1121-1130. IEEE, 2006. http://dx.doi.org/10.1109/JMEMS.2006.879669

[87] MicroChem. Nano SU-8 2000 Negative Tone Photoresist Formulations 2035 - 2100, Microchem products guide. http://www.microchem.com/

[88] 2-Methoxy-1-Methylethyl Acetate (PGMA) Summary Risk Assessment Report, Case No: 108-65-6, EINECS No: 203-603-9, European Communities, 2006. https://echa.europa.eu/documents/10162/158513c7-4aa9-4dd1-a775-cf89d728a6b0

[89] F.J. Blanco, M. Agirregabiria, J. Garcia, J. Berganzo, M. Tijero, M.T. Arroyo, J.M. Ruano, I. Aramburu and K. Mayora . *Novel three-dimensional embedded SU-8 microchannels fabricated using a low temperature full wafer adhesive bonding*. Journal of Micromechanics and Microengineering, 14: 1047. IOP, 2004. http://dx.doi.org/10.1088/0960-1317/14/7/027

[90] B. Bilenberg, T. Nielsen, B. Clausen and A. Kristensen. *PMMA to SU-8 bonding for polymer based lab-on-a-chip systems with integrated optics*. Journal of Micromechanics and icroeMngineering, 14: 814. IOP, 2004. http://dx.doi.org/10.1088/0960-1317/14/6/008

[91] S. Tuomikoski and S. Franssila. *Wafer-Level Bonding of MEMS Structures with SU-8 Epoxy*. Physica Scripta, 2004: 223. IOP, 2004. http://dx.doi.org/10.1088/0031-8949/2004/T114/056

[92] M. Agirregabiria, F.J. Blanco, J. Berganzo, M.T. Arroyo, A. Fullaondo, K. Mayoraa and J.M. Ruano-Lópeza. *Fabrication of SU-8 multilayer microstructures based on successive CMOS compatible adhesive bonding and releasing steps*. Lab Chip, 5: 545-552. Royal Society of Chemistry, 2005. http://dx.doi.org/10.1039/B500519A

[93] S. Tuomikoski and S. Franssila. *Free-standing SU-8 microfluidic chips by adhesive bonding and release etching*. Sensors and Actuators A: Physical, 120(2): 408-415. Elsevier, 2005. http://dx.doi.org/10.1016/j.sna.2005.01.012

[94] T. Sikanen, S. Tuomikoski, R.A. Ketola, R. Kostiainen, S. Franssilab and T. Kotiaho. *Characterization of SU-8 for electrokinetic microfluidic applications.* Lab on a Chip, 5: 888-896. Royal Society of Chemistry, 2005. http://dx.doi.org/10.1039/B503016A

[95] M. Agirregabiria, F.J. Blanco, J. Berganzo, A. Fullaondo, A.M. Zubiaga, K. Mayora and J.M. Ruano-López.

SDS-CGE of proteins in microchannels made of SU-8 films. ELECTROPHORESIS, 27: 3627–3634. Wiley, 2006. http://dx.doi.org/10.1002/elps.200600103

[96] H. Sato, H. Matsumura, S. Keino and S. Shoji. *An all SU-8 microfluidic chip with built-in 3D fine microstructures*. Journal of Micromechanics and Microengineering, 16(11): 2318. IOP, 2006. http://dx.doi.org/10.1088/0960-1317/16/11/010

[97] J.M. Ruano-Lopez, M. Aguirregabiria, M. Tijero, M.T. Arroya, J.Berganzo, I. Aranburu, F.J. Blanco, K. Mayora. *A new SU-8 process to integrate buried waveguides and sealed microchannels for a Lab-on-a-Chip*. Sensors and Actuators B, 114,542-551. Elsevier, 2005. http://dx.doi.org/10.1016/j.snb.2005.05.011

[98] Y.T. Chen and D. Lee. *A bonding technique using hydrophilic SU-8*. Research Express@NCKU, 8(4). 2009. http://research.ncku.edu.tw/re/articles/e/20090410/5.html

[99] J. Steigert, O. Brett, C. Müller, M. Strasser, N. Wangler, H. Reinecke, M. Daub and R Zengerle. *A versatile and flexible low-temperature full-wafer bonding process of monolithic 3D microfluidic structures in SU-8*. Journal of Micromechanics and Microengineering, 18: 095013. IOP, 2008. http://dx.doi.org/10.1088/0960-1317/18/9/095013

[100] L.J. Fernández, A. Altuna, M. Tijero, G. Gabriel, R. Villa, M.J. Rodríguez, M. Batlle, R. Vilares, J. Berganzo and F.J. Blanco. *Study of functional viability of SU-8-based microneedles for neural applications*. Journal of Micromechanics and Microengineering, 19: 025007. IOP, 2009. http://dx.doi.org/10.1088/0960-1317/19/2/025007

[101] L. Gutierrez-Rivera, J. Martinez-Quijada, R. Johnstone, D. Elliott, C. Backhouse and D. Sameoto. *Multilayer bonding using a conformal adsorbate film (CAF) for the fabrication of 3D monolithic microfluidic devices in photopolymer*. Journal of Micromechanics and Microengineering, 22: 085018. IOP, 2012. http://dx.doi.org/10.1088/0960-1317/22/8/085018

[102] E. Mitri, G. Birard, L. Vaccari, S. Kenig, M. Tormena and G. Grenciaf. *SU-8 bonding protocol for the fabrication of microfluidic devices dedicated to FTIR microspectroscopy of live cells*. Lab Chip, 14: 210-218. Royal Society of Chemistry,

2014.
http://dx.doi.org/10.1039/C3LC50878A

[103] K. Gut and D.Nabaglo. *Measurements of the attenuation by means of the scattered light of planar waveguide structure, basing on the polymer SU8 on a substrate of sodium-calcium glass*. Acta Physica Polonica A, 116:307-322. 2009.
http://dx.doi.org/10.12693/APhysPolA.116.307

[104] F. Niklaus, G. Stemme, J.Q. Lu and R.J. Gutmann. *Adhesive wafer bonding*. Journal of Applied Physics, 99(3): 031101. AIP, 2006.
http://dx.doi.org/10.1063/1.2168512

[105] M.U. Kopp, A.J. de Mello and A. Manz. *Chemical Amplification: Continuous-flow PCR on a chip.* Science, 280 (5366): 1046-1048. 1998.
http://dx.doi.org/10.1126/science.280.5366.1046

[106] P. England. *Fabrication and characterization of polymer based microstructures and microfluidic structures*. MSc Thesis, Heriot Watt Universty, 2007.

[107] J. Brackbill, D. Kothe, C. Zemach. *A continuum method for modeling surface tension.* Journal of computational physics, 100: 335–354. 1992.
http://doi.org/10.1016/0021-9991(92)90240-Y

Appendix A – Chip 1

The Excel sheet of the calculations and parameters of Chip 1.

Oil Flow rate (ml/hr)	Oil Velocity (m/s)	Reynolds Number	Capillary number	Oil Flow rate (ml/s)	Water Flow rate (ml/s)	Exp Water Flow	Flow rate ratio (water/oil)
0.1	0.001312998	0.00297746	0.001705584	0.000027778	0.00000174	0.00000139	0.063
					0.00000278	0.00000278	0.100
					0.00000417	0.00000417	0.150
					0.00000557	0.00000556	0.200
					0.00000696	0.00000694	0.250
					0.00000835	0.00000833	0.300
0.2	0.002625995	0.00595491	0.003411168	0.000055556	0.00000278	0.00000278	0.050
					0.00000557	0.00000556	0.100
					0.00000835	0.00000833	0.150
					0.00001113	0.00001111	0.200
					0.00001386	0.00001389	0.249
					0.00001669	0.00001667	0.300
0.3	0.003938993	0.00893237	0.005116752	0.000083333	0.00000417	0.00000417	0.050
					0.00000835	0.00000833	0.100
					0.00001252	0.00001250	0.150

Oil Flow rate (ml/hr)	Oil Velocity (m/s)	Reynolds Number	Capillary number	Oil Flow rate (ml/s)	Water Flow rate (ml/s)	Exp Water Flow	Flow rate ratio (water/oil)
					0.00001669	0.00001667	0.200
					0.00002082	0.00002083	0.250
					0.00002500	0.00002500	0.300
0.4	0.005251991	0.01190983	0.006822336	0.000111111	0.00000557	0.00000556	0.050
					0.00001113	0.00001111	0.100
					0.00001669	0.00001667	0.150
					0.00002221	0.00002222	0.200
					0.00002778	0.00002778	0.250
					0.00003334	0.00003333	0.300
0.5	0.006564988	0.01488729	0.0085279196	0.000138889	0.00000696	0.00000694	0.050
					0.00001386	0.00001389	0.100
					0.00002082	0.00002083	0.150
					0.00002778	0.00002778	0.200
					0.00003473	0.00003472	0.250
					0.00004169	0.00004167	0.300
0.55	0.007221487	0.01637601	0.0093807115	0.000152778	0.00000765	0.00000764	0.050
					0.00001526	0.00001528	0.100
					0.00002291	0.00002292	0.150
					0.00003057	0.00003056	0.200
					0.00003817	0.00003819	0.250

Oil Flow rate (ml/hr)	Oil Velocity (m/s)	Reynolds Number	Capillary number	Oil Flow rate (ml/s)	Water Flow rate (ml/s)	Exp Water Flow	Flow rate ratio (water/oil)
					0.00004608	0.00004583	0.302
0.6	0.007877986	0.01786474	0.0102335035	0.000166667	0.00000835	0.00000833	0.050
					0.00001669	0.00001667	0.100
					0.00002500	0.00002500	0.150
					0.00003334	0.00003333	0.200
					0.00004169	0.00004167	0.250
					0.00005000	0.00005000	0.300
0.65	0.008534485	0.01935347	0.0110862955	0.000180556	0.00000904	0.00000903	0.050
					0.00001808	0.00001806	0.100
					0.00002708	0.00002708	0.150
					0.00003613	0.00003611	0.200
					0.00004521	0.00004514	0.250
					0.00005434	0.00005417	0.301
0.7	0.009190983	0.02084220	0.0119390874	0.000194444	0.00000974	0.00000972	0.050
					0.00001943	0.00001944	0.100
					0.00002917	0.00002917	0.150
					0.00003891	0.00003889	0.200
					0.00004869	0.00004861	0.250
					0.00005826	0.00005833	0.300
0.8	0.010503981	0.02381966	0.0136446713	0.000222222	0.00001108	0.00001111	0.050

Oil Flow rate (ml/hr)	Oil Velocity (m/s)	Reynolds Number	Capillary number	Oil Flow rate (ml/s)	Water Flow rate (ml/s)	Exp Water Flow	Flow rate ratio (water/oil)
					0.00002221	0.00002222	0.100
					0.00003434	0.00003333	0.155
					0.00004434	0.00004444	0.200
					0.00005565	0.00005556	0.250
					0.00006652	0.00006667	0.299
0.9	0.011816979	0.02679711	0.0153502552	0.00025	0.00001252	0.00001250	0.050
					0.00002500	0.00002500	0.100
					0.00003752	0.00003750	0.150
					0.00005000	0.00005000	0.200
					0.00006260	0.00006250	0.250
					0.00007521	0.00007500	0.301
1	0.013129976	0.02977457	0.0170558392	0.000277778	0.00001391	0.00001389	0.050
					0.00002778	0.00002778	0.100
					0.00004169	0.00004167	0.150
					0.00005565	0.00005556	0.200
					0.00006956	0.00006944	0.250
					0.00008347	0.00008333	0.300
1.1	0.014442974	0.03275203	0.0187614231	0.000305556	0.00001526	0.00001528	0.050
					0.00003057	0.00003056	0.100
					0.00004565	0.00004583	0.149
					0.00006130	0.00006111	0.201

Oil Flow rate (ml/hr)	Oil Velocity (m/s)	Reynolds Number	Capillary number	Oil Flow rate (ml/s)	Water Flow rate (ml/s)	Exp Water Flow	Flow rate ratio (water/oil)
					0.00007652	0.00007639	0.250
					0.00009173	0.00009167	0.300
1.2	0.015755972	0.03572949	0.0204670070	0.000333333	0.00001669	0.00001667	0.050
					0.00003434	0.00003333	0.103
					0.00005000	0.00005000	0.150
					0.00006652	0.00006667	0.200
					0.00008347	0.00008333	0.250
					0.00010000	0.00010000	0.300

Appendix B – Chip 2

The Excel sheet of the calculations and parameters of Chip 2.

Oil Flow rate (ml/hr)	Oil Velocity (m/s)	Reynolds Number	Capillary number	Oil Flow rate (ml/s)	Water Flow rate (ml/s)	Exp Water Flow	Flow rate ratio (water/oil)
0.1	0.001559673	0.00356426	0.002026015	0.000027778	0.00000174	0.00000139	0.063
					0.00000278	0.00000278	0.100
					0.00000417	0.00000417	0.150
					0.00000557	0.00000556	0.200
					0.00000696	0.00000694	0.250
					0.00000835	0.00000833	0.300
0.2	0.003119346	0.00712851	0.004052031	0.000055556	0.00000278	0.00000278	0.050
					0.00000557	0.00000556	0.100
					0.00000835	0.00000833	0.150
					0.00001113	0.00001111	0.200
					0.00001386	0.00001389	0.249
					0.00001669	0.00001667	0.300
0.3	0.004679019	0.01069277	0.006078046	0.000083333	0.00000417	0.00000417	0.050
					0.00000835	0.00000833	0.100
					0.00001252	0.00001250	0.150
					0.00001669	0.00001667	0.200

Oil Flow rate (ml/hr)	Oil Velocity (m/s)	Reynolds Number	Capillary number	Oil Flow rate (ml/s)	Water Flow rate (ml/s)	Exp Water Flow	Flow rate ratio (water/oil)
					0.00002082	0.00002083	0.250
					0.00002500	0.00002500	0.300
0.4	0.006238692	0.01425702	0.008104061	0.000111111	0.00000557	0.00000556	0.050
					0.00001113	0.00001111	0.100
					0.00001669	0.00001667	0.150
					0.00002221	0.00002222	0.200
					0.00002778	0.00002778	0.250
					0.00003334	0.00003333	0.300
0.5	0.007798365	0.01782128	0.0101300767	0.000138889	0.00000696	0.00000694	0.050
					0.00001386	0.00001389	0.100
					0.00002082	0.00002083	0.150
					0.00002778	0.00002778	0.200
					0.00003473	0.00003472	0.250
					0.00004169	0.00004167	0.300
0.55	0.008578202	0.01960340	0.0111430844	0.000152778	0.00000765	0.00000764	0.050
					0.00001526	0.00001528	0.100
					0.00002291	0.00002292	0.150
					0.00003057	0.00003056	0.200
					0.00003817	0.00003819	0.250
					0.00004608	0.00004583	0.302

Oil Flow rate (ml/hr)	Oil Velocity (m/s)	Reynolds Number	Capillary number	Oil Flow rate (ml/s)	Water Flow rate (ml/s)	Exp Water Flow	Flow rate ratio (water/oil)
0.6	0.009358039	0.02138553	0.0121560921	0.000166667	0.00000835	0.00000833	0.050
					0.00001669	0.00001667	0.100
					0.00002500	0.00002500	0.150
					0.00003334	0.00003333	0.200
					0.00004169	0.00004167	0.250
					0.00005000	0.00005000	0.300
0.65	0.010137875	0.02316766	0.0131690998	0.000180556	0.00000904	0.00000903	0.050
					0.00001808	0.00001806	0.100
					0.00002708	0.00002708	0.150
					0.00003613	0.00003611	0.200
					0.00004521	0.00004514	0.250
					0.00005434	0.00005417	0.301
0.7	0.010917712	0.02494979	0.0141821074	0.000194444	0.00000974	0.00000972	0.050
					0.00001943	0.00001944	0.100
					0.00002917	0.00002917	0.150
					0.00003891	0.00003889	0.200
					0.00004869	0.00004861	0.250
					0.00005826	0.00005833	0.300
0.8	0.012477385	0.02851404	0.0162081228	0.000222222	0.00001108	0.00001111	0.050
					0.00002221	0.00002222	0.100
					0.00003434	0.00003333	0.155

Oil Flow rate (ml/hr)	Oil Velocity (m/s)	Reynolds Number	Capillary number	Oil Flow rate (ml/s)	Water Flow rate (ml/s)	Exp Water Flow	Flow rate ratio (water/oil)
					0.00004434	0.00004444	0.200
					0.00005565	0.00005556	0.250
					0.00006652	0.00006667	0.299
0.9	0.014037058	0.03207830	0.0182341381	0.00025	0.00001252	0.00001250	0.050
					0.00002500	0.00002500	0.100
					0.00003752	0.00003750	0.150
					0.00005000	0.00005000	0.200
					0.00006260	0.00006250	0.250
					0.00007521	0.00007500	0.301
1	0.015596731	0.03564255	0.0202601535	0.000277778	0.00001391	0.00001389	0.050
					0.00002778	0.00002778	0.100
					0.00004169	0.00004167	0.150
					0.00005565	0.00005556	0.200
					0.00006956	0.00006944	0.250
					0.00008347	0.00008333	0.300
1.1	0.017156404	0.03920681	0.0222861688	0.000305556	0.00001526	0.00001528	0.050
					0.00003057	0.00003056	0.100
					0.00004565	0.00004583	0.149
					0.00006130	0.00006111	0.201
					0.00007652	0.00007639	0.250
					0.00009173	0.00009167	0.300

Oil Flow rate (ml/hr)	Oil Velocity (m/s)	Reynolds Number	Capillary number	Oil Flow rate (ml/s)	Water Flow rate (ml/s)	Exp Water Flow	Flow rate ratio (water/oil)
1.2	0.018716077	0.04277106	0.0243121842	0.000333333	0.00001669	0.00001667	0.050
					0.00003434	0.00003333	0.103
					0.00005000	0.00005000	0.150
					0.00006652	0.00006667	0.200
					0.00008347	0.00008333	0.250
					0.00010000	0.00010000	0.300

Appendix C – Chip 3

The Excel sheet of the calculations and parameters of Chip 3.

Oil Flow rate (ml/hr)	Oil Velocity (m/s)	Reynolds Number	Capillary number	Oil Flow rate (ml/s)	Water Flow rate (ml/s)	Exp Water Flow	Flow rate ratio (water/oil)
0.1	0.001538083	0.00348788	0.00199797	0.000027778	0.00000174	0.00000139	0.063
					0.00000278	0.00000278	0.100
					0.00000417	0.00000417	0.150
					0.00000557	0.00000556	0.200
					0.00000696	0.00000694	0.250
					0.00000835	0.00000833	0.300
0.2	0.003076166	0.00697576	0.003995939	0.000055556	0.00000278	0.00000278	0.050
					0.00000557	0.00000556	0.100
					0.00000835	0.00000833	0.150
					0.00001113	0.00001111	0.200
					0.00001386	0.00001389	0.249
					0.00001669	0.00001667	0.300
0.3	0.004614249	0.01046364	0.005993909	0.000083333	0.00000417	0.00000417	0.050
					0.00000835	0.00000833	0.100
					0.00001252	0.00001250	0.150
					0.00001669	0.00001667	0.200

Oil Flow rate (ml/hr)	Oil Velocity (m/s)	Reynolds Number	Capillary number	Oil Flow rate (ml/s)	Water Flow rate (ml/s)	Exp Water Flow	Flow rate ratio (water/oil)
					0.00002082	0.00002083	0.250
					0.00002500	0.00002500	0.300
0.4	0.006152332	0.01395151	0.007991879	0.000111111	0.00000557	0.00000556	0.050
					0.00001113	0.00001111	0.100
					0.00001669	0.00001667	0.150
					0.00002221	0.00002222	0.200
					0.00002778	0.00002778	0.250
					0.00003334	0.00003333	0.300
0.5	0.007690415	0.01743939	0.0099898487	0.000138889	0.00000696	0.00000694	0.050
					0.00001386	0.00001389	0.100
					0.00002082	0.00002083	0.150
					0.00002778	0.00002778	0.200
					0.00003473	0.00003472	0.250
					0.00004169	0.00004167	0.300
0.55	0.008459456	0.01918333	0.0109888335	0.000152778	0.00000765	0.00000764	0.050
					0.00001526	0.00001528	0.100
					0.00002291	0.00002292	0.150
					0.00003057	0.00003056	0.200
					0.00003817	0.00003819	0.250
					0.00004608	0.00004583	0.302

Oil Flow rate (ml/hr)	Oil Velocity (m/s)	Reynolds Number	Capillary number	Oil Flow rate (ml/s)	Water Flow rate (ml/s)	Exp Water Flow	Flow rate ratio (water/oil)
0.6	0.009228498	0.02092727	0.0119878184	0.000166667	0.00000835	0.00000833	0.050
					0.00001669	0.00001667	0.100
					0.00002500	0.00002500	0.150
					0.00003334	0.00003333	0.200
					0.00004169	0.00004167	0.250
					0.00005000	0.00005000	0.300
0.65	0.009997539	0.02267121	0.0129868032	0.000180556	0.00000904	0.00000903	0.050
					0.00001808	0.00001806	0.100
					0.00002708	0.00002708	0.150
					0.00003613	0.00003611	0.200
					0.00004521	0.00004514	0.250
					0.00005434	0.00005417	0.301
0.7	0.010766581	0.02441515	0.0139857881	0.000194444	0.00000974	0.00000972	0.050
					0.00001943	0.00001944	0.100
					0.00002917	0.00002917	0.150
					0.00003891	0.00003889	0.200
					0.00004869	0.00004861	0.250
					0.00005826	0.00005833	0.300
0.8	0.012304663	0.02790303	0.0159837578	0.000222222	0.00001108	0.00001111	0.050
					0.00002221	0.00002222	0.100
					0.00003434	0.00003333	0.155

Oil Flow rate (ml/hr)	Oil Velocity (m/s)	Reynolds Number	Capillary number	Oil Flow rate (ml/s)	Water Flow rate (ml/s)	Exp Water Flow	Flow rate ratio (water/oil)
					0.00004434	0.00004444	0.200
					0.00005565	0.00005556	0.250
					0.00006652	0.00006667	0.299
0.9	0.013842746	0.03139091	0.0179817276	0.00025	0.00001252	0.00001250	0.050
					0.00002500	0.00002500	0.100
					0.00003752	0.00003750	0.150
					0.00005000	0.00005000	0.200
					0.00006260	0.00006250	0.250
					0.00007521	0.00007500	0.301
1	0.015380829	0.03487878	0.0199796973	0.000277778	0.00001391	0.00001389	0.050
					0.00002778	0.00002778	0.100
					0.00004169	0.00004167	0.150
					0.00005565	0.00005556	0.200
					0.00006956	0.00006944	0.250
					0.00008347	0.00008333	0.300
1.1	0.016918912	0.03836666	0.0219776670	0.000305556	0.00001526	0.00001528	0.050
					0.00003057	0.00003056	0.100
					0.00004565	0.00004583	0.149
					0.00006130	0.00006111	0.201
					0.00007652	0.00007639	0.250
					0.00009173	0.00009167	0.300

Oil Flow rate (ml/hr)	Oil Velocity (m/s)	Reynolds Number	Capillary number	Oil Flow rate (ml/s)	Water Flow rate (ml/s)	Exp Water Flow	Flow rate ratio (water/oil)
1.2	0.018456995	0.04185454	0.0239756368	0.000333333	0.00001669	0.00001667	0.050
					0.00003434	0.00003333	0.103
					0.00005000	0.00005000	0.150
					0.00006652	0.00006667	0.200
					0.00008347	0.00008333	0.250
					0.00010000	0.00010000	0.300

Appendix D – Results for Chip1, 2 and 3

The Excel sheet of the measured droplet diameters (µm) and standard error results of Chip 1 for Q= 0.05, 0.1, 0.15, 0.2, 0.25, 0.3.

Chip1	Capillary Number	0.05	S.E	0.1	S.E	0.15	S.E	0.2	S.E	0.25	S.E	0.3	S.E
0.10	0.001705584	159.272789	2.50	175.241376	2.71	187.248721	2.11	186.857779	0.83	193.905835	1.30	195.630103	1.00
0.20	0.003411168	151.016726	1.99	166.950009	1.04	172.937162	0.81	183.329774	0.69	178.707954	1.63	189.362777	0.54
0.30	0.005116752	143.883984	1.82	153.505046	1.10	152.138208	1.24	169.960003	1.65	172.482119	0.79	181.113203	0.85
0.40	0.006822336	140.533477	0.70	151.027786	1.06	162.831046	1.05	168.711864	1.13	170.249121	0.92	173.863344	0.50
0.50	0.0085279196	141.583465	1.28	144.559072	0.76	155.50366	0.48	160.569583	1.05	170.010025	1.37	170.261329	0.81
0.55	0.0093807115	140.248654	1.15	148.731113	0.97	154.565152	0.80	161.372695	0.64	162.490399	1.02	167.508946	0.53
0.60	0.0102335035	136.707199	0.95	151.609767	1.42	160.685868	0.68	162.918524	1.41	170.288112	0.82	169.096204	0.94
0.65	0.0110862955	135.043095	1.94	149.628636	0.88	151.504882	0.78	161.711829	0.66	165.164791	1.05	168.324477	0.47
0.70	0.0119390874	140.360514	1.24	151.610224	0.59	155.732748	0.54	156.667536	0.63	159.209103	0.53	163.45973	0.48
0.80	0.0136446713	133.657888	1.11	140.816899	0.71	149.273245	0.42	153.115363	0.22	157.259096	0.54	165.507227	1.20
0.90	0.0153502552	131.653738	0.80	134.656815	1.92	143.33572	0.64	144.450625	0.23	153.707404	0.60	161.675985	0.66
1.00	0.0170558392	125.811798	0.66	138.482759	0.69	139.577828	0.92	152.45914	0.89	167.268622	0.85	170.037383	0.79
1.10	0.0187614231	126.958342	0.89	143.936666	0.95	143.943028	0.56	152.348922	1.00	156.285929	0.75	158.719146	1.01
1.20	0.0204670070	112.01428	1.46	139.893032	0.74	136.058149	0.74	147.874482	1.01	145.070606	1.18	154.15564	0.74

The Excel sheet of the measured droplet diameters (µm) and standard error results of Chip 2 for Q= 0.05, 0.1, 0.15, 0.2, 0.25, 0.3.

Chip2	Capillary Number	0.05	S.E	0.1	S.E	0.15	S.E	0.2	S.E	0.25	S.E	0.3	S.E
0.10	0.002026015	183.105037	1.15	191.192703	0.55	203.284689	1.13	209.658159	1.07	208.823577	1.27	210.396186	0.85
0.20	0.004052031	160.25258	0.66	172.158515	1.06	171.303495	0.83	174.542994	0.61	182.72385	1.16	183.766484	0.78
0.30	0.006078046	149.093943	0.97	155.73249	1.00	160.932546	0.35	166.433041	0.58	166.862598	0.72	173.190425	0.77
0.40	0.008104061	141.837201	1.04	149.901046	0.88	154.227952	0.67	160.307014	0.76	163.556616	0.82	171.15537	0.59
0.50	0.0101300767	138.243421	0.75	142.90264	1.32	150.918439	0.59	157.326995	0.40	157.11123	0.44	160.025255	0.51
0.55	0.0111430844	136.669276	0.40	143.974868	0.67	150.721372	0.70	153.864108	0.75	158.688796	0.89	159.135703	0.23
0.60	0.0121560921	135.205346	0.28	143.102386	0.33	146.00966	0.74	150.143793	0.46	154.673918	0.44	155.156487	0.66
0.65	0.0131690998	133.647416	0.69	139.737588	0.47	146.457564	0.31	151.504964	0.57	151.150092	0.50	157.05341	0.59
0.70	0.0141821074	130.9773	0.83	140.223697	0.46	144.511042	0.51	148.413255	1.18	148.294383	0.78	155.242201	0.49
0.80	0.0162081228	125.484526	0.83	138.050969	0.73	145.875377	0.52	142.252468	0.84	151.233124	0.89	152.957298	0.43
0.90	0.0182341381	123.853933	0.39	134.560122	0.70	141.016702	0.57	141.964812	0.53	149.945026	0.70	152.16718	0.47
1.00	0.0202601535	120.882921	0.80	133.331614	0.69	138.582136	0.65	141.253263	0.91	142.247718	0.64	147.674542	0.41
1.10	0.0222861688	118.872491	0.72	128.723349	0.52	133.602106	0.67	141.076919	0.88	143.4365	0.71	149.690928	0.60
1.20	0.0243121842	115.963201	0.71	126.371199	0.35	131.006115	0.60	136.060774	0.83	138.686745	1.49	138.283796	1.15

The Excel sheet of the measured droplet diameters (μm) and standard error results of Chip 3 for Q= 0.05, 0.1, 0.15, 0.2, 0.25, 0.3.

Chip3	Capillary Number	0.05	S.E	0.1	S.E	0.15	S.E	0.2	S.E	0.25	S.E	0.3	S.E
0.10	0.00199797	173.819727	1.20	184.703882	0.79	198.895626	0.88	204.068966	0.55	205.875607	0.55	198.711299	1.25
0.20	0.003995939	169.965078	0.76	179.339521	0.73	174.603305	0.65	178.830905	0.54	183.485641	0.48	184.201502	0.89
0.30	0.005993909	156.849845	0.89	161.817427	0.70	161.575165	0.49	172.186404	1.02	179.362832	0.67	175.885523	0.97
0.40	0.007991879	152.915888	0.77	154.760657	0.59	151.623128	2.17	160.001779	1.19	166.421659	0.77	169.449381	1.04
0.50	0.009989849	141.122273	0.83	154.791307	0.62	150.426591	0.29	156.437841	0.31	159.888366	1.01	164.515417	1.12
0.55	0.010988834	130.448902	0.68	144.445845	0.53	148.570062	0.68	158.096593	0.76	157.902886	0.96	159.113629	1.60
0.60	0.011987818	140.330731	1.17	140.391279	0.36	147.341562	1.09	155.357042	1.06	157.59093	0.85	159.623281	1.12
0.65	0.012986803	132.852202	0.62	133.346802	0.76	149.880664	0.05	151.560953	0.30	153.909735	1.00	159.640373	1.03
0.70	0.013985788	131.423396	1.18	132.914345	0.63	147.435488	0.53	151.658618	1.51	154.041502	1.30	156.364835	1.14
0.80	0.015983758	125.485245	1.03	130.68478	0.85	143.51515	0.76	143.637114	0.62	151.052853	1.43	154.892319	0.94
0.90	0.017981728	100.684989	0.95	129.963325	0.93	141.370279	0.41	138.872118	0.73	146.591449	2.31	155.173065	0.52
1.00	0.019979697	113.336601	0.83	134.727456	0.78	135.156358	0.54	138.028515	0.90	149.614736	0.87	148.616225	0.85
1.10	0.021977667	119.103108	1.51	131.116503	0.81	131.509044	0.75	136.797924	1.72	140.040918	1.15	144.126614	1.12
1.20	0.023975637	117.033878	0.72	129.180284	0.87	133.042065	2.27	132.132686	1.40	144.078532	0.77	147.748756	1.08

Appendix E – SU-8 Fabrication Datasheet

This appendix contains part of a list that was used to monitor the microfluidic device fabrication.

Name	Design No		1st Layer						2nd Layer						Development	Notes
	Design	Depth (µm)	Rpm	PreBake		Energy mJ/cm2	Post Exposure Bake		Rpm	PreBake		Energy mJ/cm2	Post Exposure Bake			
				65^0 C	95^0 C		65^0 C	95^0 C		65^0 C	95^0 C		65^0 C	95^0C		
21611-01	D53	110	1000	5	20	300	1	6	750	5	26	300	1	12	08:33	
21611-02	D63	120	1000	5	20	300	1	6	750	5	30	400	1	12	08:30	Bad alignment.
21611-03	SLG	N/A	1000	5	20	300	1	6	750	5	30	400	1	12	08:30	
23611-02	D42	117	1000	5	20	300	1	6	750	5	25	350	1	15	13:13	Advise 18min. More dev.
23611-05	LG	105	2000	3	6	300	1	6	2000	3	6	350	1	6	04:10	partially

Name	Design No		1st Layer						2nd Layer						Development	Notes
	Design	Depth (µm)	Rpm	PreBake		Energy mJ/cm2	Post Exposure Bake		Rpm	PreBake		Energy mJ/cm2	Post Exposure Bake			
				65^0 C	95^0 C		65^0 C	95^0 C		65^0 C	95^0 C		65^0 C	95^0C		
23611-06	LG	43	2000	3	6	350	1	6	2000	3	6	350	1	7	04:34	
23611-07	D94	43	2000	3	6	350	1	6	2000	3	6	350	1	6	05:03	
28611-01	D33	121	1000	5	20	400	1	07:30	1000	5	20	450	1	6	09:10	More dev.
28611-02	D43	121	1000	5	20	400	1	6	1000	5	20	350	1	6	04:24	
28611-03	LG	35	1000	7	20	400	1	6	2000	3	6	400	1	6	04:20	
30611-01	D41	164	1000	5	25	400	1	6	1000	5	25	400	1	6	14:10	Sides not smooth.
30611-02	D33	232	1000	5	20	400	1	6	1000	5	32	400	1	10	18:18	Very good.

Name	Design No		1st Layer						2nd Layer						Development	Notes
	Design	Depth (µm)	Rpm	PreBake		Energy mJ/cm2	Post Exposure Bake		Rpm	PreBake		Energy mJ/cm2	Post Exposure Bake			
				65^0 C	95^0 C		65^0 C	95^0 C		65^0 C	95^0 C		65^0 C	95^0C		
30611-03	LG	N/A	1000	5	20	400	1	6	1000	5	25	400	1	10	18:16	Small bits problematic
30611-04	D21	N/A	1000	5	20	400	1	6	1000	5	20	400	1	6	18:00	White fringes, not open
10611-05	LG	N/A	1000	5	20	400	1	6	2000	3	6	400	1	6	04:25	small channels not open
5711-04	LG	71	1000	5	20	400	1	6	2000	3	6	400	1	6	05:01	Very good.
5711-06	D23	N/A	1000	5	20	400	1	6	2000	3	6	400	1	6	04:50	Erased, over developed
5611-01	D71	80	1000	5	20	400	1	6	1000	5	32	400	1	10	18:04	Very good.
5711-02	D32	132	1000	5	20	400	1	6	1000	5	32	400	1	10	20:35	Good.

Name	Design No		1st Layer						2nd Layer						Development	Notes
	Design	Depth (µm)	Rpm	PreBake		Energy mJ/cm2	Post Exposure Bake		Rpm	PreBake		Energy mJ/cm2	Post Exposure Bake			
				65^0 C	95^0 C		65^0 C	95^0 C		65^0 C	95^0 C		65^0 C	95^0C		
5711-03	LG	113	1000	5	20	400	1	6	1000	5	32	400	1	10	25:20	Good, last bit problematic
12711-05	D72	75	2000	3	6	400	1	6	1800	3	6	400	1	6	05:20	
21711-01	D72	111	2000	3	6	400	1	6	1000	10	65	400	1	12	07:17	Perfect
21711-03	LG	68	2000	3	7	400	1	6	2000	3	6	400	1	6	05:34	Very good.
21711-04	LG	60	2000	3	6	400	1	6	2000	4	8	400	1	6	07:28	Very good.
26711-01	LG	117	2000	3	6	400	1	6	1000	10	65	400	1	12	07:55	Good.
26711-02	D42	132	2000	3	6	400	1	6	1000	10	65	400	1	12	08:47	Good. Less Dev

Name	Design No		1st Layer						2nd Layer						Development	Notes
	Design	Depth (µm)	Rpm	PreBake		Energy mJ/cm2	Post Exposure Bake		Rpm	PreBake		Energy mJ/cm2	Post Exposure Bake			
				65^0 C	95^0 C		65^0 C	95^0 C		65^0 C	95^0 C		65^0 C	95^0C		
26711-03	LG	64	2000	3	6	400	1	6	2000	3	6	400	1	6	06:00	T-junction
28711-01	D93	195	1000	5	20	400	1	6	1000	10	65	400	1	42	08:25	Good.
28711-02	LG	58	1000	5	20	400	1	6	1000	5	32	400	1	62	20:12	T-junction
28711-03	LG	264	1000	5	20	400	1	6	1000	10	65	400	1	12	09:23	T-junction
28711-04	D72	224	1000	5	21:30	400	1	6	1000	5	25	400	1	12	15:12	Good.
2811-01	LG	249	1000	05:14	21:39	400	1	6	1000	10	65	400	1	12	10:02	
2811-02	LG	229	1000	06:30	20	400	1	6	1000	10	65	400	1	12	09:32	

Name	Design No		1st Layer						2nd Layer						Development	Notes
	Design	Depth (µm)	Rpm	PreBake		Energy mJ/cm2	Post Exposure Bake		Rpm	PreBake		Energy mJ/cm2	Post Exposure Bake			
				65^0 C	95^0 C		65^0 C	95^0 C		65^0 C	95^0 C		65^0 C	95^0C		
2811-03	LG	264	1000	5	20	400	1	6	1000	10	65	400	1	12	09:12	
2811-04	D22	142	1000	5	20	400	1	6	1000	10	65	400	1	12	09:53	
2811-05	D42	375	1000	5	21:40	400	1	6	1000	10	65	400	1	12	09:20	
4811-02	LG	116	1000	5	20	400	1	10	1000	5	65	400	2	12	09:28	Good.
4811-06	LG	40	1000	5	25	400	1	6	2000	5	40	400	1	12	05:31	
4811-07	LG	40	2000	3	6	400	1	6	2000	5	20	400	1	12	05:20	
16811-04	LG	200	1000	5	20	400	1	8	1000	5	65	400	1	12	12:15	

Name	Design No		1st Layer						2nd Layer						Development	Notes
	Design	Depth (µm)	Rpm	PreBake		Energy mJ/cm2	Post Exposure Bake		Rpm	PreBake		Energy mJ/cm2	Post Exposure Bake			
				65^0 C	95^0 C		65^0 C	95^0 C		65^0 C	95^0 C		65^0 C	95^0C		
16811-06	D83	125	1000	07:30	20	400	1	6	1000	5	65	400	1	12	12:27	
18811 01	D41	102	1000	5	20	400	1	6	1000	5	65	400	1	12	11:37	Good.
18811 02	D83	112	1000	5	20	400	1	6	1000	5	65	400	1	12	12:20	Good.
18811 03	LG	132	1000	5	20	400	1	6	2000	3	6	400	1	6	07:25	Mostly Formed.
30811-01	D33	44	1000	05:03	20	400	1	07:39	1000	5	65	400	1	12	12:07	Very good.
30811-02	D73	57	1000	05:10	20	400	1	9	1000	5	65	400	1	12	12:15	Good.
30811-03	LG	53	1000	5	20	400	1	6	2000	3	6	400	1	6	06:36	Bonding fail.

Name	Design No		1st Layer						2nd Layer						Development	Notes
	Design	Depth (µm)	Rpm	PreBake		Energy mJ/cm2	Post Exposure Bake		Rpm	PreBake		Energy mJ/cm2	Post Exposure Bake			
				65^0 C	95^0 C		65^0 C	95^0 C		65^0 C	95^0 C		65^0 C	95^0C		
30811-04	LG	57	1000	5	20	400	1	6	2000	3	6	400	1	6	06:14	Good. Problem at inlet.
30811-05	LG	45	1000	05:12	20	400	1	6	2000	3	6	400	1	6	06:42	Mostly Formed.
1911-02	LG	48	1000	5	20	400	1	6	2000	3	6	400	1	6	06:20	Good
1911-05	LG	48	1000	5	20	400	1	6	2000	3	6	400	1	6	06:40	Good
1911-06	LG	49	1000	5	20	400	1	6	2000	3	6	400	1	6	07:09	
6911-01	LG	69	1000	5	20	400	01:30	6	2000	3	6	400	1	6	06:53	
6911-02	LG	52	1000	5	20	400	1	6	2000	3	7	400	1	6	06:40	Good

Name	Design No		1st Layer						2nd Layer						Development	Notes
	Design	Depth (µm)	Rpm	PreBake		Energy mJ/cm2	Post Exposure Bake		Rpm	PreBake		Energy mJ/cm2	Post Exposure Bake			
				65^0 C	95^0 C		65^0 C	95^0 C		65^0 C	95^0 C		65^0 C	95^0C		
6911-03	LG	41	1000	5	20	400	1	6	2000	3	6	400	1	6	06:45	Good
6911-04	LG	48	1000	5	20	400	1	6	2000	3	8	372	1	6	06:47	out
8911-01	LG	130	1000	5	20	400	1	6	1000	3	65	400	7	12	02:30	
8911-02	LG	44	1000	5	20	400	1	6	2000	3	3	400	1	6	06:55	small channels.
8911-03	LG	52	1000	5	20	400	1	6	2000	3	6	400	1	6	06:52	small channels.
20911-01	LG	42	1000	5	20	400	1	6	2000	3	6	400	1	6	06:11	Very good.
20911-02	LG	N/A	1000	06:30	20	400	1	6	2000	3	6	400	1	6	06:40	Fail - small channels

Name	Design No		1st Layer						2nd Layer						Development	Notes
	Design	Depth (µm)	Rpm	PreBake		Energy mJ/cm2	Post Exposure Bake		Rpm	PreBake		Energy mJ/cm2	Post Exposure Bake			
				65^0 C	95^0 C		65^0 C	95^0 C		65^0 C	95^0 C		65^0 C	95^0C		
20911-03	LG	N/A	1000	5	20	400	1	6	2000	3	7	400	1	6	07:07	Fail - Partially opened
22911-01	LG	N/A	1000	5	20	400	01:30	6	2000	3	6	400	1	6	10:28	Fail - old SU8
22911-02	LG	118	1000	5	20	400	1	8	2000	3	6	400	2	6	12:19	Good - old SU8
22911-03	LG	N/A	1000	5	20	400	1	6	2000	3	6	400	1	6	06:50	Partially opened
22911-04	LG	38	1000	5	20	400	1	6	2000	3	7	400	1	6	08:15	Well formed.
22911-05	LG	49	1000	5	20	400	01:45	6	2000	03:25	6	400	1	6	08:27	Very good.
22911-06	LG	46	1000	5	20	400	1	6	2000	3	6	400	1	6	08:29	Very good.

Name	Design No		1st Layer						2nd Layer						Development	Notes
	Design	Depth (µm)	Rpm	PreBake		Energy mJ/cm2	Post Exposure Bake		Rpm	PreBake		Energy mJ/cm2	Post Exposure Bake			
				65^0 C	95^0 C		65^0 C	95^0 C		65^0 C	95^0 C		65^0 C	95^0C		
29911-01	LG	49	1000	05:27	20	400	1	6	2000	3	6	400	1	6	07:35	Good structure
29911-02	LG	N/A	1000	05:36	20	400	1	6	2000	3	6	400	1	6	07:53	spinner error - thickness ?
29911-05	D82	49	1000	5	20	400	1	6	2000	3	6	400	1	6	08:20	
41011-01	LG	47	1000	5	20	400	1	6	2000	3	6	400	1	6	08:31	good
41011-02	LG	63	1000	5	20	400	1	6	2000	3	6	400	1	6	07:30	good
41011-03	LG	53	1000	5	20	400	1	6	2000	3	6	400	1	6	12:35	scratch
41011-04	LG	159	1000	5	20	400	1	6	2000	3	6	400	1	6	09:10	good

Name	Design No		1st Layer						2nd Layer						Development	Notes
	Design	Depth (µm)	Rpm	PreBake		Energy mJ/cm2	Post Exposure Bake		Rpm	PreBake		Energy mJ/cm2	Post Exposure Bake			
				65^0 C	95^0 C		65^0 C	95^0 C		65^0 C	95^0 C		65^0 C	95^0C		
41011-05	LG	56	1000	5	20	400	1	6	2000	3	6	400	1	6	08:53	good
111011-03	LG	45	1000	5	20	400	01:08	6	2000	3	6	400	1	6	08:37	
111011-06	LG	59	1000	5	20	400	1	6	2000	3	6	400	1	6	08:35	
181011-01	LG	50	1000	5	20	400	1	6	2000	3	6	400	1	6	08:50	
181011-02	LG	54	1000	5	20	400	1	6	2000	3	6	400	1	6	08:44	
181011-03	LG	51	1000	05:30	20	400	1	6	2000	3	6	400	1	6	08:48	
181011-04	LG	60	1000	5	20	400	1	6	2000	3	6	400	1	6	10:11	

Name	Design No		1st Layer						2nd Layer						Development	Notes
	Design	Depth (µm)	Rpm	PreBake		Energy mJ/cm2	Post Exposure Bake		Rpm	PreBake		Energy mJ/cm2	Post Exposure Bake			
				65^0 C	95^0 C		65^0 C	95^0 C		65^0 C	95^0 C		65^0 C	95^0C		
181011-05	LG	58	1000	5	20	400	1	6	2000	03:10	6	400	1	6	09:14	
181011-06	LG	46	1000	5	20	400	1	6	2000	3	6	400	1	6	09:12	
201011-01	LG	43.5	1000	5	20	400	1	6	2000	3	6	400	1	6	09:05	
201011-02	LG	48	1000	5	20	400	1	6	2000	3	6	400	1	6	09:18	
201011-03	LG	68	1000	5	20	400	1	6	2000	3	6	400	01:30	6	09:16	
201011-04	LG	50	1000	5	20	400	1	6	2000	3	6	400	1	6	09:10	
201011-05	LG	58	1000	5	20	400	1	6	2000	3	6	400	1	6	09:46	

Name	Design No		1st Layer						2nd Layer						Development	Notes
	Design	Depth (µm)	Rpm	PreBake		Energy mJ/cm2	Post Exposure Bake		Rpm	PreBake		Energy mJ/cm2	Post Exposure Bake			
				65^0 C	95^0 C		65^0 C	95^0 C		65^0 C	95^0 C		65^0 C	95^0C		
271011-02	LG	54	1000	05:12	20	400	1	6	2000	3	6	400	1	6	09:04	
211011-03	LG	61	1000	5	20	400	1	6	2000	3	6	400	1	6	09:22	
11111-01	LG	N/A	1000	5	20	400	1	6	2000	3	6	400	1	6	08:30	Fail - soft SU8
11111-02	LG	33	1000	5	20	400	1	6	2000	03:16	6	400	1	6	09:19	good
11111-03	LG	56	1000	5	20	400	1	6	2000	3	6	400	1	6	08:57	good
11111-04	LG	75	1000	5	20	400	1	6	2000	3	6	400	1	6	09:16	good
31111-03	LG	37	1000	5	20	400	1	6	2000	3	6	400	1	6	09:04	

Name	Design No		1st Layer						2nd Layer						Development	Notes
	Design	Depth (µm)	Rpm	PreBake		Energy mJ/cm2	Post Exposure Bake		Rpm	PreBake		Energy mJ/cm2	Post Exposure Bake			
				65^0 C	95^0 C		65^0 C	95^0 C		65^0 C	95^0 C		65^0 C	95^0C		
31111-04	LG	31	1000	5	20	400	1	6	2000	3	6	400	1	6	09:22	
81111-05	LG	30	1000	5	20	400	1	6	2000	3	6	400	1	6	10:05	
221111-01	LG	50	1000	5	20	400	1	6	2000	03:16	10	400	1	6	09:10	
221111-04	LG	50	1000	5	20	400	1	6	2000	3	6	400	1	6	09:10	
221111-06	LG	46	1000	5	20	400	1	6	2000	3	6	400	1	6	09:00	
221111-07	LG	50	1000	5	20	400	1	6	2000	3	6	400	1	6	09:35	
221111-08	LG	50	1000	5	20	400	1	6	2000	3	6	400	1	6	10:12	

Name	Design No		1st Layer						2nd Layer						Development	Notes
	Design	Depth (µm)	Rpm	PreBake		Energy mJ/cm2	Post Exposure Bake		Rpm	PreBake		Energy mJ/cm2	Post Exposure Bake			
				65^0 C	95^0 C		65^0 C	95^0 C		65^0 C	95^0 C		65^0 C	95^0C		
Bonding Layer	-	-	1000	5	30	400	-	-	2000	1	02:54					